NTNU – Trondheim
Norwegian University of
Science and Technology

Numerical modelling of the effect of waterflooding and surfactant injection in a matrix-fracture system

Vinh Vuong Tran

Petroleum Geoscience and Engineering (2 year)
Submission date: June 2015
Supervisor: Ole Torsæter, IPT

Norwegian University of Science and Technology
Department of Petroleum Engineering and Applied Geophysics

Acknowledgement

I would like to express my greatest appreciation to my supervisor, Professor Ole Torsæter, for assigning this very interesting topic for my thesis. His guidance and scientific discussions has contributed in the better understanding of the topic and success of this study.

I would also give a warm thanks to Professor Jon Kleppe, for the support and help in times of need and thanks to Ying Guo for introducing this topic.

A warm and special thanks to all my fellow students, which has been encouraging, supportive and a helping hand throughout the whole master period at NTNU.

Finally, I want to thank my parents and my brother for their mental support during my whole degree. Their utterly valuable presence and support have been the backbone for all my achievements. I cannot express how much appreciation I feel for them.

Abstract

Naturally fractured reservoirs in carbonate rocks usually contain more residual oil in the matrix than other reservoirs, due to the high permeability fracture zones that carries the flooded fluids, leaving parts of the reservoir untouched.

Studies on spontaneous imbibition with both water and surfactant has been conducted through simulations to exploit the fractures as a network to reach out to the matrices. Capillary pressure and interfacial tension modification on relative permeability curves has been done to represent the effect of surfactant injection

This study show that reducing the interfacial tension and capillary pressure by surfactant injection, will result in a slightly lower oil production initially, compared to regular waterflooding. However, the simulation study indicate that the oil production will eventually intersect the oil production curve for waterflooding and reach a higher final recovery.

The reservoir performance is improved through higher surfactant concentration as the CMC is being reached faster. In other words, the amount of surfactant in the system impact the reservoir performance significantly.

Sammendrag

Naturlig oppsprukne reservoarer i karbonatbergarter inneholder vanligvis større andel av residuell olje i matriksblokkene sammenlignet med andre reservoarer på grunn av de høy-permeable sprekksonene som frakter strømmende fluider, og etterlater deler av reservoaret urørt.

Studier på spontan imbibering med både vann og tensid har blitt studert gjennom simuleringer for å prøve å utnytte sprekksystemet i reservoarer som et nettverk som kan nå ut til matriksblokkene. Endringer i kapillær trykk og grenseflatespenningskurver har blitt gjort for å kunne representere effekten av tensid injeksjon.

Studiet viser at reduksjon i grenseflatespenning og kapillær trykk ved tensid injeksjon, vil føre til noe lavere oljeproduksjon i starten, sammenlignet med vanlig vanninjeksjon. Likevel viser simuleringsstudiet at oljeproduksjonen vil etter hvert krysse oljeproduksjonskurven for vannflømming og ende opp med en høyere utvinningsgrad.

Reservoarytelsen er forbedret gjennom høyere tensid konsentrasjon på grunn av at den kritiske micellekonsentrasjonen nås raskere. Med andre ord blir reservoarytelsen påvirket betraktelig av mengden tensid i systemet.

Table of Contents

Acknowledgement ..... **I**

Abstract ..... **III**

Sammendrag ..... **V**

Table of Contents ..... **VII**

List of Figures ..... **XI**

List of Tables ..... **XV**

1 Introduction **1**

2 Reservoir Properties **3**

2.1 Porosity 3

2.1.1 Dual porosity 4

2.1.2 Fracture Porosity 4

2.2 Permeability 5

2.2.1 Dual permeability 5

2.2.2 Fracture Permeability 5

2.3 Saturation 6

2.4 Wettability 7

2.4.1 Contact Angle 7

2.4.2 Interfacial Tension 9

2.4.3 Effect of Interfacial Tension on Relative Permeability 10

2.4.4 States of Wettability 11

3 Displacement Forces **13**

3.1 Capillary Forces 13

3.1.1 Capillary Pressure Measurements 16

3.2 Gravity Forces 17

3.3 Viscous Forces 18

3.3.1 Viscous Fingering 18

4 Fluid Flow in Porous Media **19**

4.1 Fluid Flow Conditions 19

4.1.1 Unsteady-state flow 19

4.1.2 Steady-state flow 20
4.1.3 Pseudosteady-state flow 20
4.2 Darcy's Law 21
4.3 Mobility Ratio 22
4.4 Imbibition Process 23
4.4.1 Spontaneous Imbibition 24
4.4.2 Forced Imbibition 24
4.5 Drainage Process 25
5 NFR – Description and Geometry in Carbonates 27
5.1 Characterization of Carbonate Fractures 27
5.1.1 Single Fracture 27
5.1.2 Group of Fractures 28
5.2 Warren-Root model 30
6 Fracture-Matrix Fluid Transfer 31
6.1 Water Invading the Fractures 33
7 Surfactant flooding 35
7.1 Surfactant Properties 35
7.2 Surfactant types 36
7.2.1 Anionic 36
7.2.2 Cationic 36
7.2.3 Nonionic 36
7.2.4 Zwitterionic 36
7.3 Critical Micelle Concentration, CMC 37
7.4 Microemulsions 38
7.5 Capillary Number 39
7.6 IFT Reduction through Surfactant Flooding 40
7.7 Wettability Alteration through Surfactant Flooding in Carbonates 41
7.7.1 Adsorption with Cationic-based Surfactant 41
7.7.2 Adsorption of Anionic-based Surfactants 42
8 Numerical Simulation 43
8.1 Two Models Surrounded by Fractures 43
8.1.1 Single Matrix Block Model 43
8.1.2 Expanded Matrix Block Model (Basecase) 44
8.1.3 Basecase Parameters 45
8.2 Grid Design 46

8.3 Well Design and Location 46
8.4 Basecase - Relative Permeability and Capillary Pressure Curves 47
8.4.1 Matrix 48
8.4.2 Fracture 49
8.5 Other Reservoir Properties and Input Data 50
8.6 Imbibition Process in Eclipse E100 51
8.7 Surfactant Model in Eclipse E100 51
8.7.1 Relative Permeability and Capillary Pressure Curves for Miscible Fluid Displacement 51
8.7.2 Calculation of Capillary Number 54
8.7.3 Water PVT Properties 55
8.7.4 Adsorption 55
8.7.5 Keywords to Activate the Surfactant Model 56
9 Results 61
9.1 Waterflooding – Single Matrix Block 61
9.1.1 Effect of Well Location and Geometry 61
9.1.2 Effect of Injection Rate 65
9.2 Waterflooding – Three Matrix Block (Basecase) 68
9.2.1 Effect of Fracture Width 68
9.2.2 Effect of Injection Rate 71
9.3 Surfactant flooding 74
9.3.1 Effect of Surfactant Concentration 74
9.3.2 Effect of Adsorption 77
9.3.3 Effect of Surfactant Injection after Waterflooding 80
9.3.4 Effect of Surfactant Slug 83
9.3.5 Comparison of Basecase, Slug and Continuous Surfactant Flooding 87
10 Discussion 89
10.1 Reservoir Parameters 89
10.1.1 Fracture Permeability 89
10.1.2 Fracture Porosity 90
10.2 Simulation Model 91
10.3 Waterflooding – Single Matrix Block Model 92
10.3.1 Effect of Well Geometry 92
10.3.2 Effect of Injection Rate 93
10.4 Waterflooding – Three Matrix Block Model 94

10.4.1 Effect of Gravity 94
10.4.2 Effect of Fracture Opening 96
10.5 Surfactant flooding – Three Matrix Block Model 97
10.5.1 Effect of Surfactant Concentration – Continuous Flooding 97
10.5.2 Effect of Adsorption – Continuous Flooding 98
10.5.3 Effect of Surfactant Slug Size 100
10.6 Simulation Uncertainties 101
10.7 Complete Evaluation 102
11 Conclusion 103
12 Recommendation 105
Nomenclature 107
Bibliography 111
APPENDIX A 115
A.1 – Table of Input Parameters 115
A.2 - Fluid in Place – Regions 117
APPENDIX B 121

List of Figures

Figure 1.1 – Simplistic model of the fracture-matrix system studied. 2
Figure 2.1 – Simplistic representation of matrix, fracture and vug pore space. 4
Figure 2.2 – Imaging Method for measuring contact angle (Torsæter & Abtahi, 2003) 8
Figure 2.3 – Contact angle 8
Figure 2.4 – Interfacial Tension between oil and water at molecular level 9
Figure 2.5 – Simplistic overview of the wettability states (Abdallah et al., 2007). 12
Figure 3.1 – Wetting of spheres showing the radii of curvature. Modified figure from Green and Willhite (1998). 14
Figure 3.2 – Capillary Tubes 15
Figure 3.3 – Restored capillary pressure technique using a porous membrane 16
Figure 3.4 –Composite capillary pressure curve including the role of gravity force 17
Figure 4.1 – Linear horizontal flow 21
Figure 4.2 – Water saturation distribution as function of distance between injection and production well 23
Figure 4.3 – Relative permeability curve and capillary pressure curve for a typical imbibition process for a completely water-wet system 24
Figure 4.4 – Relative permeability curve and capillary pressure curve for a typical drainage process for a completely water-wet system 25
Figure 5.1 – Single fracture orientation 28
Figure 5.2 - Simplified geometrical figures (Torsæter, 2014) 29
Figure 5.3 - Idealization of a fractured reservoir. Actual reservoir (left) and idealized reservoir model 30
Figure 6.1 - Matrix-Fracture fluid exchange during flow between wells 31
Figure 7.1 – Schematic structure of a surfactant molecule 35
Figure 7.2 – Formation of micelles in a hydrocarbon solvent 37
Figure 7.3 – Comparison of micelle and microemulsions. (Tadros, 2006) 38
Figure 7.4 –Correlation between residual oil saturation and capillary number 39
Figure 7.5 – Schematic model of suggested wettability alteration mechanism by cationic surfactant flooding 41

Figure 7.6 – Schematic model of suggested wettability alteration mechanism by anionic surfactant flooding and bilayer formation 42
Figure 8.1 – Single matrix block surrounded by fractures on all surfaces @T = 0 days. 44
Figure 8.2 – Three matrix blocks surrounded by fractures on all surfaces @T = 0 days. 44
Figure 8.3 – Well location and design 46
Figure 8.4 – Capillary pressure curve in matrix block during immiscible fluid displacement 48
Figure 8.5 – Relative permeability curves for matrix (dashed lines) and fracture. 49
Figure 8.6 – Oil formation volume factor. 50
Figure 8.7 – Oil viscosity 50
Figure 8.8 – Calculation of the relative permeability 52
Figure 8.9 – Relative permeability curves for immiscible and miscible (dashed lines) fluid displacement. 52
Figure 8.10 – Capillary pressure curves for immiscible and miscible (dashed line) fluid displacement in matrix. 53
Figure 9.1 – Well placement in the single matrix block model 61
Figure 9.2 - Oil recovery efficiency for two cases of well placement (horizontal and vertical). 62
Figure 9.3 – Field oil production for two cases of well placement (horizontal and vertical). . 63
Figure 9.4 – Field watercut for two cases of well placement (horizontal and vertical). 64
Figure 9.5 – Oil recovery efficiency for three injection rate cases 65
Figure 9.6 – Field oil production rate for three injection rate cases 66
Figure 9.7 – Field watercut for three injection rate cases 67
Figure 9.8 – Oil recovery efficiency for three different fracture widths 68
Figure 9.9 – Field oil production rate for three different fracture widths 69
Figure 9.10 – Field watercut for three different fracture widths 70
Figure 9.11 – Oil recovery efficiency for two injection rate cases 71
Figure 9.12 – Field oil production rate for two injection rate cases 72
Figure 9.13 – Field watercut for two injection rate cases 73
Figure 9.14 - Oil recovery efficiency for three different surfactant concentrations (0.03, 0.003 and 0.0003 g/cm^3) compared to basecase. 74
Figure 9.15 - Oil production rate in scm^3/hr for three different surfactant concentrations (0.03, 0.003 and 0.0003 g/cm^3) compared to basecase. 75
Figure 9.16 - Field watercut for three different surfactant concentrations (0.03, 0.003 and 0.0003 g/cm^3) compared to basecase. 76

Figure 9.17 – Recovery efficiency for three cases of surfactant adsorption (0, 0.0005 and 0.005 g/g) 77
Figure 9.18 – Field oil production rate for three cases of surfactant adsorption (0, 0.0005 and 0.005 g/g) 78
Figure 9.19 – Field watercut for three cases of surfactant adsorption (0, 0.0005 and 0.005 g/g) 79
Figure 9.20 – Oil recovery efficiency for waterflooding, continuous surfactant injection and delayed surfactant injection. 80
Figure 9.21 – Oil production rate for waterflooding, continuous surfactant injection and delayed surfactant injection. 81
Figure 9.22 – Field watercut for waterflooding, continuous surfactant injection and delayed surfactant injection. 82
Figure 9.23 – Oil recovery efficiency for waterflooding, continuous surfactant injection and different slug sizes. 83
Figure 9.24 – A part of oil recovery efficiency for waterflooding, continuous surfactant injection and different slug sizes found in Figure 9.23. 84
Figure 9.25 – Oil production rate for waterflooding, continuous surfactant injection and different slug sizes. 85
Figure 9.26 – Field watercut for waterflooding, continuous surfactant injection and different slug sizes. 86
Figure 10.1 – Fracture between two matrix blocks 90
Figure 10.2 – Sideview of horizontal well and topview of vertical well. 92
Figure 10.3 – Comparison of the effect of injection rate 93
Figure 10.4 – Sideview (y, z) of fracture, showing the effect of gravity, after 14 days of waterflooding 94
Figure 10.5 – Sideview (y, z) of fracture, showing the effect of gravity, after 60 days of waterflooding 95
Figure 10.6 – Topview comparing adsorption and no adsorption case with same surfactant concentration 99
Figure 10.7 – Water injection followed by a surfactant slug and then water injection. 100

List of Tables

Table 2.1 – Wettability Preferences 9
Table 8.1 – Fracture and Matrix parameters for basecase 45
Table 8.2 – Location of production and injection well 46
Table 8.3 - Fluid properties 50
Table 9.1 – Oil recovery efficiency for waterflooding, continuous surfactant injection and slug size cases. 84
Table 9.2 – Cases for comparison 87
Table 9.3 - Fluid in place report from Eclipse for matrix and fracture 87
Table 9.4 – Comparison of oil saturation in the three block model for five different cases. 88

1 Introduction

Naturally fractured networks exist due to different tectonic activities. These huge networks spread out over huge areas with great hydrocarbon potential.

One of the biggest and oldest fields in the Norwegian continental shelf is the Greater Ekofisk Field, which has been producing since 1971. The field has had such a great production history due to its good reservoir properties with an average reservoir permeability of 200mD. The high permeability is a result of the big fracture network that covers the whole field.

One of the reasons the Greater Ekofisk Field has been producing at such an impressive rate is the result of the second stage of oil recovery, water injection. Different recovery mechanisms have played an important role in the increased reservoir recovery rate, and spontaneous imbibition is one of them.

Water that is injected in a highly fractured reservoir tends to flush straight through the fracture system, leaving parts of the matrices unswept. Decreasing the residual oil saturation in the matrix is today one of the challenges that is being faced in natural fractured reservoirs.

This thesis will take imbibition with water and surfactants in chalk into consideration. A study in reservoir simulation of a single matrix block and an expanded model with three matrix blocks surrounded by fractyre will be discussed with different surfactant conditions compared with normal waterflooding.

The main part of this thesis is the study of surfactant injection with different concentrations, adsorption functions and surfactant slug sizes on reservoir performance. Other cases including the effect of well placement, injection rate and fracture width with waterflooding has also been discussed.

Figure 1.1 shows the simulation concept of this study.

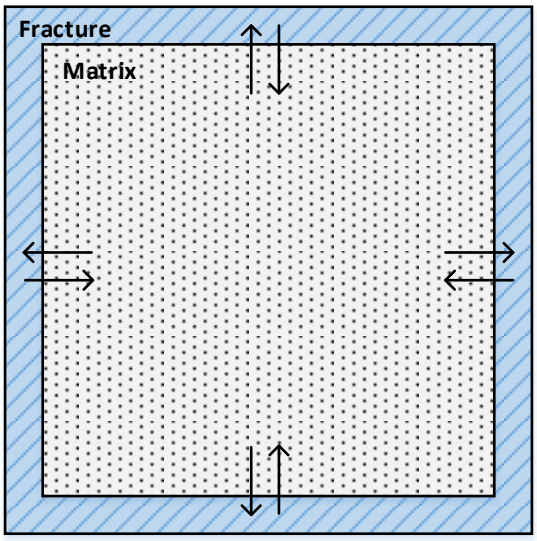

Figure 1.1 – Simplistic model of the fracture-matrix system studied.

2 Reservoir Properties

Rock and fluid properties is of great importance in the understanding of a reservoir system. These properties make the foundation of deciding whether to produce from the particular field or not, weighting it upon its feasibility.

The storage capacity of the reservoir, the interconnectivity between the pores and the saturation of hydrocarbons are the most important factors.

2.1 Porosity

Porosity is a measure of the storage capacity in a reservoir to store hydrocarbons or other fluids such as water. The ratio between the pore volume, V_p, and the total volume of the reservoir, V_b determine the porosity, φ:

$$\varphi = \frac{V_p}{V_b} \tag{2.1}$$

There are different types of porosities that have to be accounted for, such as absolute porosity, effective porosity and dual porosity.

The absolute porosity is the ratio between total volume of pores in the reservoir and the total reservoir volume:

$$\varphi_a = \frac{V_{p,tot}}{V_b} \tag{2.2}$$

The effective porosity is only taking the interconnected pores into consideration when determining the porosity, and is also the porosity factor that is used in all reservoir-engineering calculations.

2.1.1 Dual porosity

There exist two types of porosities in a fractured reservoir system, the conventional matrix porosity and the porosity of fractures and vugs. See Figure 2.1

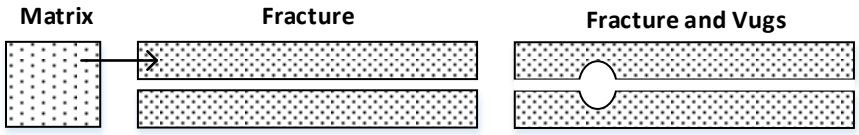

Figure 2.1 – Simplistic representation of matrix, fracture and vug pore space.

The porosity in the matrix is usually referred to as the primary porosity, while the fracture porosity is referred to as the secondary porosity. To determine the average porosity of a fractured reservoir system, it is necessary to calculate the total porosity (Van Golf-Racht, 1982).

The total porosity is determined by simply adding the two porosities.

$$\varphi_{tot} = \varphi_m + \varphi_f \tag{2.3}$$

Where:

φ_{tot} Total porosity

φ_m Matrix porosity

φ_f Fracture porosity

The two porosities can be expressed as:

$$\varphi_m = \frac{V_{p,matrix}}{V_b} \tag{2.4}$$

$$\varphi_f = \frac{V_{p,fracture}}{V_b} \tag{2.5}$$

Where:

$V_{p,m}$ Volume of matrix porosity

$V_{p,f}$ Volume of fracture porosity

2.1.2 Fracture Porosity

The fracture porosity, also referred to as secondary porosity, exists due to tectonic activities. The fractures does not have big storage capacity, but by joining the pre-existing pores enhances the permeability significantly.

2.2 Permeability

Permeability is defined as the capacity and the ability of the formation to transmit fluid between porous mediums. The rock permeability is a property that controls the directional movement and the flow rate of the fluids in the formation (Ahmed, 2010a)

The mathematical formula that describes the fluid flow in a porous media is called Darcy's law and is described in Chapter 4.2.

2.2.1 Dual permeability

In a fractured reservoir system, there are two systems present with different permeability. The two systems are associated as the matrix and the fracture.

The permeability of a fracture-matrix system can be represented as the sum of the two permeabilities of matrix and fractures:

$$k_t = k_m + k_f \tag{2.6}$$

Where:

k_t	System permeability, mD
k_m	Matrix permeability, mD
k_f	Fracture network permeability, mD

2.2.2 Fracture Permeability

The fracture permeability is determined by equation (2.7):

$$k_f = \frac{e^3}{12D} \tag{2.7}$$

Where:

e	Fracture width, m
D	Average fracture width and where the fracture plane is parallel to the fluid pressure gradient.

(Nelson, 2001)

2.3 Saturation

Saturation is defined as the fraction of different fluids that are occupying the pore volume of a rock. Typical reservoir fluids that can fill up the pore space are water, oil and gas. Since the saturation is a measure of the fraction of these fluids, the mathematical relationship can be described as:

$$S_i = \frac{V_i}{V_p} \qquad ; \boldsymbol{i = o, g, w} \qquad \textbf{(2.8)}$$

Where:

S_i	Saturation of fluid i
V_i	Total volume of fluid i
V_p	Pore volume

The sum of all the fluid saturations combined is by definition 100%, which result in the expression:

$$S_o + S_g + S_w = 1.0 \qquad \textbf{(2.9)}$$

Where:

S_o	Oil saturation
S_g	Gas saturation
S_w	Water saturation

2.4 Wettability

Wettability is a reservoir property that determines the tendency of a fluid to spread on, or adhere to, a solid's surface in the presence of another immiscible fluid (Zolotukhin & Ursin, 2000). The property describes the preference of a solid to react with one of two immiscible fluids that are present in a formation more strongly than the other. One of the two phases will be attracted by the surface of the solid and be identified as the wetting phase, while the other phase is identified as the non-wetting phase (Green & Willhite, 1998).

Reservoir rocks contain different minerals and pore structures, which is of big importance regarding wettability. The pore surface of different rocks contain a wide variety of exposed minerals that have preferential affinities for water, hydrocarbons or constituents suspended and dissolved in the fluids (Donaldson & Alam, 2008).

2.4.1 Contact Angle

Measuring the contact angle between two immiscible fluids in contact with each other is related to the preferred wettability of the wetted surface.

An oil drop resting on top of a horizontal water-wet surface immersed in water will adopt a position between completely spread and a round drop resting lightly on the surface. The two extreme positions have a contact angle of 0° and 180°, respectively (Donaldson & Alam, 2008) and can be measured in the lab by different methods, such as the imaging method.

The imaging method is a basic method for measuring the contact angle, where a small drop (2-3mm^3) of water is laid on top of a smooth surface of a rock that have been pre-submerged in an oil-filled cell. See Figure 2.2. Then, by taking a picture and enlarging the image of the water drop, it is possible to calculate the contact angle in the system by using the drop dimensions. (Torsæter & Abtahi, 2003)

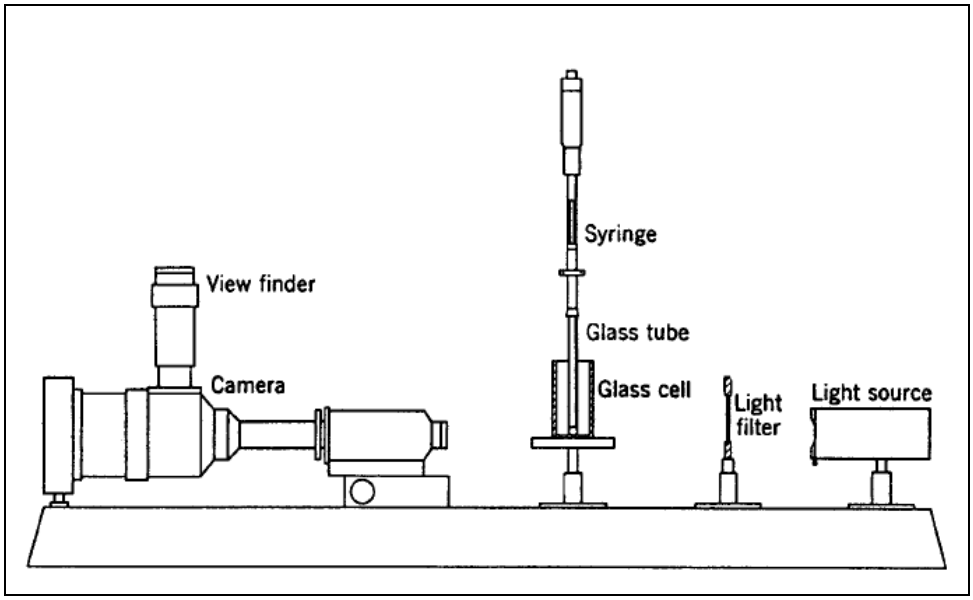

Figure 2.2 – Imaging Method for measuring contact angle (Torsæter & Abtahi, 2003)

The system consisting of two immiscible fluid, oil and water, possess three types of interfacial tensions: σ_{os}, σ_{ws} and σ_{wo}, which can describe the contact angle through the following equation:

$$\sigma_{os} = \sigma_{ws} - \sigma_{wo} \cos\theta \tag{2.10}$$

Where;

σ_{os}	Tension between oil droplet and surface
σ_{ws}	Tension between water and surface
σ_{wo}	Interfacial tension between water and oil droplet
θ	Contact angle

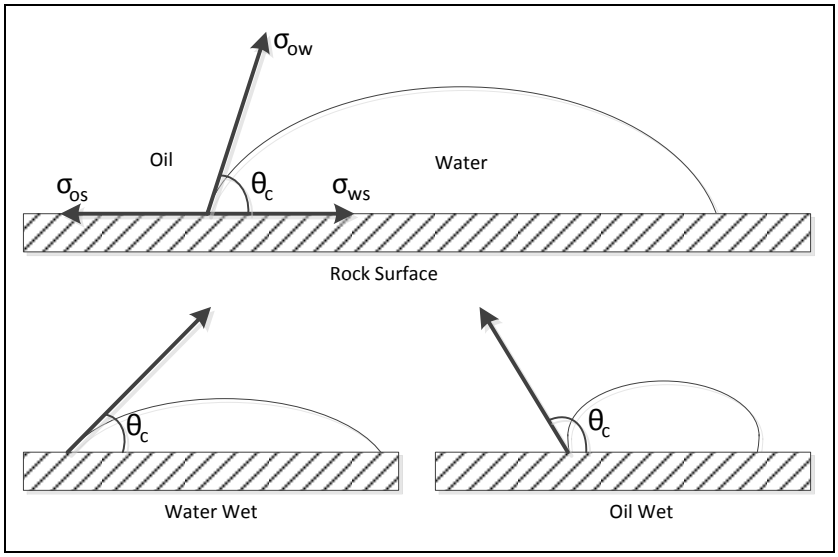

Figure 2.3 – Contact angle

From the determination of the contact angle as seen in Figure 2.3, also called wetting angle, the wettability preference of the surface can be determined as listed in Table 2.1.

Table 2.1 – Wettability Preferences

Wetting angle θ (˚)	Wettability Preference
0-30	Strongly water-wet
30-90	Preferentially water-wet
90	Neutral wet
90-150	Preferentially oil-wet
150-180	Strongly oil-wet

(Zolotukhin & Ursin, 2000)

2.4.2 Interfacial Tension

The tension between two liquids is commonly termed as interfacial tension and is measured as force per unit length. To understand this concept, a system with two immiscible fluids is considered. Looking in the molecular level, the two separate fluids are surrounded by similar molecules remote from the interface. Oil molecules surround oil molecules and water molecules likewise, making the net attractive force equal to 0, as the molecules are pulled in all directions (Dandekar, 2013).

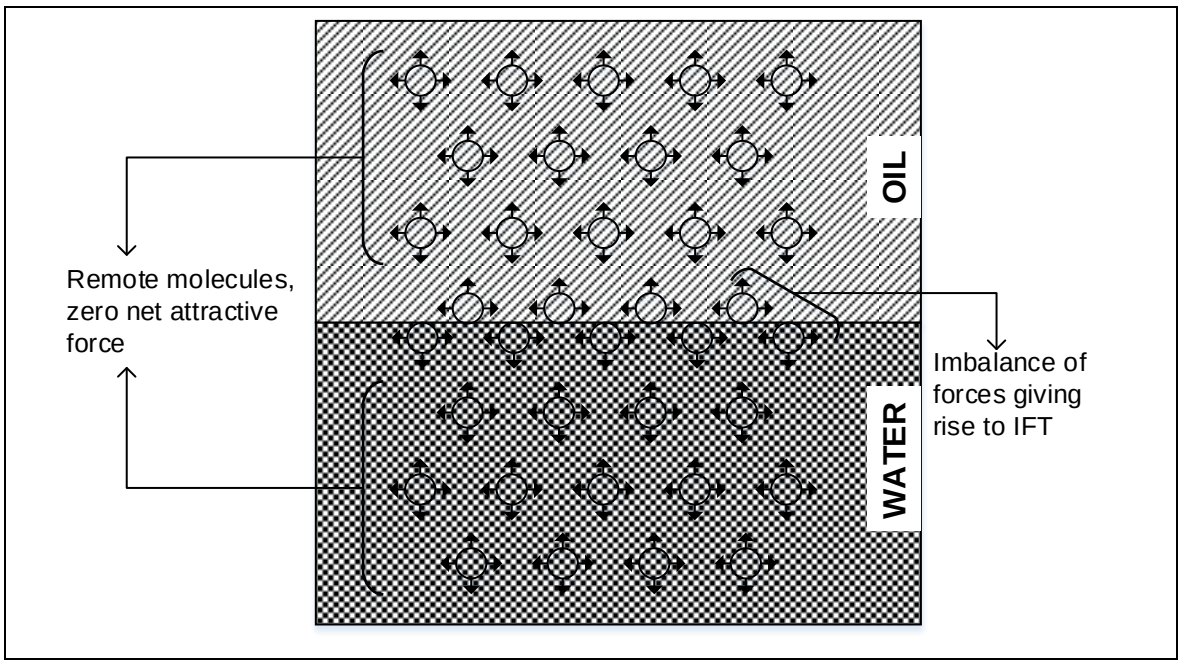

Figure 2.4 – Interfacial Tension between oil and water at molecular level. Modified model from Dandekar, 2013.

There are forces acting on the molecules between the two fluids, at the interface from the oil lying immediately above the interface and the water molecules lying below. The resulting forces are not balanced due to the magnitude of the forces above and below the interface, and by that give rise to interfacial tension (Dandekar, 2013). See Figure 2.4.

As interfacial tension is the best-known property for describing the interface between two fluids, and because it influences wettability, capillary pressure and relative permeability that affects the reservoir performance; it is an important factor to consider in a reservoir system. (Dandekar, 2013)

2.4.3 Effect of Interfacial Tension on Relative Permeability

The curvature of the relative permeability curves is dependent on the interfacial tension between the two fluid phases. Experimental studies show that the relative permeability values increase continuously as the interfacial tension decreases. Residual oil saturation also decreases with decreasing IFT, meaning that the displacement efficiency increases. (Shen, Zhu, Li, & Wu, 2010)

A correlation between the exponential indices of oil and water, n_o and n_w, respectively, and the interfacial tension exist:

$$n_o = n_o(\sigma_{wo}, \lambda_o) \quad \textbf{(2.11)}$$

$$n_w = n_w(\sigma_{wo}, \lambda_w) \quad \textbf{(2.12)}$$

Where:

- n_o Empirical exponent for oil-phase
- n_w Empirical exponent for water-phase
- σ_{wo} Interfacial tension between water and oil droplet
- λ_o Pore size distribution constant for oil relative permeability
- λ_w Pore size distribution constant for water relative permeability

(Shen et al., 2010)

IFT has a significant effect on n_w and n_o, when the tension between the two fluids are lower than 3.0mN/m. The oil and water exponential indices decrease as the IFT decreases, and result in a more straight relative permeability curve for both oil and water. (Shen et al., 2010)

The exponents and relative permeability calculations for this study are described in Chapter 8.4, trough equation (8.4) and (8.5).

2.4.4 States of Wettability

Different factors affect the rocks preferential wettability, which is why different wettability states exist:

- Reservoir rock material and geometry
- Geological mechanisms (accumulation and migration)
- Composition and amount of oil and brine
- Pressure and Temperature
- Mechanisms occurring during production, like saturations, pressure and composition

(Torsæter & Abtahi, 2003)

There exist three main states of wettability, see Figure 2.5:

2.4.4.1 Water-wet system

A water-wet system exists when more than 50% of the rock surface is wet by water. The water occupies the small pores, dead ends and is arranged in such a way that it makes a film of water on the surface of the larger pores. Oil droplets that are present can be found in larger pores or as elongated droplets that runs through several large pores. In this state, water is the continuous phase throughout the whole porous system, while the non-wetting phase, oil, is the discontinuous phase surrounded by water. (Donaldson & Alam, 2008)

2.4.4.2 Neutral-wet system

Neutral-wet systems are frequently used as a term for both fractional- and mixed-wet systems, and describe the porous system as 50% water-wet and 50% oil-wet.

Fractional-wet system

A system where the pore surface contain of different mineral that are randomly distributed throughout the rock, making the wetting preferential random with no continuous oil network through the rock is called a fractional-wet system. (Donaldson & Alam, 2008)

Mixed wet system

For a mixed wet condition to take place, the small pores in the system has to be water-wet and saturated with water, while the larger pores are oil-wet and filled with oil, in a way that it forms a continuous path through the length of the rock. (Donaldson & Alam, 2008)

2.4.4.3 Oil-wet system

An oil-wet system is the exact opposite of a water-wet system. Oil globules occupy the smaller pores without the present of water. The oil is also arranged as a thin film in contact with the pore surface in the larger pores, while the water droplets are present in the center surrounded by oil. (Donaldson & Alam, 2008)

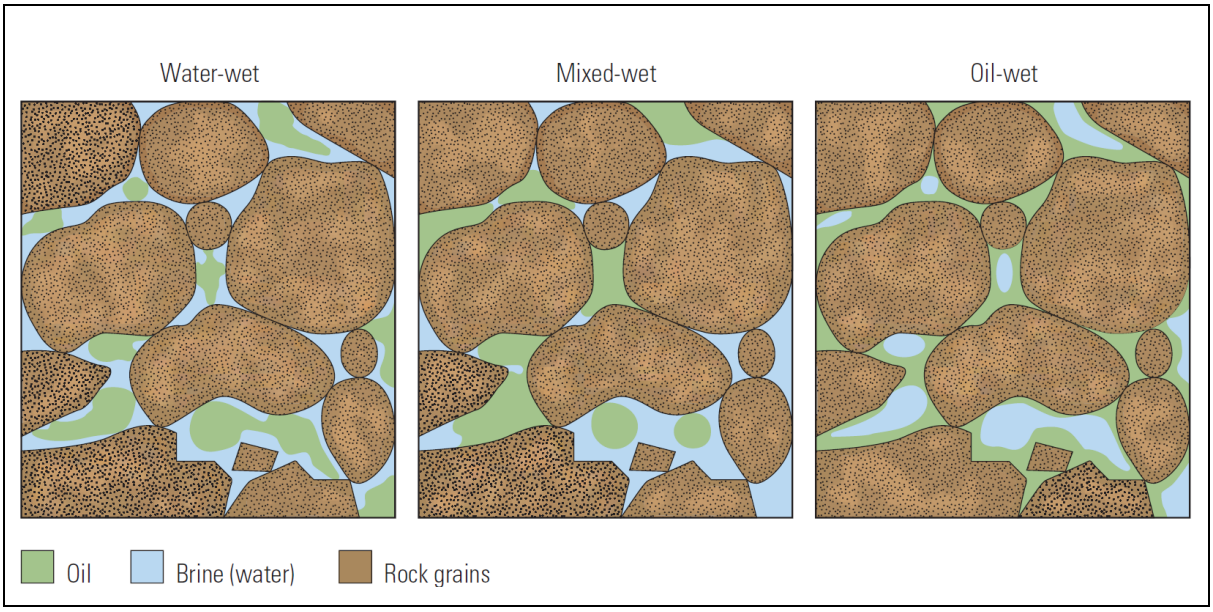

Figure 2.5 – Simplistic overview of the wettability states (Abdallah et al., 2007).

3 Displacement Forces

To understand how production of hydrocarbons from a reservoir is taking place, it is necessary to study different displacement forces together with flow in porous media. The displacement forces to consider is capillary, viscous and gravity forces.

3.1 Capillary Forces

The existence of capillary forces in a reservoir is the result of a combined effect between several factors, such as the surface and interfacial tension of the rock and the fluid, pore size and geometry, and the wetting characteristics of the system (Ahmed, 2010a)

The pressure difference between two fluids is a result of discontinuity in pressure, and is called capillary pressure. The capillary pressure is basically the pressure in the non-wetting phase minus the pressure in the wetting phase. (Fanchi, 2006a)

$$P_c = P_{non-wetting} - P_{wetting} \tag{3.1}$$

The capillary pressure may either have positive or negative values. This can be related to the capillary pressure curves for spontaneous imbibition and forced imbibition. The pressure is also a result of the curvature of the fluid interface according to the Young-Laplace equation:

$$P_c = \sigma\left(\frac{1}{r_1} + \frac{1}{r_2}\right) \tag{3.2}$$

Where:

- σ Interfacial tension between the two fluids
- r_1 and r_2 Principle radii of curvature (see Figure 3.1)

(Torsæter & Abtahi, 2003)

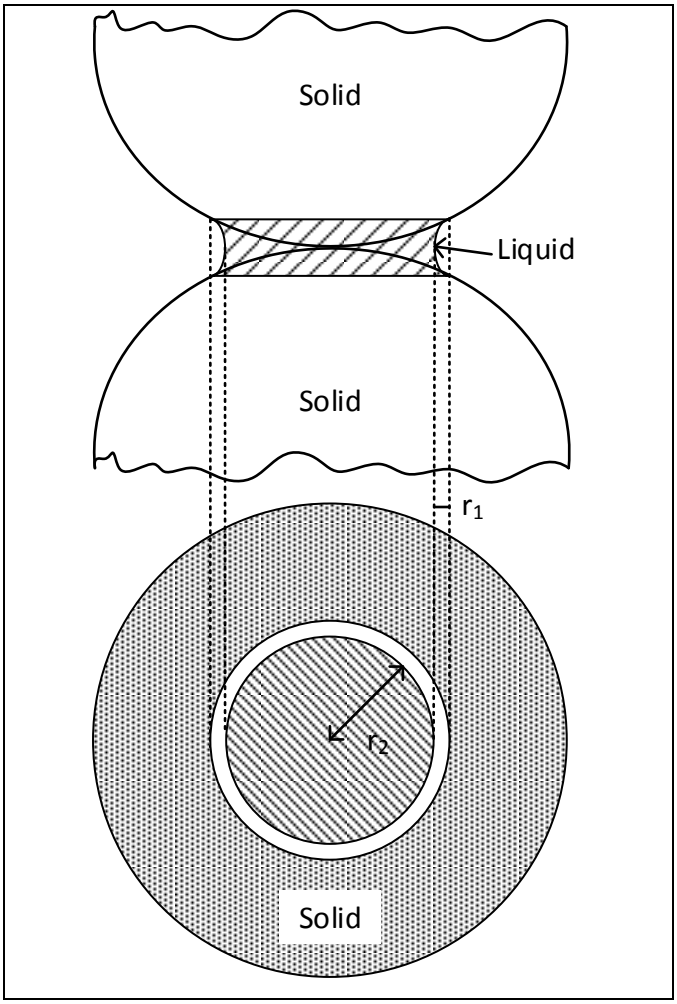

Figure 3.1 – Wetting of spheres showing the radii of curvature. Modified figure from Green and Willhite (1998).

Figure 3.1 shows the oil-bearing, uniform spherical rock particles. The values of r_1 and r_2 are related to the saturation of the wetting phase fluid within a porous medium. The capillary pressure is therefore dependent on the saturation of the fluid phase that wets the system. (Green & Willhite, 1998)

The displacement of one fluid by another in the pores in a porous medium is either aided or opposed by the surface forces of capillary pressure. (Ahmed, 2010a)

In a system with oil and water the capillary pressure can be described as:

$$P_c = \frac{2\sigma_{ow}\cos\theta}{r} \quad \textbf{(3.3)}$$

And

$$h = \frac{2\sigma_{wo}\cos\theta}{rg(\rho_w - \rho_o)} \quad \textbf{(3.4)}$$

Where:

- σ_{ow} Interfacial tension between oil and water
- θ Contact angle
- r Capillary radius
- h Capillary rise
- g Acceleration due to gravity
- ρ_w Water density
- ρ_o Oil density

(Ahmed, 2010a)

The capillary pressure phenomena that take place in the capillary tubes also exist in the porous media in a reservoir. Bundles of interconnected capillaries vary in size resembling the case in Figure 3.2 with different radii.

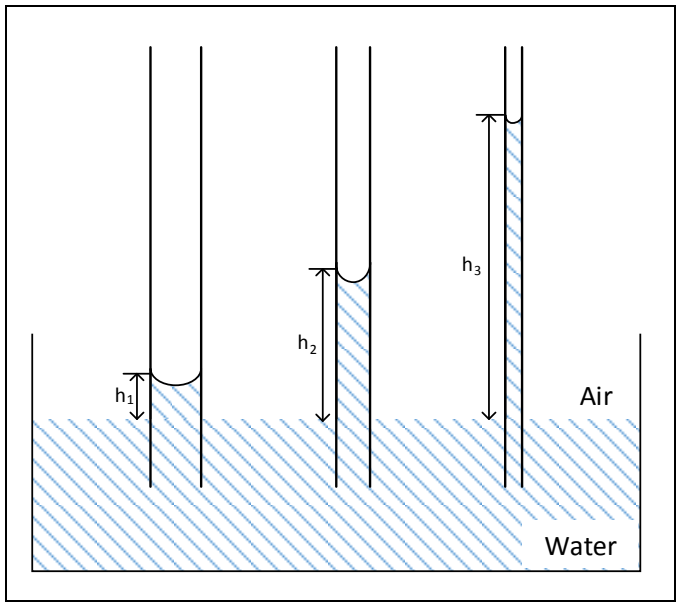

Figure 3.2 – Capillary Tubes

3.1.1 Capillary Pressure Measurements

Several methods have been developed to simulate the displacing forces in a reservoir in order to determine the magnitude of the capillary forces in a reservoir, the fluid saturation distribution and connate water saturation. Techniques such as the centrifuge method and mercury injection are among the methods used. In this study the restored capillary pressure technique will be introduced.

A core is 100% saturated with reservoir brine, and laid on top of a porous membrane, which is saturated with 100% water and permeable to that particular water only. The membrane with the core on top is placed in a chamber, where air pressure is applied. The pressure is increased until a small amount of water is displaced through the porous, semi-permeable membrane into a graduated container placed below the membrane. The pressure is then held constant until no more water is displaced. (Ahmed, 2010a)

The core is then taken out from the chamber and weighted to determine the water saturation, before repeating the procedure with increased pressure until the water saturation is reduced to a minimum. Since the pressure required to displace the wetting phase from the core is exactly equal to the capillary forces holding the remaining water within the core after equilibrium has been reached, the pressure data can be plotted as the capillary pressure data. (Ahmed, 2010a)

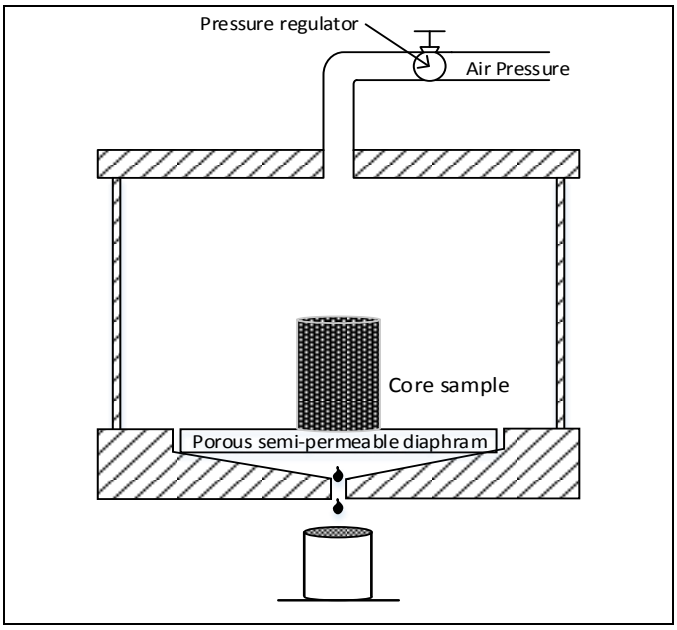

Figure 3.3 – Restored capillary pressure technique using a porous membrane. Modified figure from Ahmed (2010a).

3.2 Gravity Forces

Displacement due to gravity forces are dependent on the two key elements: pore size distribution and pore interconnectivity. The gravity force acts more in the medium to large pores, while the capillary forces displace the non-wetting phase more from the medium to small pores. Due to the contrast in pore size, some of the displaced fluid might get trapped as a result of connection of medium to large pores with small pores leading to blockage of oil in large pores. (Chilingarian, Mazzullo, & Rieke, 1996)

The gravity force, P_g vs. water saturation, S_w, curve may be considered similar to a capillary pressure curve. Negative capillary pressure is then considered as gravity force. See Figure 3.4.

$$P_G = -P_C \tag{3.5}$$

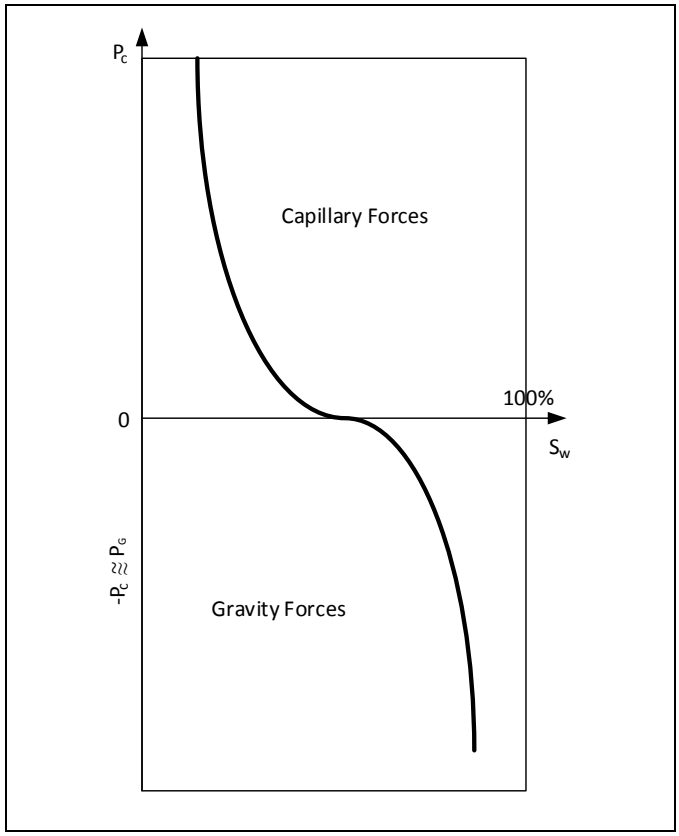

Figure 3.4 –Composite capillary pressure curve including the role of gravity force. Modified figure from Chilingarian et al. (1996).

3.3 Viscous Forces

The viscous forces that act as a displacement force in a porous medium are reflected in the magnitude of the pressure drop that occurs as a result of flow of a fluid through the medium. One approximation used to calculate the viscous force is simply to consider the porous medium as a bundle of parallel capillary tubes. With this assumption, the pressure drop for laminar flow through a single tube is given by Poiseuille's law. (Green & Willhite, 1998)

$$\Delta P = -\frac{8\mu L\bar{v}}{r^2 g_c} \tag{3.6}$$

Where:

ΔP	Pressure drop across the capillary tube, lbf/ft^2
L	Capillary tube length, ft
r	Capillary tube radius, ft
$\bar{v}$	Average velocity in the capillary tube, ft/sec
μ	Viscosity of flowing fluid, lbm/ft-sec
g_c	Conversion factor

3.3.1 Viscous Fingering

Viscous fingering occurs when a less viscous fluid is being injected into a porous system and displacing the higher viscosity fluid. The flow can influence the reservoir flow behavior and adversely impact the recovery. In details the low viscosity fluid will form fingers while moving through the fluid. (Fanchi, 2006b)

4 Fluid Flow in Porous Media

There are several factors that determine the fluid flow property in a porous media. The fluid flow in subsurface reservoirs is characterized by flow conditions, geometry, fluid state and the phases of fluid flowing through the porous media. (Satter, Iqbal, & Buchwalter, 2008)

In this study two fluid phases is being considered, oil and water. This means that it exists a wetting and a non-wetting phase that will flow separately and in distinct paths.

4.1 Fluid Flow Conditions

The flow conditions that are usually considered are the unsteady-state, steady-state and the pseudosteady-state flow, that relates to how the reservoir pressure changes in time and space during production, injection and due to boundary effects. (Satter et al., 2008)

4.1.1 Unsteady-state flow

Unsteady-state flow is encountered as soon as the production well is opened due to the rate of change in the reservoir pressure is at its greatest in the immediate vicinity of the wellbore. (Satter et al., 2008)

Since both pressure and flow rate change in the both time and location, unsteady-state flow condition can be described as:

$$\frac{\delta P(x,y)}{\delta t} = f(t) \tag{4.1}$$

Where:

P Fluid pressure at a location (x, y) in a 2D flow geometry

f(t) Function of time

(Satter et al., 2008)

4.1.2 Steady-state flow

Steady-state flow is present when pressure and rate distributions throughout the reservoir do not change with time. This occurs when the mass balance is in equilibrium, and mass flow rate into the reservoir equals the mass flow rate out of the reservoir. These conditions can be closely related to a reservoir with a strong water-drive, gas-cap drive or secondary recovery. (Slider, 1983)

The steady-state flow in a two-dimensional plane (x, y) can be characterized as follows:

$$\frac{\delta P(x,y)}{\delta t} = 0 \tag{4.2}$$

A finite fluid pressure gradient directed towards the wellbore must also exist for a well to produce. This give rise to following assumption:

$$\frac{\delta P}{\delta x} \neq 0, \qquad \frac{\delta P}{\delta y} \neq 0 \tag{4.3}$$

(Satter et al., 2008)

4.1.3 Pseudosteady-state flow

The rate at which the reservoir pressure declines due to production becomes the same everywhere within the reservoir and a constant change in pressure with time at all radii that result in parallel pressure distributions and corresponding constant rate distributions is usually referred to as pseudosteady-state condition. (Slider, 1983)

The following equation describes the flow condition:

$$\frac{\delta P(x,y)}{\delta t} = C \tag{4.4}$$

Where;

C Constant, psi/day

4.2 Darcy's Law

The fundamental law of fluid flow in porous media is described in Darcy's law. The law that was derived by Henry Darcy in 1856, states that the velocity of a homogenous fluid in a porous media is proportional to the pressure gradient and inversely proportional to the fluid viscosity. For a horizontal linear system (See Figure 4.1) the following equation is applicable:

$$v = \frac{q}{A} = -\frac{k}{\mu}\frac{dP}{dx} \tag{4.5}$$

Where:

v	Apparent velocity, cm/s
q	Volumetric flow rate, cm^3/s
A	Total cross-sectional area, cm^2
k	Permeability, D
μ	Viscosity, cP
dP/dx	Pressure gradient, atm/cm

(Ahmed, 2010a)

Darcy's law is applicable only when certain conditions exist:

- Laminar flow
- Steady-state flow
- Incompressible fluids
- Homogeneous formation.

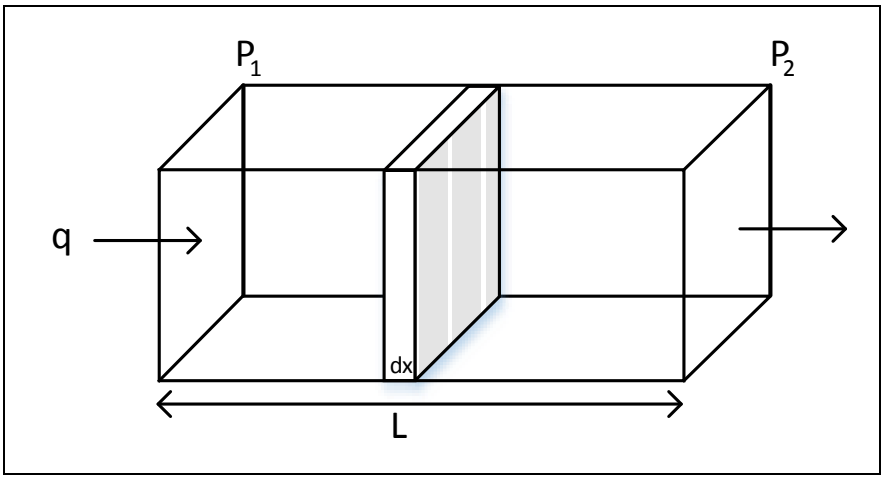

Figure 4.1 – Linear horizontal flow

4.3 Mobility Ratio

The mobility ratio is defined as the displacing fluid's mobility divided by that of the displaced fluid. (Nind, 1989)

The ratio k/μ for a particular fluid is known as the mobility, λ, of that fluid in the reservoir. The mobility ratio, M, between two fluids will then be described with the formula:

$$M = \frac{\lambda_1}{\lambda_2} = \left(\frac{k_1}{\mu_1}\right) \Big/ \left(\frac{k_2}{\mu_2}\right) \quad \textbf{(4.6)}$$

Where:

1 Displacing fluid

2 Displaced fluid

(Nind, 1989)

Considering the case where the displacing fluid is water and the displaced fluid is oil. The value of the mobility ratio tells something about the displaced fluid's velocity compared to the displacing fluid's velocity.

Intuitively, an M value equal or less than 1 would be favorable. Under an imposed pressure difference, the oil is capable of travelling with a velocity which is equal to or greater than that of the water (Dake, 1983). The water is the phase that pushes the oil and with no tendency for the oil to be by-passed and by that, result in a sharp interface between the fluids, which can be related to the term: "piston-like displacement". This can be observed in Figure 4.2 (a).

Non-ideal displacement, is unfortunately the most common in nature, and occurs when M is greater than 1. In this case, water is capable of travelling faster than the oil and, as the water pushes the oil through the reservoir, the latter will be by-passed. Water tongues will develop and lead to an unfavorable water saturation profile (Dake, 1983), as shown in Figure 4.2 (b).

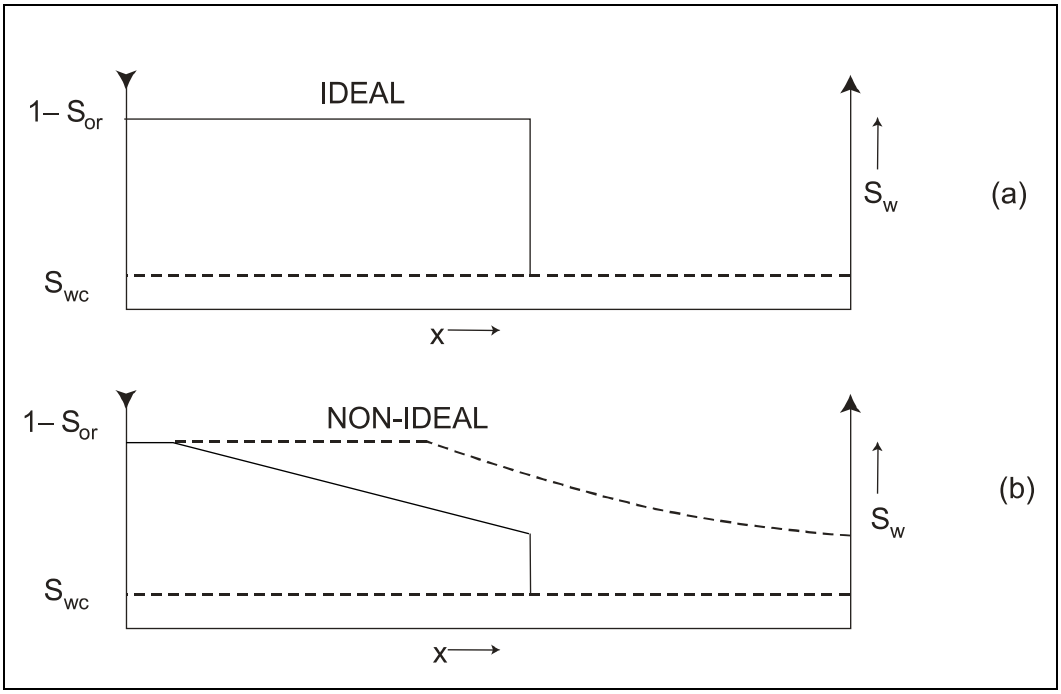

Figure 4.2 – Water saturation distribution as function of distance between injection and production well. (Dake, 1983)

4.4 Imbibition Process

The imbibition process is usually analogues to waterflooding, and is a process where the preferred wetting phase is absorbed into the porous rock.

The imbibition process can be obtained through a simple laboratory experiment by first saturating the core with water, which is the wetting phase, and then displace the water with oil until desired connate water saturation is reached. Water is then reintroduced into the core and the water will continuously increase in saturation due to spontaneous imbibition and by that produce relative permeability data.

Figure 4.3, shows the relative permeability curves for a spontaneous imbibition process. The capillary pressure curve on the right is a typical curve for a completely water-wet system. Less water-wet systems would result in negative capillary pressure values at high water saturation (Kleppe, 2014).

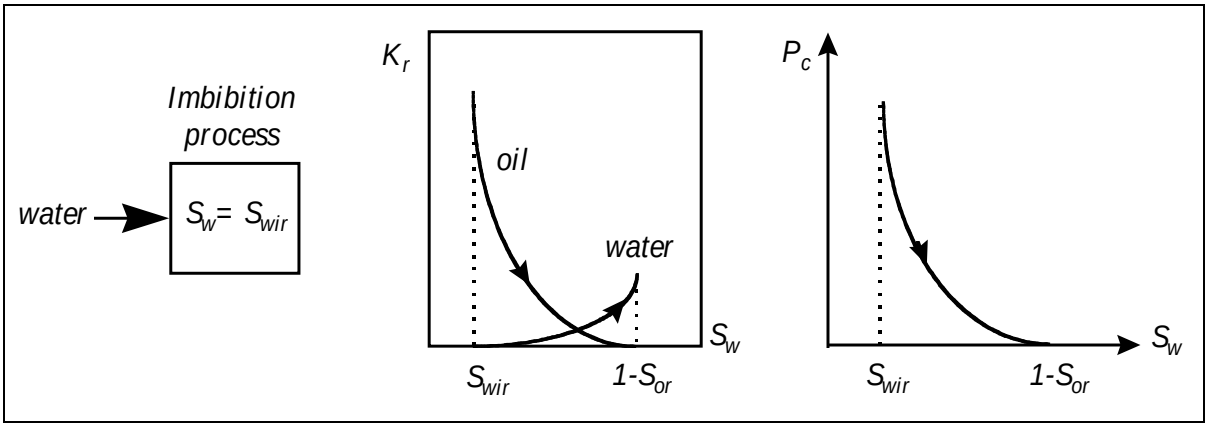

Figure 4.3 – Relative permeability curve and capillary pressure curve for a typical imbibition process for a completely water-wet system. (Kleppe, 2014)

4.4.1 Spontaneous Imbibition

During a spontaneous imbibition process no pressure is needed to drive the wetting phase into the rock. Graphically this corresponds to the positive capillary pressure values in the capillary pressure vs. water saturation graph as seen in Figure 4.3.

4.4.2 Forced Imbibition

After the wetting phase has been absorbed into the porous rock, some of the non-wetting phase fluid still remains. Applying a pressure allows the wetting phase to be pushed into the porous media and produce the remaining fluids until residual oil saturation remains.

Forced imbibition is typical in systems where the preferred wettability is closer to neutral wet, where viscous displacement forces is necessary to displace the remaining oil. The capillary pressure curve will then have a negative part.

4.5 Drainage Process

The process of increasing the non-wetting fluid phase in a system while continuously decreasing the wetting fluid phase is called drainage or depletion process.

Initially, the saturations that are present in the reservoir rocks are normally the result of a drainage process during the time of oil accumulation (Kleppe, 2014). The pore spaces of the reservoir rocks where originally filled with water, after which oil moved into the reservoir and displacing some of the water, and reducing the water to some residual saturation (Ahmed, 2010b).

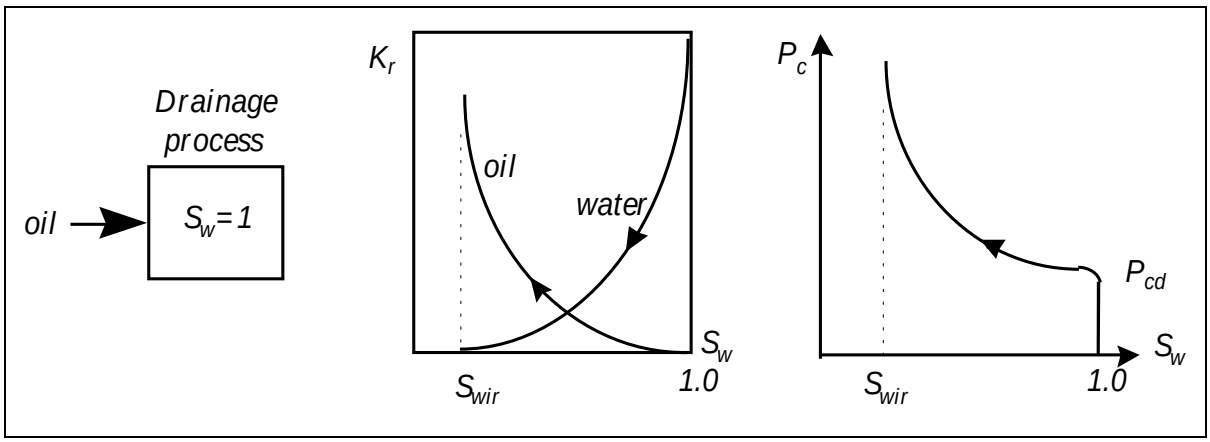

Figure 4.4 – Relative permeability curve and capillary pressure curve for a typical drainage process for a completely water-wet system. (Kleppe, 2014)

5 NFR – Description and Geometry in Carbonates

The introduction of the general aspects of a fractured system leads to a better understanding of the specific features of a naturally fractured reservoir.

The absence of the transition zone, small pressure drops around the producing well at high rates and fractured network gas cap, are few of the specific features that can be found in natural fractured carbonate reservoirs. (Chilingarian et al., 1996)

This section describes the characteristics of carbonate fracture systems and introduces the Warren and Root model for simulation studies.

5.1 Characterization of Carbonate Fractures

A fractured system in reservoir scale is usually referred to as a group of fractures. To understand the nature of these groups of fractures it is necessary to look at one single fracture and then expand it to a multi-fractured system that can refer to geometry arrangement, which further generates the matrix block. (Chilingarian et al., 1996)

5.1.1 Single Fracture

Single fracture parameters refer to intrinsic characteristics, such as fracture width and orientation, see Figure 5.1. The distance between the fracture walls, which can vary between 10-200 microns, represents these. Orientation of the fractures connects the single fracture to the environment (Chilingarian et al., 1996).

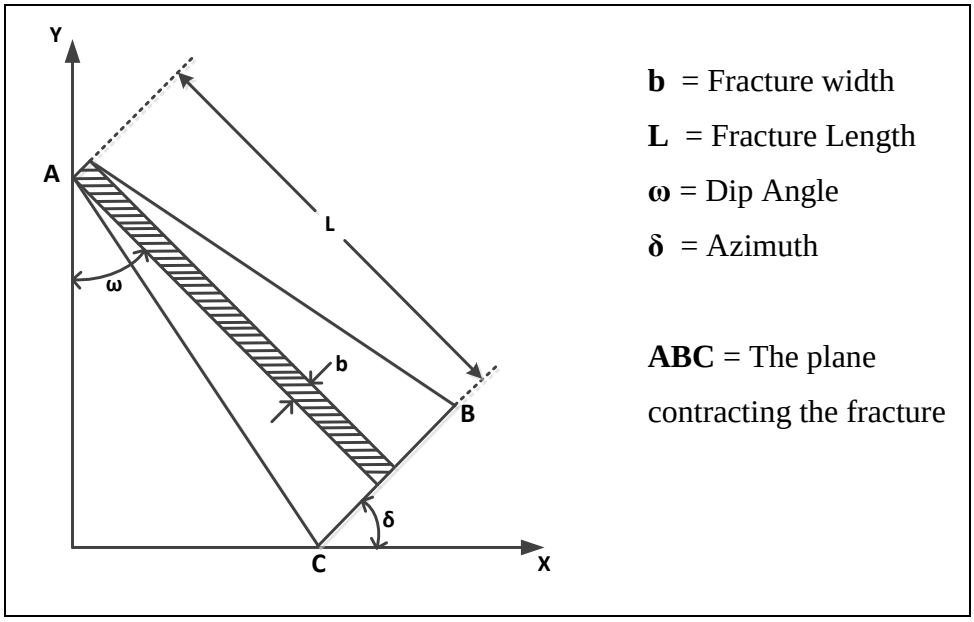

Figure 5.1 – Single fracture orientation. Modified figure from Chilingarian et al. (1996).

5.1.2 Group of Fractures

A group of fractures, referred to as a fracture network, contain two or more fracture systems that have been generated by different stress. (Chilingarian et al., 1996)

The fracture density expresses the frequency of fractures along a given direction and the extension of several orthogonal fractures. Single matrix blocks of different sizes and shapes are the result of the intersection of several orthogonal fracture systems. (Chilingarian et al., 1996)

To give a measure of the fracture density along a direction X, the linear fracture density (LFD) is introduced.

$$[LFD]_X = \frac{n_f}{L_X} = \frac{Number\ of\ fracture}{Length} \quad \textbf{(5.1)}$$

Rearranging the equation above, the block length between the two fractures, L_x can be determined:

$$L_X = \frac{n_f}{[LFD]_X} \quad \textbf{(5.2)}$$

Taking this approach into consideration it is possible to generate idealized block shapes due to the various distributions of fractures in the fracture network. The blocks can be structured with different geometry, by which has been described by Reiss in 1966 (Torsæter, 2014), see Figure 5.2.

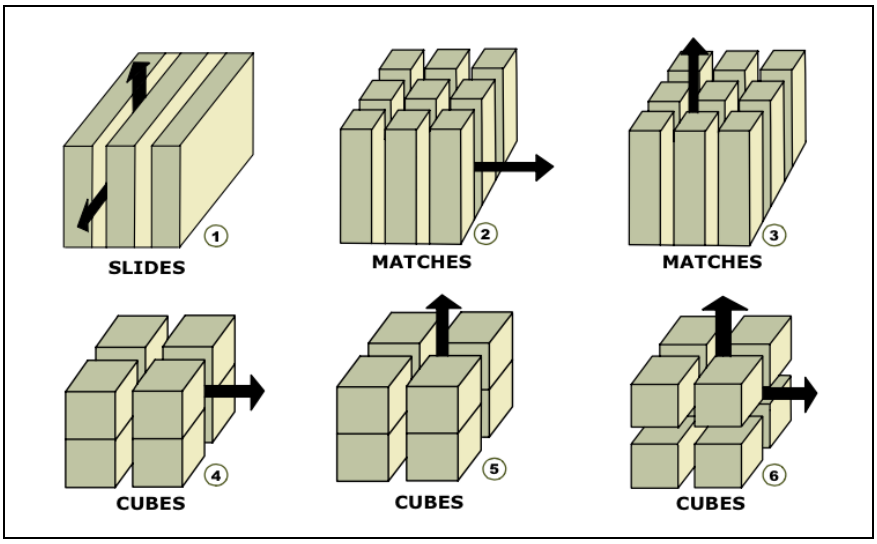

Figure 5.2 - Simplified geometrical figures (Torsæter, 2014)

In order to recognize the tectonic effects against lithology, when a single layer productive zone is small, all fractures should be referred to the single layer pay. If the pay is large and the fractures are both vertical and horizontal, the fractures in some cases can be interpreted as normal and parallel fracture to the stratification. Fracture intensity can therefore be introduced as the ratio between the vertical and the horizontal fracture density:

$$FINT = \frac{LFDV}{LFDH} = \frac{Linear\ fracture\ density\ (vertical)}{Linear\ fracture\ density\ (horizontal)} \quad \textbf{(5.3)}$$

(Chilingarian et al., 1996)

5.2 Warren-Root model

In 1962, Warren and Root proposed a model that describes an intermediate reservoir, which is defined as a complex of discrete volumetric elements with primary porosity that is anisotropically coupled by secondary voids (Warren & Root, 1963). See Figure 5.3.

The model is an idealized system, formed with identical rectangular parallelepipeds, separated by an orthogonal network of fractures (Van Golf-Racht, 1982).

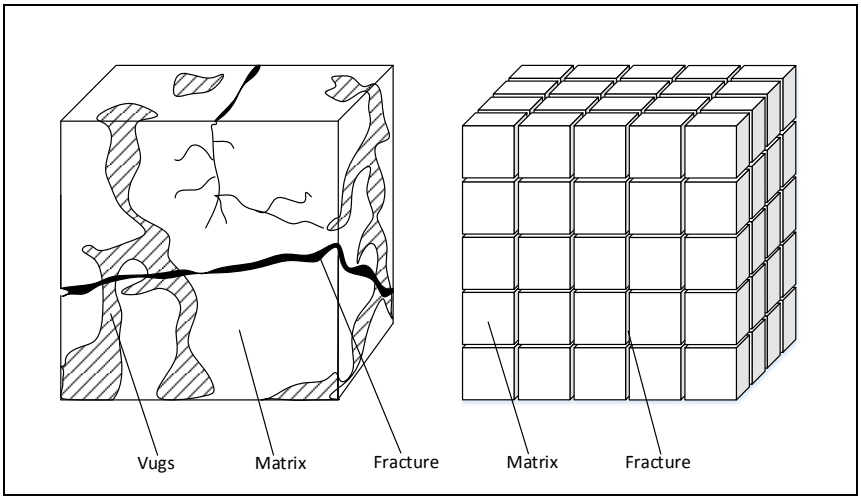

Figure 5.3 - Idealization of a fractured reservoir. Actual reservoir (left) and idealized reservoir model. Modified figure from Warren and Root (1963).

The flow towards the wellbore is considered to only take place in the fractured network, while the matrix continuously feeds the system of fractures under quasi-steady flow conditions. (Van Golf-Racht, 1982)

The Warren-Root model is based on a few general assumptions:

1) The material that contains the primary porosity is homogenous and isotropic and contained within a systematic array and identical, rectangular parallelepipeds.
2) The secondary porosities are contained within an orthogonal system of continuous, uniform fracture that is oriented so that each fracture is parallel to one of the principal axes of permeability.
3) The two porosities are homogeneous anisotropic. The fluid flow can only occur between the primary and secondary porosities, while flow between the primary porosity elements cannot occur.

(Warren & Root, 1963)

6 Fracture-Matrix Fluid Transfer

A fracture network makes the reservoir complex and studies regarding the fluid-exchange between the fracture and the matrix are of great importance. The principle is that a single matrix block is surrounded by fractures on all sides with fluid different than the fluid in the matrix. There is also no communication between the matrix blocks, which gives similarities to the Warren-Root model described in section 5.2.

Since the matrix blocks are isolated matrix units, the fluid displacement will be dependent on different characteristics, i.e. rock, fluid and fluid type saturating the matrix and fractures. The presence of these characteristics give rise to two types of displacement forces; drainage and imbibition, which is described in Chapter 4.4 and 4.5.

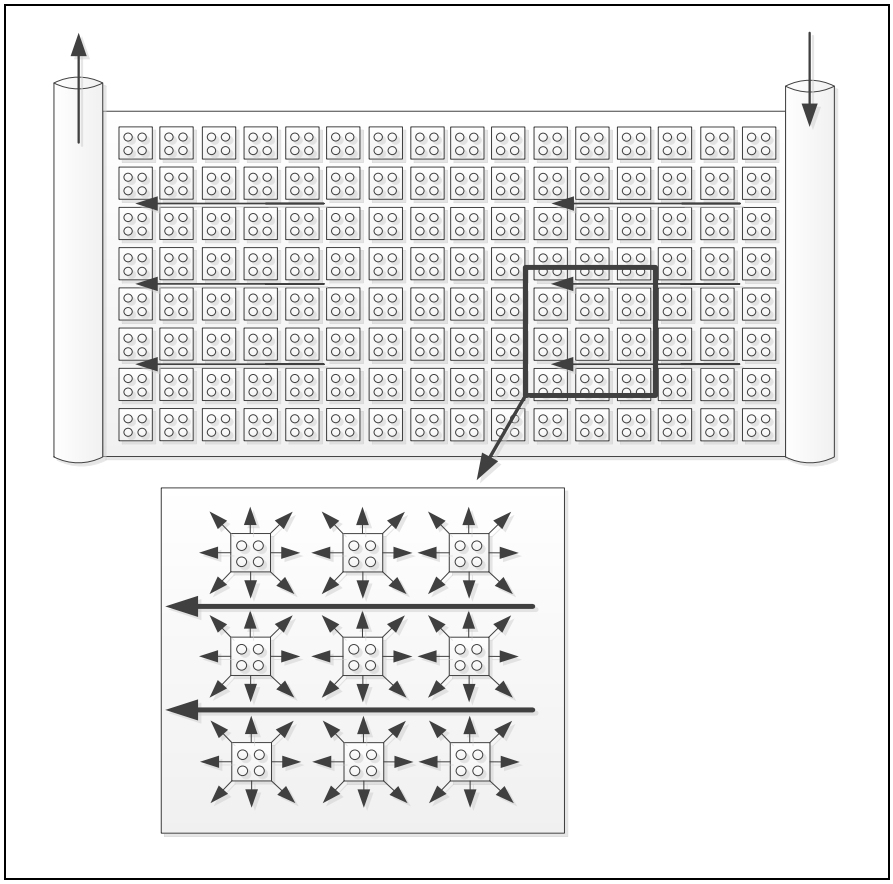

Figure 6.1 - Matrix-Fracture fluid exchange during flow between wells. Modified figure from Torsæter (2014).

Considering a single matrix block that is saturated with oil and surrounded by a different fluid, such as gas or water, it is necessary to interpret the displacement processes that can occur due to the difference in fluid property. This project will only consider water-invaded fractures.

In 1963, Warrren and Root presented a fluid transfer function between matrix and fracture, where the fractures act as conduits to the wellbore. Assuming that the fluid flow in the formation from the matrix blocks into the fracture system is under pseudosteady-state conditions, the transferability of fluid between fracture and matrix can be described through the mathematical relationship:

$$\Gamma = \sigma \left(\frac{k_m}{\mu}\right) V (p_m - p_f) \quad \textbf{(6.1)}$$

Where,

k_m Matrix permeability

σ Block-shape factor

μ Fluid viscosity

V Matrix rock volume

p_m Matrix pressure

p_f Fracture pressure

(Ahmed, 2010c)

The shape factor that has been mentioned in Section **5.1.2** is a measure of the geometry and the characteristic shape of the matrix-fissure system and is defined by the expression:

$$\sigma = \frac{A}{Vx} \quad \textbf{(6.2)}$$

Where,

A = Surface are of the matrix block

V = Volume of the matrix block

x = Characteristic length of the matrix block

(Ahmed, 2010c)

6.1 Water Invading the Fractures

In a system with only one single matrix block surrounded by fractures in all directions the water-oil contact will raise in the fractured network, either partially or fully surround the matrix block that is assumed to be fully saturated with oil. In this case the capillary forces and gravity work in favor of an upward displacement of oil, and the process is called imbibition displacement (Chilingarian et al., 1996).

7 Surfactant flooding

Post waterflooding, hydrocarbons remain in the reservoir either as capillary-trapped oil or oil that has been bypassed by the water (Fanchi, 2006b). Surfactant flooding is a tertiary recovery mechanism that aims to recover the capillary-trapped residual oil by reducing the interfacial tension between the fluid interfaces as well as the surface tension between fluid and the pore surface (Zolotukhin & Ursin, 2000).

Surfactant is by definition a blend of surface acting agents (Sheng, 2011) and are usually comprised of organic compounds that are amphiphillic, meaning they are composed of a hydrocarbon chain and a polar hydrophilic group.

7.1 Surfactant Properties

Surfactant is soluble in both organic solvents and water due to the surfactant molecule being built up by two parts, a non-polar lypophile (tail) and a polar hydrophile (head). See Figure 7.1. (Zolotukhin & Ursin, 2000)

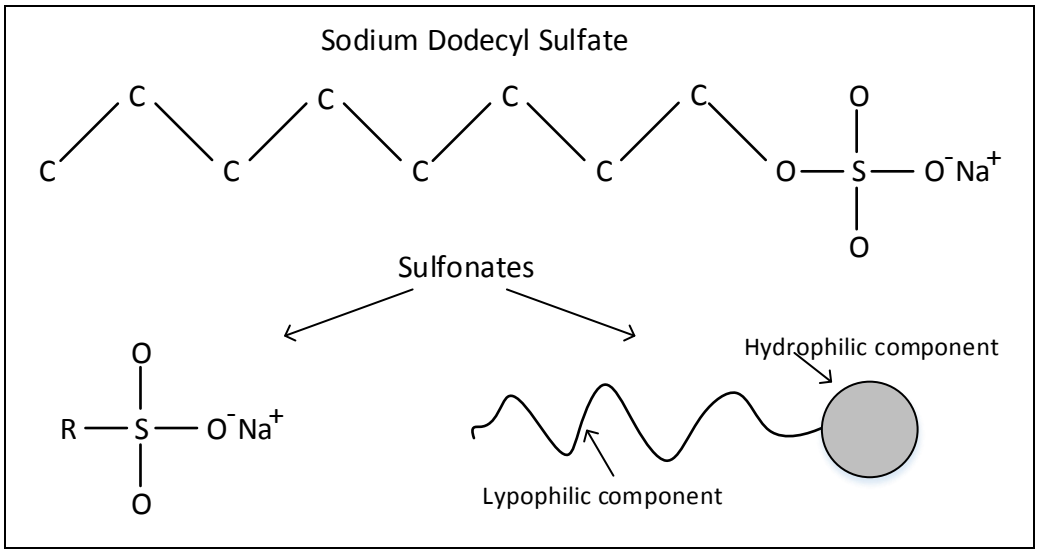

Figure 7.1 – Schematic structure of a surfactant molecule. Modified figure from Zolotukhin and Ursin (2000)

7.2 Surfactant types

Surfactants can be classified according to their polar moieties and the nature of their hydrophilic head.

7.2.1 Anionic

Anionic surfactants are most commonly used in oil recovery due to its solubility in the aqueous phase and its ability to reduce interfacial tension efficiently (Zolotukhin & Ursin, 2000). It gives rise to a negatively charged surfactant ion and a positively charged counter-ion upon dissolution in water (Lowe, Oubre, & Ward, 1999).

7.2.2 Cationic

Cationic surfactants yield a positively charged surfactant ion and a negatively charged counter-ion upon dissolution in water. This type of surfactant also tend to easily adsorb to anionic surfaces (Lowe et al., 1999), such as sandstone rocks, which is why they are not used in sandstone reservoirs. In carbonate rocks the surfactant has the ability to change the surface wettability from oil-wet to more water-wet (Sheng, 2011).

7.2.3 Nonionic

Hydrophilic head groups that do not ionize appreciably in water, characterize nonionic surfactants, and are easily blended with other types of surfactants making it applicable as cosurfactants (Lowe et al., 1999). Nonionic surfactants are more tolerant of high salinity, but its ability to reduce interfacial tension is not as good as anionic surfactant (Sheng, 2011). The head group of the surfactant molecule is larger than the tail group (Green & Willhite, 1998).

7.2.4 Zwitterionic

Zwitterionic surfactant, also called amphoteric surfactants, has two groups of opposite charge. They contain both a cationic and an anionic group (Lowe et al., 1999). These types of surfactant are tolerant to both temperature and salinity (Sheng, 2011).

7.3 Critical Micelle Concentration, CMC

One important characteristic of surfactants is the critical micelle concentration, CMC, that is defined as the concentration of surfactants where micelles are spontaneously formed. (Sheng, 2011)

When a surfactant is added to a solvent at very low concentrations, the dissolved surfactant molecules are dispersed as monomers, and as the concentration of surface-active agents increases, the molecules tend to aggregate. After a certain surfactant concentration, further addition of surfactants results in the formation of micelles (Green & Willhite, 1998).

The micelles are formed depending on the solvent. If the solvent is water, the micelles tend to form with the tail portion directed inwards and the head portion outward. The orientation of the surfactant molecules is reversed for a hydrocarbon solvent (Green & Willhite, 1998). See Figure 7.2.

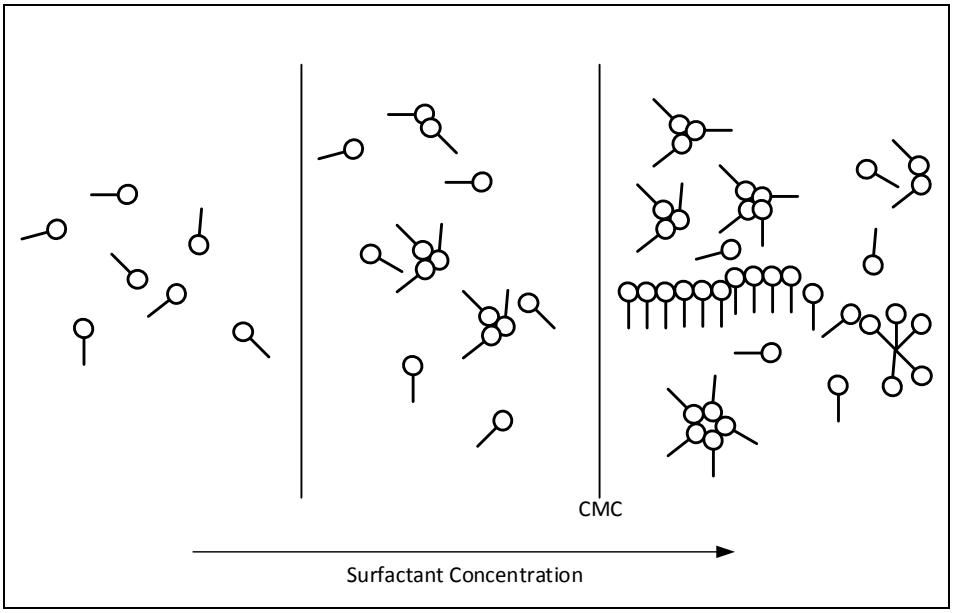

Figure 7.2 – Formation of micelles in a hydrocarbon solvent. Modified figure from Green and Willhite (1998).

7.4 Microemulsions

Microemulsions is defined as "…stable, translucent micellar solution of oil, water that may contain electrolytes, and on or more amphiphillic compounds" (Green & Willhite, 1998) and are often described as "swollen micelles" (Tadros, 2006).

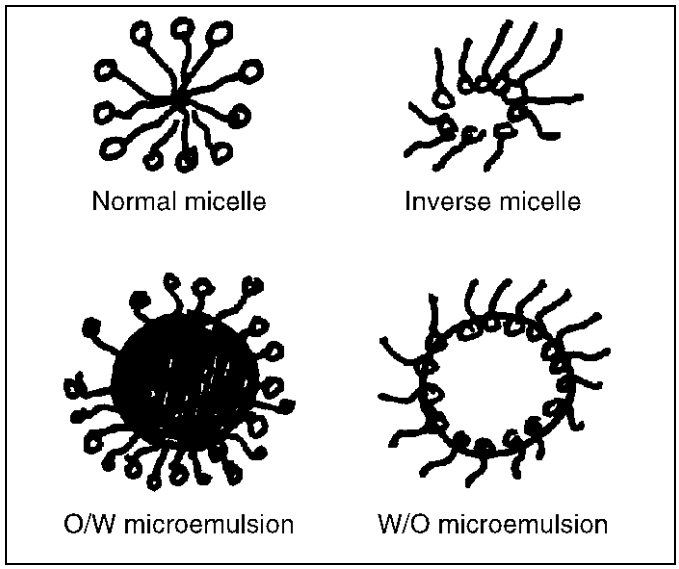

Figure 7.3 – Comparison of micelle and microemulsions. (Tadros, 2006)

The cores of spherically shaped micelles formed in aqueous solution are capable of solubilizing organics, and under the right conditions, significantly amounts of either oil or water can be solubilized into the interior of the micelle. (Green & Willhite, 1998)

7.5 Capillary Number

Surfactant flooding is used as a tertiary recovery mechanism with the main objective of reducing the residual oil saturation in the reservoir. Capillary number is a concept that is closely related to this and defined as the ratio of viscous-to-capillary force (Sheng, 2011).

$$N_C = \frac{F_v}{F_c} = \frac{v\mu}{\sigma \cos\theta} \tag{7.1}$$

Where:

F_v	Vicsous force, N
F_c	Capillary force, N
v	Darcy velocity of the displacing fluid, m/s
μ	Viscosity of the displacing fluid, mPa s
σ	Interfacial tension between displaced and displacing fluid, mN/m
θ	Contact angle

Conventional waterfloods generally operate at or close to N_c of 10^{-6}. From studies conducted by Bardon and Longeron (1980), Foster (1973) and Lefebvre du Prey (1973), it is evident that to reduce the residual oil saturation, the capillary number must be increased to at least 10^{-4}. Since v and μ cannot be varied with an order of 10^2 or more, IFT, which is amenable to being reduced by such order of magnitude, is therefore the only parameter that can be modified. (Donaldson, Chilingarian, & Yen, 1989)

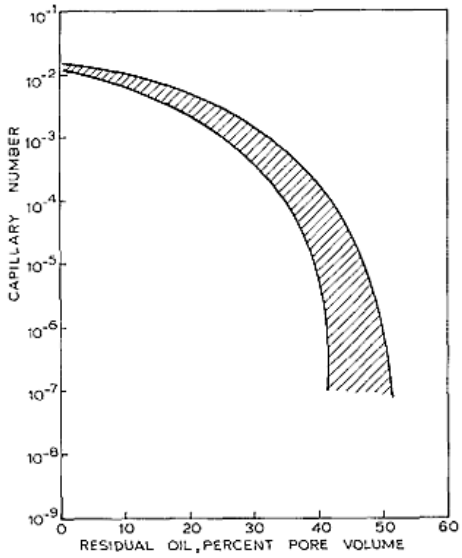

Figure 7.4 –Correlation between residual oil saturation and capillary number. (Donaldson et al., 1989)

7.6 IFT Reduction through Surfactant Flooding

Considering a two-phase system with oil and water, separated by a planar interface. The water phase is on the bottom due to its high density compared to oil. The interface has a certain thickness measured in Angstrom ($1x10^{-10}$ meters) and the system is at hydrostatic equilibrium. (Green & Willhite, 1998)

The pressure distribution through the two phases are affected by the presence of the interface, and the interface zone is considered to be inhomogeneous due to the densities and compositions within the interfacial zone vary with direction and position (Green & Willhite, 1998). When surfactants are added into the system, surfactant molecules adsorb at the interface, displacing some of the water and hydrocarbon molecules there.

The surfactant molecules will then orient themselves such that the hydrophilic part is directed into the water phase and hydrophobic part into the oil phase. This accumulation of surfactants in the interfacial zone disrupts the fluid structure in the region that leads to rapid decrease in the interfacial tension as the surfactant concentration increases until the CMC is reached. (Green & Willhite, 1998)

The rapid decrease in IFT due to increase in surfactant concentration will diminish beyond the CMC, as additional surfactant added in excess of the CMC contributes to the formation of micelles and does not increase the concentration of the water-hydrocarbon interface. (Green & Willhite, 1998)

7.7 Wettability Alteration through Surfactant Flooding in Carbonates

The wettability in an oil-wet reservoir rock can be altered through surfactant flooding to a more water-wet state that can result in higher recovery efficiency. Transitioning to a more water-wet state accelerates the spontaneous imbibition of water into the matrix blocks and thereby increasing the oil recovery during waterflooding. (Salehi, Johnson, & Liang, 2008)

Earlier studies reveal that the two main mechanisms responsible for the wettability alteration is the ion-pair formation and the adsorption of surfactant molecules through interactions with the adsorbed crude oil components that lies on the rock surface. (Salehi et al., 2008)

The effectiveness of the wettability alteration is highly dependent upon the ionic nature of the surfactant involved and the charged components in the crude oil, such as acid and base. Carbonate rocks usually carry positive charges on the surface that makes it more attracted to acidic components in crude oil. (Salehi et al., 2008)

7.7.1 Adsorption with Cationic-based Surfactant

Organic components in the crude oil that contains negatively charged carboxyl-groups, $-COO^-$ are the most strongly adsorbed components onto the chalk surface. When introducing a cationic type surfactant into the system, the negatively charged carboxylic groups form ion-pairs with the cations and be desorbed from the carbonate surface. See Figure 7.5. Once the adsorbed organic material has been released from the surface, the chalk becomes more water-wet and imbibition of water is then governed by capillary forces. (Standnes & Austad, 2000)

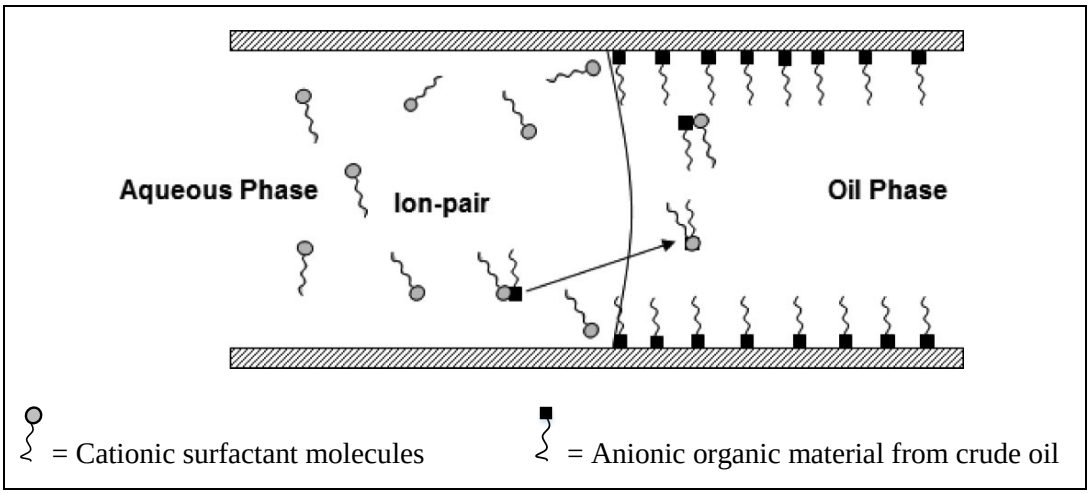

Figure 7.5 – Schematic model of suggested wettability alteration mechanism by cationic surfactant flooding. (Salehi et al., 2008)

7.7.2 Adsorption of Anionic-based Surfactants

Previous experimental studies done by Standnes and Austad (2000), have shown that anionic surfactants can also improve the spontaneous imbibition process in oil-wet chalk, but not as effective as cationic surfactants.

The anionic head groups from the surfactant and the negatively charged components from the crude oil on the rock surface leads to electrostatic repulsion forces. The suggested mechanism for wettability alteration with anionic-based surfactants is therefore the formation of a surfactant monolayer on the oil-wet rock surface. The surfactant molecules is adsorbed through hydrophobic interaction, leading the water-soluble headgroup of the surfactant oriented toward the solution, making a thin waterzone layer and create weak capillary forces during the imbibition process. (Salehi et al., 2008)

Since the hydrophobic tail from the surfactant is oriented towards the hydrophobic surface, as seen in Figure 7.6, the hydrophilic headgroup will be oriented toward the solution and change the wettability of the surface to less oil-wet. (Salehi et al., 2008)

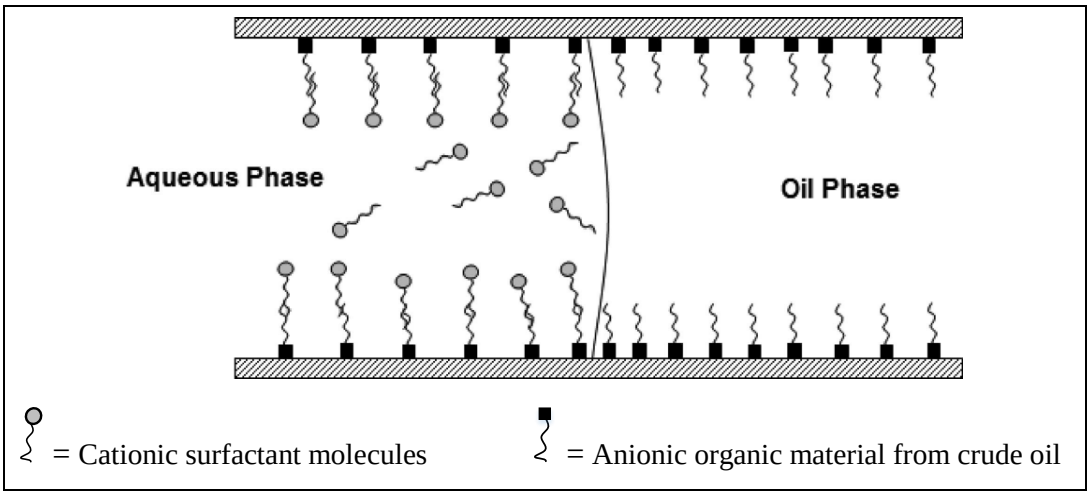

Figure 7.6 – Schematic model of suggested wettability alteration mechanism by anionic surfactant flooding and bilayer formation. (Salehi et al., 2008)

8 Numerical Simulation

A geological model is always constructed to understand the details during field development. The reservoir model is then designed, which is basically turning the geological model into a gridded discrete system, where fluid flow can be calculated.

In this section, details of a matrix block surrounded by fractures in all three dimensions will be discussed. Different displacement processes take place including imbibition, gravity force and viscous forces

8.1 Two Models Surrounded by Fractures

Two models have been designed with the same concept as having a core submersed in water with imbibition as the main driving force to produce from the low permeable matrix. Different simulations have been conducted in order to investigate and to achieve increased production performance.

8.1.1 Single Matrix Block Model

The matrix block that has been designed is $1m^3$ with 25x25x25 gridblocks. The fracture surrounding the matrix accounts for 3 cells on each surface, meaning 6 gridcells in each direction has been allocated to the fracture. The full model is 31x31x31, a total of 29791 gridblocks, whereas 15625 are the matrix and the rest, 14166, is the fracture surrounding it.

Figure 8.1 shows the single block model before production. The figure to the right shows that the model is surrounded by fractures with higher initial oil saturation than the matrix block.

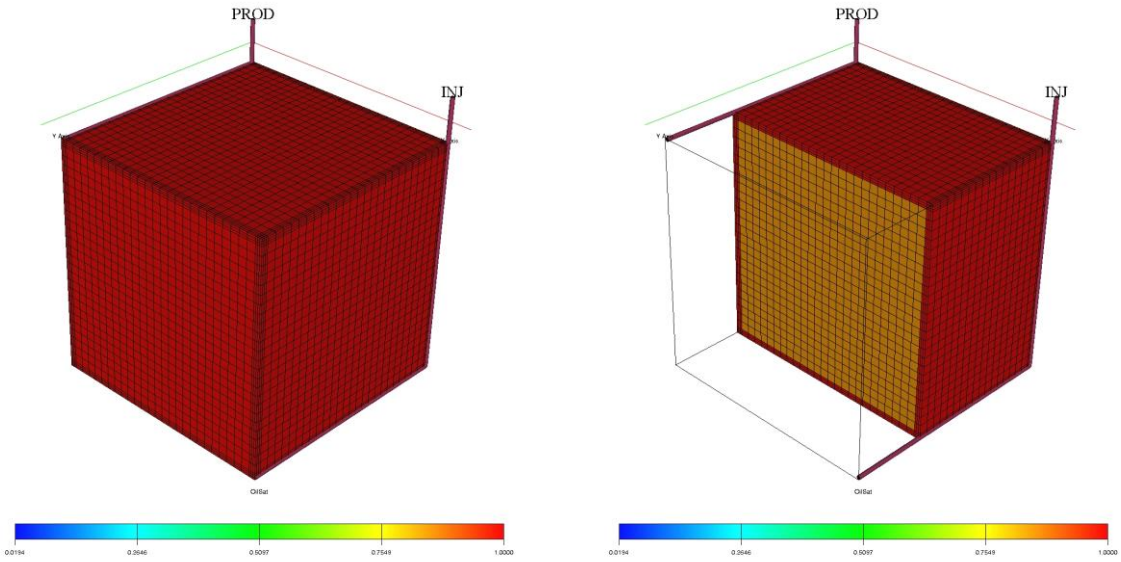

Figure 8.1 – Single matrix block surrounded by fractures on all surfaces @T = 0 days.

8.1.2 Expanded Matrix Block Model (Basecase)

The model is then expanded by two additional matrix blocks separated by fractures in Y-direction. Figure 8.2 shows the full model and a sliced model. The initial oil saturation is described in the color code and shows higher initial oil saturation in the fractures.

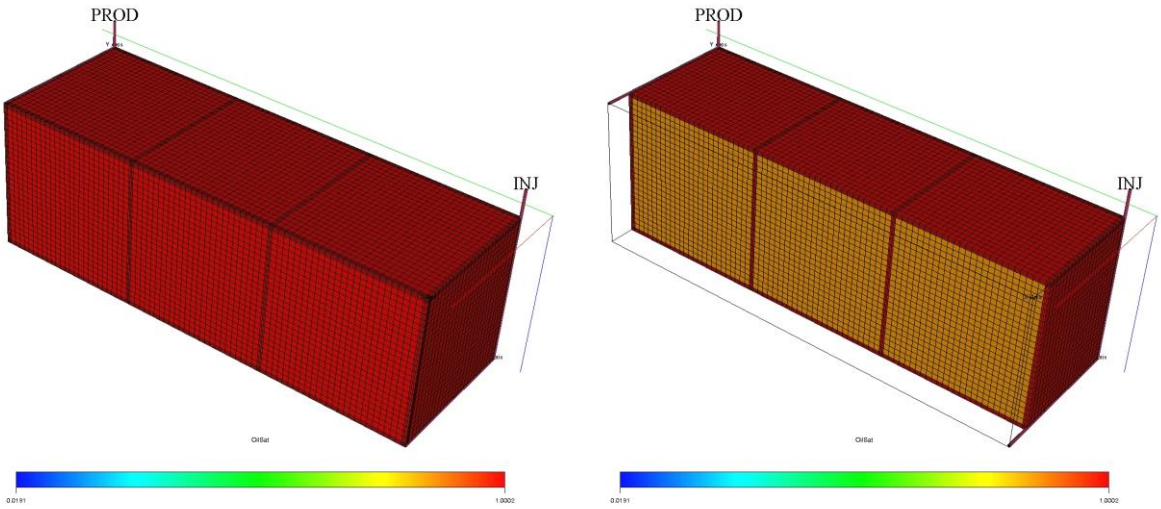

Figure 8.2 – Three matrix blocks surrounded by fractures on all surfaces @T = 0 days.

8.1.3 Basecase Parameters

Both models described in 8.1.1 and 8.1.2 has the same fracture and matrix parameters as basecase. The parameters are listed in Table 8.1.

Table 8.1 – Fracture and Matrix parameters for basecase

	Matrix	**Fracture**
Fracture width [cm]	-	0.9
Matrix dimensions [cm^3]	100 x 100 x 100	-
Permeability [mD]	1.0	5000
Porosity	0.2	0.99
Initial oil saturation	0.75	1.0
Residual oil saturation	0.15	0.02

From the fracture width and the matrix dimensions listed, it is possible to calculate the total bulk volume of both models, and by that calculate the fraction of fractures to the total model and the pore volume.

$$Fracture\ \% = \frac{V_f}{V_m} \tag{8.1}$$

$$PV = V_m \varphi_m + V_f \varphi_f \tag{8.2}$$

Model	**V_b** [m^3]	**V_m** [m^3]	**V_f** [m^3]	**PV** [m^3]	**Fracture** %
Single matrix block	1.64	1.0	0.64	0.837	64.3
Three matrix blocks	4.68	3.0	1.68	2.26	56.0

8.2 Grid Design

Both models are structured in such a way that each matrix block consist of 25 gridblocks in each direction that will correspond to 100 cm in. Each gridblock is therefore equal to 100/25 = $4cm^3$.

The single block model contain 31x31x31 gridcells, 25x25x25 are allocated to the matrix, while the 6 remaining gridcells in each direction is allocated to the fractures, 3 on each surface side. Since the fracture width is 0.9cm, each gridblock in the fracture will correspond $0.9/3 = 0.3cm^3$.

8.3 Well Design and Location

In basecase, the wells have been located horizontally in the fractures, in such a way that the flow occurs diagonally, through the fracture. Table 8.2 shows the coordinates of the wells.

Table 8.2 – Location of production and injection well

	Production Well	**Injection Well**
Single block model (x, y)	(1, 1)	(31, 1)
3 block model (x, y)	(1, 1)	(87, 1)

The production well is perforating the top layer (k=1) from I, J = (1, 1) and horizontally throughout j-direction (j=1, 2, 3… 31). While the injection well perforates at the opposite side of the model at the bottom layer (k = 31), from I, J = (31, 1) and horizontally throughout j-direction (j=1, 2, 3… 31) for the single matrix block model and I, J = (87, 1) for the expanded model. See Figure 8.3.

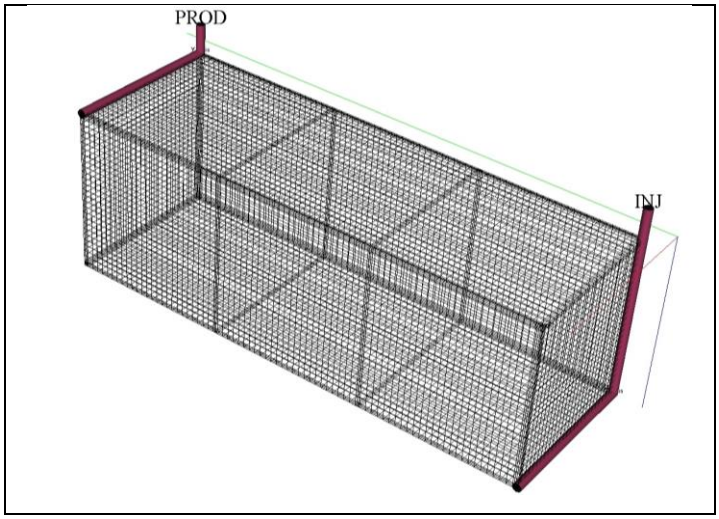

Figure 8.3 – Well location and design

8.4 Basecase - Relative Permeability and Capillary Pressure Curves

Relative permeability curves for the two regions, matrix and fracture, and the capillary pressure curve are the main parameters when deciding the displacement forces in the system as well as the residual oil saturation and initial water saturation.

The relative permeability has in this case been designed using the saturation endpoints and the corey correlation.

$$S_w^* = \frac{S_w - S_{wr}}{1 - S_{wr} - S_{or}} \tag{8.3}$$

$$k_{rw} = {S_w^*}^{n_w} \cdot k_{rw,endpoint} \tag{8.4}$$

$$k_{ro} = (1 - S_w^*)^{n_o} \cdot k_{ro,start} \tag{8.5}$$

Where;

- S_w^* Normalized water-saturation
- S_w Water saturation
- S_{wr} Residual water saturation
- S_{or} Residual Oil saturation
- k_{rw} Relative permeability for water
- k_{ro} Relative permeability for oil
- n_w Empirical exponent for water-phase
- n_o Empirical exponent for oil-phase

(Kjosavik, Ringen, & Skjaeveland, 2002)

8.4.1 Matrix

The water saturation endpoints for the matrix was set to S_{wi} = 0.75 and S_{or} = 0.15, which is the parameters in the model that tell how much of the oil in the matrix that will actually get displaced and produced.

Firstly calculate the SW* for all SW by using the saturation endpoints and secondly calculate the relative permeability for water and oil, k_{rw} and k_{ro}, using the calculated SW* and the pre-determined empirical exponents N_w and N_o.

Example calculation using equation (8.3) - (8.5):
(SW@0.40, $N_w = N_o$=2, $krw_{endpoint}$ = 0.45, kro_{start} = 0.8)

$$S_w^* = \frac{0.40 - 0.15}{1 - 0.15 - 0.25} = 0.4167$$

$$k_{rw} = 0.4167^2 \cdot 0.45 = 0.078137$$

$$k_{ro} = (1 - 0.4167)^2 \cdot 0.8 = 0.2722$$

The relative permeability curves are presented together with the fracture relative permeability curves in Figure 8.5.

Figure 8.4 shows the capillary pressure curve in the matrix block for immiscble fluid displacement.

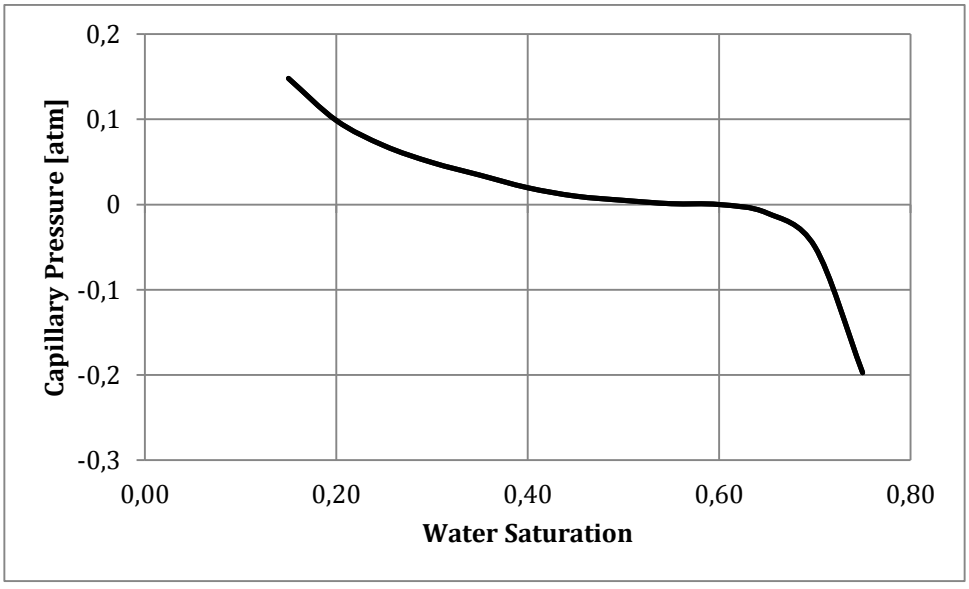

Figure 8.4 – Capillary pressure curve in matrix block during immiscible fluid displacement

8.4.2 Fracture

The fractures surrounding the matrix block have been simplified, and act as an open layer with fluid. Therefore, there is no capillary pressure that needs to be taken into consideration.

The relative permeability curves are also just designed as two straight lines, due to the fracture opening and are not supposed to have any affect in the particular region.

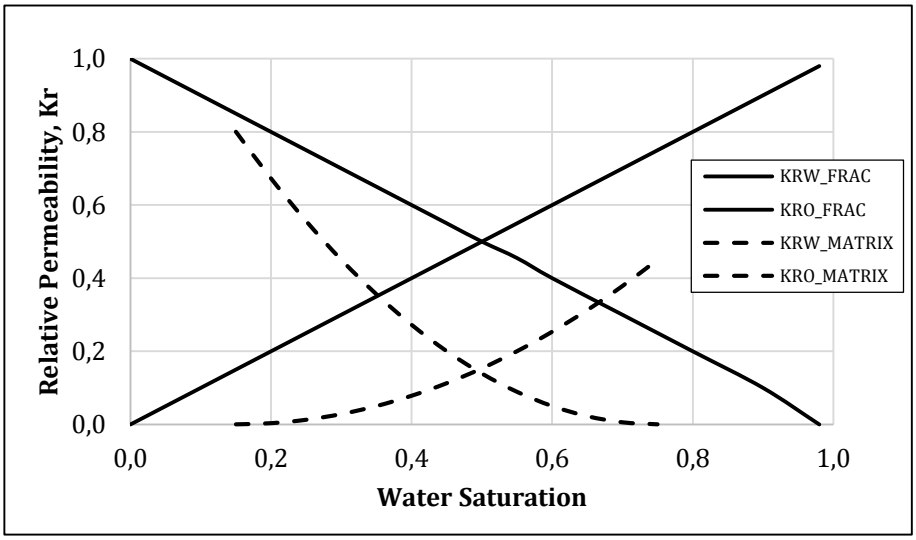

Figure 8.5 – Relative permeability curves for matrix (dashed lines) and fracture.

8.5 Other Reservoir Properties and Input Data

The following parameters have been taken from Skår (2014). Data for all figures plotted can be found in Appendix A.1 – Table of Input Parameters

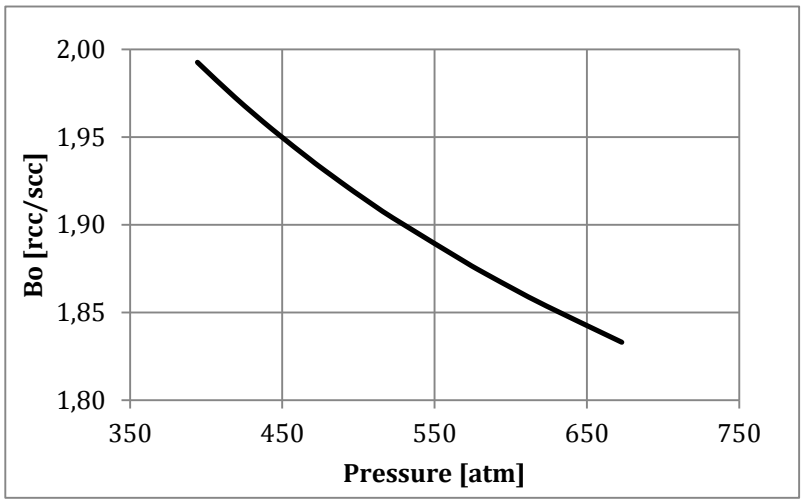

Figure 8.6 – Oil formation volume factor.

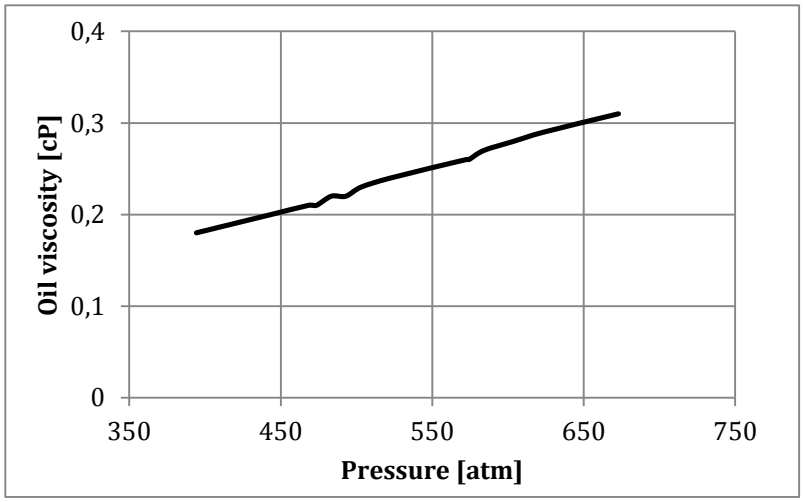

Figure 8.7 – Oil viscosity

Table 8.3 - Fluid properties

Oil density [kg/m^3]	722.2
Water density [kg/m^3]	997.35

8.6 Imbibition Process in Eclipse E100

The process of water imbibition in Eclipse is modeled by specifying different saturation table numbers for the regions that is present. In this study the two regions are the fracture and the matrix. The matrix cells typically have a water-oil capillary pressure, while the fractures usually have zero capillary pressure. (Fanchi, 2006b)

When water is introduced into the fracture that surrounds the matrix block in a water-wet system, the matrix rock has a positive water-oil capillary pressure that will make the water flow into the matrix and displace the oil.

8.7 Surfactant Model in Eclipse E100

In Eclipse E100, the distribution of surfactants is modelled by solving a conservation equation for surfactants within the water phase. The surfactant is assumed to only exist in the water phase and the concentration is calculated fully implicitly at the end of each timestep after oil, water and gas flows have been computed. (GeoQuest, 2013)

8.7.1 Relative Permeability and Capillary Pressure Curves for Miscible Fluid Displacement

When the surfactant model in Eclipse is activated the relative permeability model allows a transition from immiscible relative permeability curves at low capillary number to miscible relative permeability curves at higher capillary numbers (GeoQuest, 2013). This transition is activated by using the keyword SURFCAPD, which stands for capillary de-saturation curve.

Figure 8.8, shows in two steps how the relative permeability used at a value of miscibility function is calculated. Firstly, the endpoints for the curves are interpolated and then the miscible and immiscible curves are scaled between point A and B. The relative permeability can then be found for both curves, and the final relative permeability is taken as an interpolation between the two values.(GeoQuest, 2013)

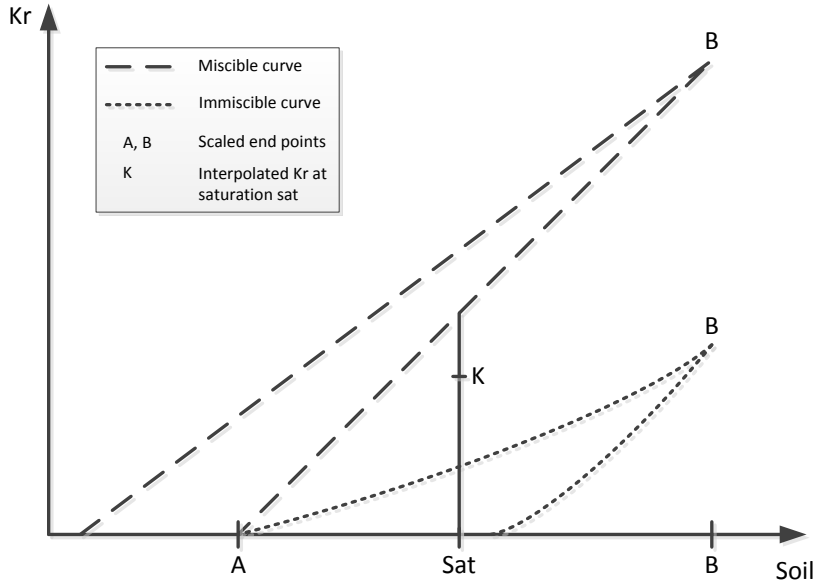

Figure 8.8 – Calculation of the relative permeability. (GeoQuest, 2013)

Figure 8.9 and Figure 8.10 show the relative permeability curves and the capillary pressure curves, respectively, for both miscible and immiscible fluid displacement that was used in the surfactant model.

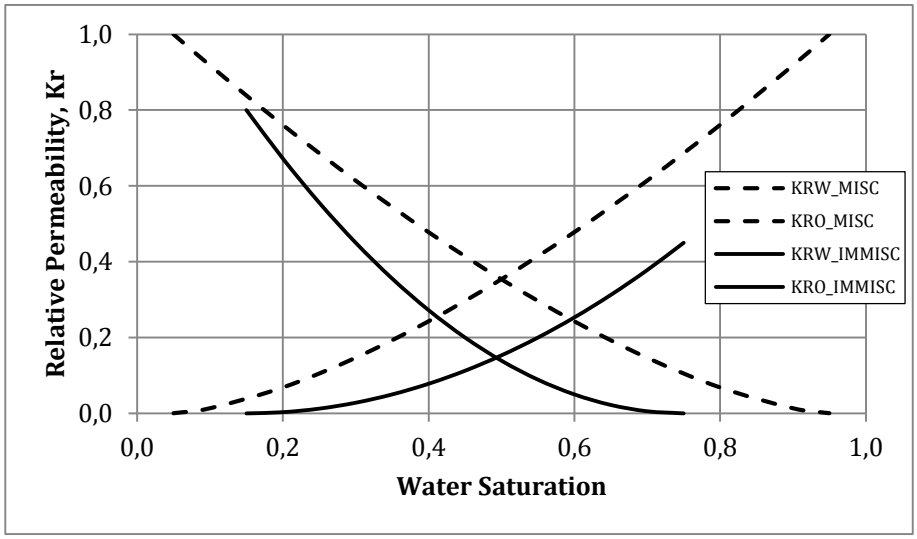

Figure 8.9 – Relative permeability curves for immiscible and miscible (dashed lines) fluid displacement.

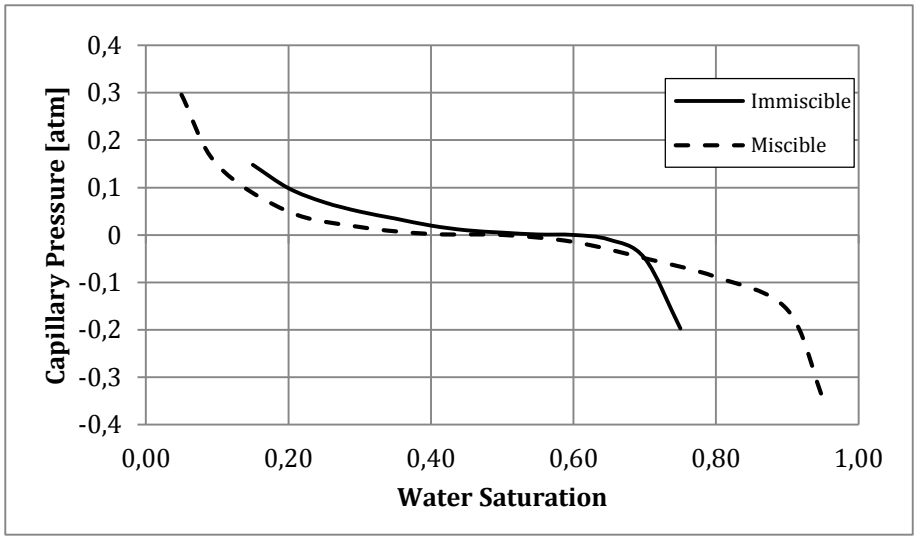

Figure 8.10 – Capillary pressure curves for immiscible and miscible (dashed line) fluid displacement in matrix.

8.7.2 Calculation of Capillary Number

The capillary number, N_c, is a dimensionless ratio between viscous forces and capillary forces, as described in Chapter 7.5. In Eclipse E100, the capillary number is calculated for each gridcell:

$$N_C = C_N \frac{|K \cdot \nabla P_p|}{\sigma} \tag{8.6}$$

Where:

C_N	Unit conversion constant, ≈1 for SI units. (Constant is dependent on the units used)
K	Permeability, mD
∇P_P	Phase potential, bar/m
σ	Interfacial tension between the displaced and displacing fluid, N/m

The oil phase potential is used together with the oil-water surface tension to determine the capillary number in the surfactant model.

$$|K \cdot \nabla P_P| = \sqrt{\left(K_x \cdot \frac{\partial P}{\partial x}\right)^2 + \left(K_y \cdot \frac{\partial P}{\partial y}\right)^2 + \left(K_z \cdot \frac{\partial P}{\partial z}\right)^2} \tag{8.7}$$

$$K_x \cdot \frac{\partial P}{\partial x} = 0.5 \left[\left(\frac{K_x}{D_x}\right)_{i-1,i} \cdot (P_i - P_{i-1}) + \left(\frac{K_x}{D_x}\right)_{i,i+1} \cdot (P_{i+1} - P_i) \right] \tag{8.8}$$

Equation (8.8) is calculated in x direction for a given cell *i*. The same procedure is applied for calculations in y and z direction. (GeoQuest, 2013)

8.7.3 Water PVT Properties

The input data for PVTW is modified when surfactant model is activated. The model calculates a water-surfactant solution viscosity through following equation:

$$\mu_{ws}(C_{surf}, P) = \mu_w(P)\frac{\mu_S(C_{surf})}{\mu_w(P_{ref})} \quad \textbf{(8.9)}$$

Where:

- μ_{ws} Viscosity of the water-surfactant mixture
- μ_w Viscosity of water
- μ_s Viscosity of surfactant
- P_{ref} Reference pressure in the PVTW keywords
- C_{surf} Surfactant concentration

(GeoQuest, 2013)

Equation (8.9) shows that the viscosity of the mixture differs from the pure water viscosity, but for low surfactant concentrations, the mixture viscosity is assumed to be similar to pure water viscosity (Kalnæs, 2009).

8.7.4 Adsorption

The adsorption of surfactant is assumed to happen instantaneously. The amount of adsorbed surfactants is a function of the surrounding surfactant concentration, which can be activated through the SURFAD keyword. The mass of adsorbed surfactant on the rock is given by:

$$Mass\ of\ adsorbed\ surfactant = PV\ \frac{1-\phi}{\phi} \cdot MD \cdot CA(C_{surf}) \quad \textbf{(8.10)}$$

Where:

- PV Pore volume in the cell
- φ Porosity
- MD Mass density of rock
- CA(C_{surf}) Adsorption isotherm as a function of local surfactant concentration in solution

(GeoQuest, 2013)

8.7.5 Keywords to Activate the Surfactant Model

Several keywords need to be specified to activate the surfactant model in Eclipse E100. A list of the required keywords in the different sections is listed together with input data for the given keyword.

RUNSPEC

SURFACT: Initializes and indicates that the surfactant model is used in the run.

PROPS

SURFST: Surface tension between oil and water is given as a function of surfactant concentration.

SURFST

-- Csurf	Water viscosity
-- (g/cm^3)	(cP)
0	5
0.001	0.5
0.005	1.0E-8
0.01	1.0E-9
0.3	1.0E-9
1	1.0E-9/

SURFVISC: Describes the effect on the surfactant viscosity when the concentration of surfactants in the water changes.

SURFVISC

-- Csurf	Solution water viscosity
-- (g/cm^3)	(cP)
0	0.61
0.03	0.8
1.00	1.0/

SURFCAPD: The surfactant capillary de-saturation function describes the transition between immiscible conditions and miscibility as a function of dimensionless capillary number. The first column is defined as the 10-logarithm of the capillary number, while the second column defines which relative permeability curves to be used (0 for immiscible and 1 for miscible).

As explained in chapter 7.5, the capillary number has to be increased to 10^{-4} before a reduction in residual oil saturation due to interfacial tension alteration can occur. This means that first column must have a value of -4 before activating the relative permeability curve for miscible condition.

```
SURFCAPD
-- Log10 Nc    Misc function
        -10     0.0
        -5      0.0
        -4      1.0
        -3      1.0
        10      1.0/
        /
        /
```

SURFADS: This keyword describes the surfactant adsorption onto the rock surface. The local surfactant concentration in the solution surrounding the rock is defined in the first column. The second column defines the saturated concentration of surfactant adsorbed by the rock formation.

In this study, the adsorption is assumed to be 0 for all surfactant concentrations, but sensitivity on adsorption has been conducted.

```
SURFADS
-- Csurf        Adsorp
-- (g/cm3)      (g/g)
0.0             0
0.001           0.000
0.03            0.000
1.00            0.000/
/
/
```

SURFROCK: Specifies the rock properties required for the surfactant model. The first column defines the adsorption index (1 for retracted surfactant whenever local surfactant concentration in the solution is decreased, 2 for no desorption). The second column defines the mass density of the rock and is used to calculate the surfactant loss due to adsorption.

It is assumed that no desorption will occur in this study. Index 2 is therefore used for all rock densities.

```
SURFROCK
-- Index        Density
-- 1/2          (g/rcc)
      2         0.253/
      2         0.253/
      2         0.253/
```

SCHEDULE

WSURFACT: Specifies the concentration of surfactant in the injection stream of the chosen well. It is required that the well is already declared to be a water injection well.

```
WSURFACT
.. Wellname    Surfactant concentration
..             (g/scc)
'INJ'          0.003/
/
```

9 Results

Different waterflooding and surfactant flooding scenarios has been conducted on the two models described in Chapter 8.1. Effect of different parameters such as injection rate, well location and geometry has been studied on the single matrix block. Surfactants is only introduced in the expanded model.

All cases were simulated for 2 years to investigate the production performance. The reservoir properties and well placement for the cases were introduced in Chapter 8.

9.1 Waterflooding – Single Matrix Block

A single matrix block was designed initially to study the effect of different displacement forces as well as studying the well geometry, to look at the most stable and preferable well geometry.

9.1.1 Effect of Well Location and Geometry

Two well cases have been studied, one vertical and one horizontal well. See Figure 9.1.

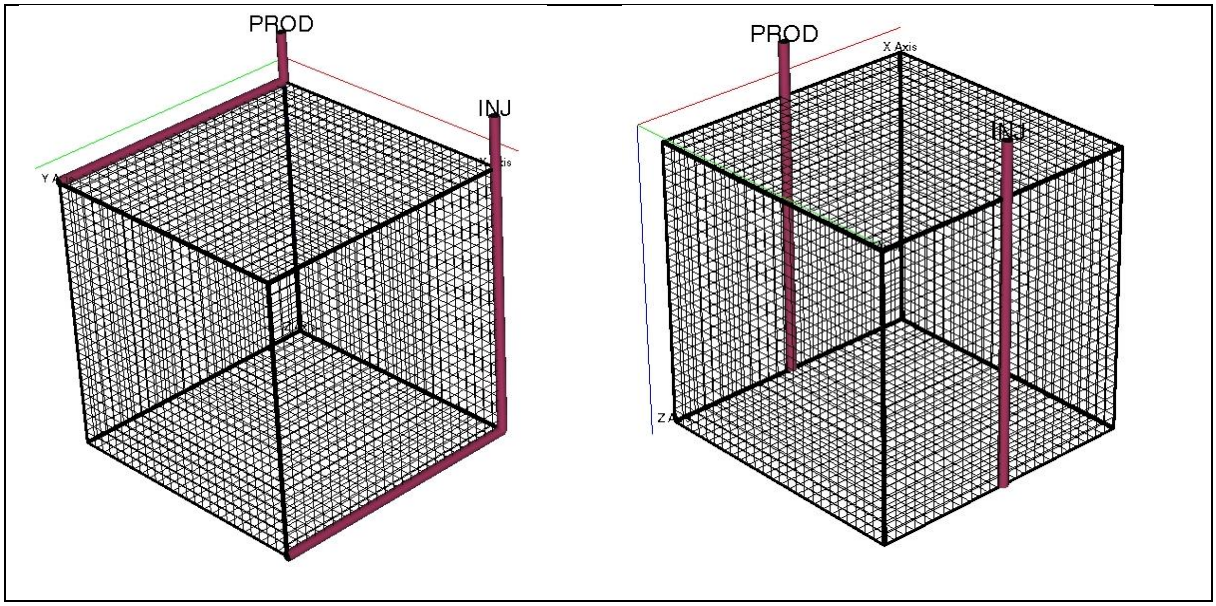

Figure 9.1 – Well placement in the single matrix block model. Both wells are located in the fracture in both cases.

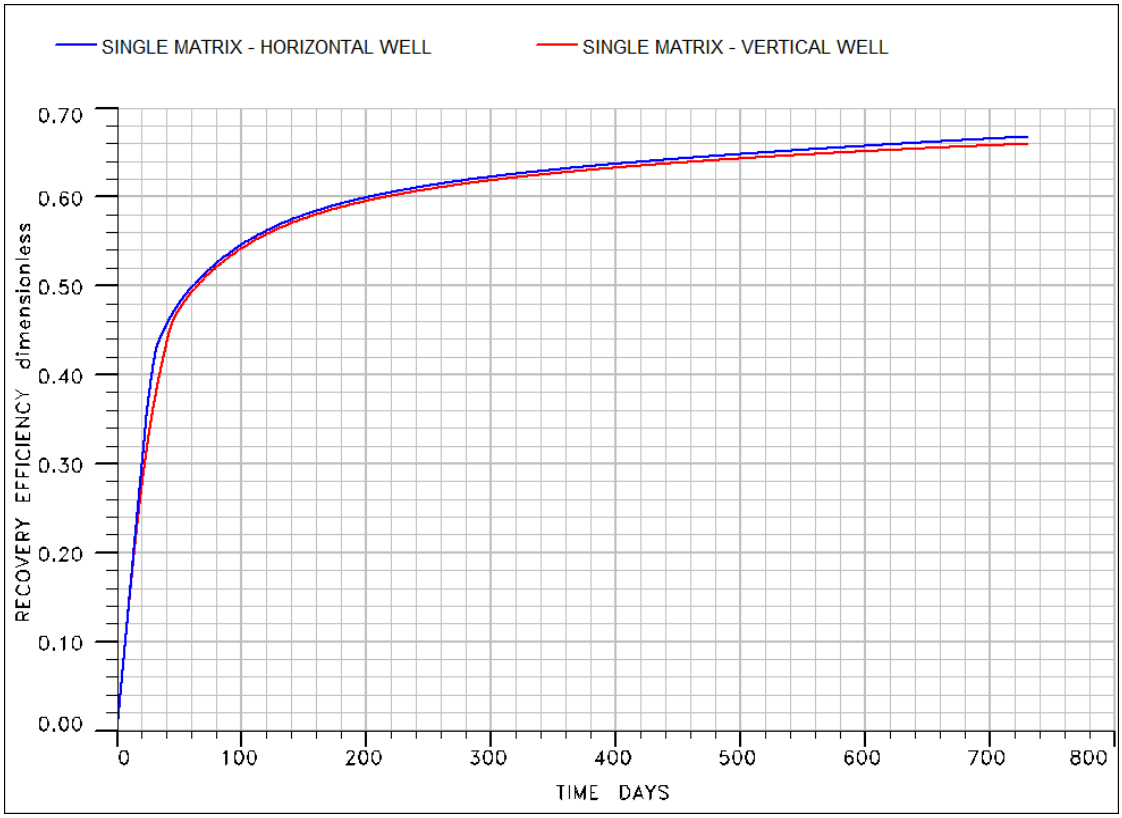

Figure 9.2 - Oil recovery efficiency for two cases of well placement (horizontal and vertical).

Figure 9.2 shows that the case with horizontal well, yield a higher recovery factor than the case with vertical well. Both recovery curves follow the same trend. As observed, the vertical well curve deviates away from the horizontal well curve after around 300 days of simulation, resulting in a lower recovery for the vertical well.

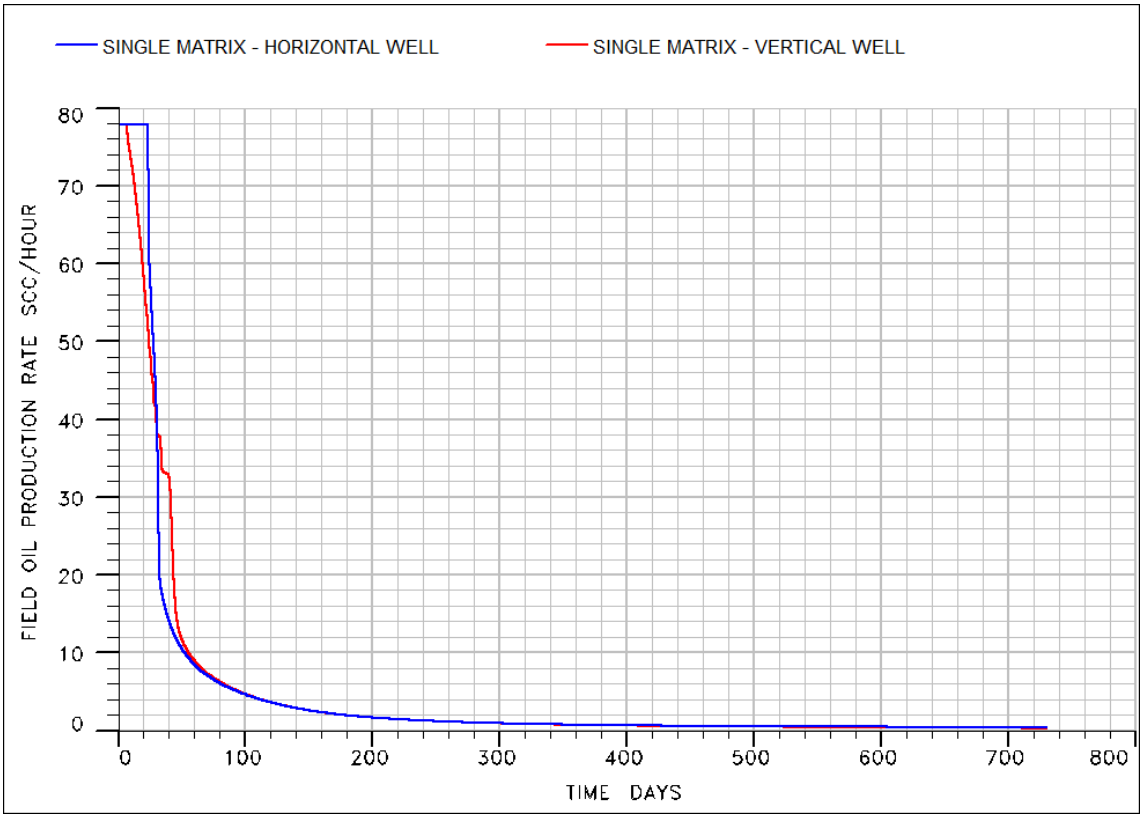

Figure 9.3 – Field oil production for two cases of well placement (horizontal and vertical).

The field oil production rate is plotted in Figure 9.3. It can be observed that for the vertical well the production starts declining after 5 days compared to the horizontal well, where a constant production rate is held for 22 days, before declining.

The production rate gets a small bump after 34 days, for the vertical well, while the horizontal well declines with a smooth inversely proportional rate.

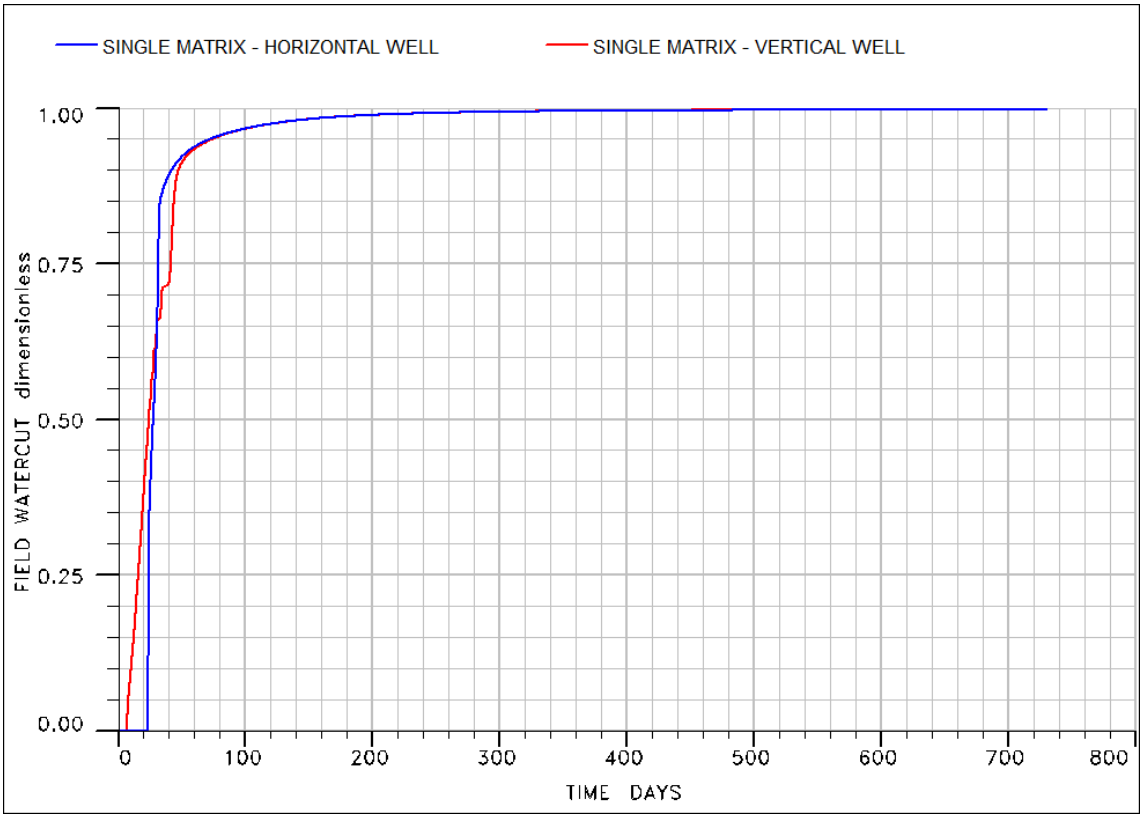

Figure 9.4 – Field watercut for two cases of well placement (horizontal and vertical).

The watercut for the two cases is plotted in Figure 9.16. The plot indicate that the water breakthrough for the vertical well occurs after 5 days, while it takes 22 days for the injected water to reach the production well in the horizontal well case.

The vertical well case increases in watercut at a lower rate than the horizontal well case between 5 and 34 days, before the two curves intersects.

9.1.2 Effect of Injection Rate

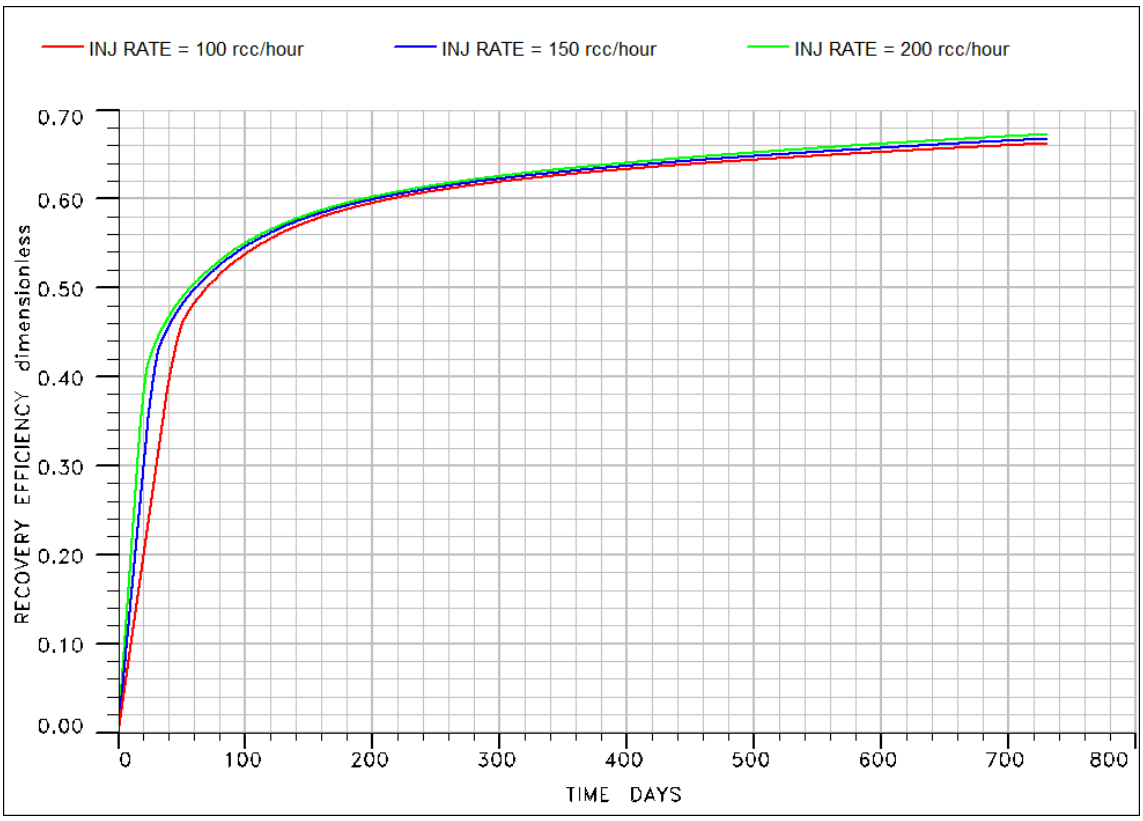

Figure 9.5 – Oil recovery efficiency for three injection rate cases, 100 (red line), 150 (blue line) and 200 rcc/hour (green line)

The oil recovery efficiency for the three injection rate cases are plotted in Figure 9.5. All the three cases follow the same recovery trend. The case with highest injection rate, 200 rcc/hr, increases at a highest rate followed by the injection rate of 150 and then 100 rcc/hr.

After about 200 days, all three cases increase in recovery in parallel. The case with highest injection rate yield the highest final recovery efficiency at 67.4% after 2 years, while the cases with injection rate of 150 and 100 rcc/hour has a final recovery of 66.8% and 66.2%, respectively.

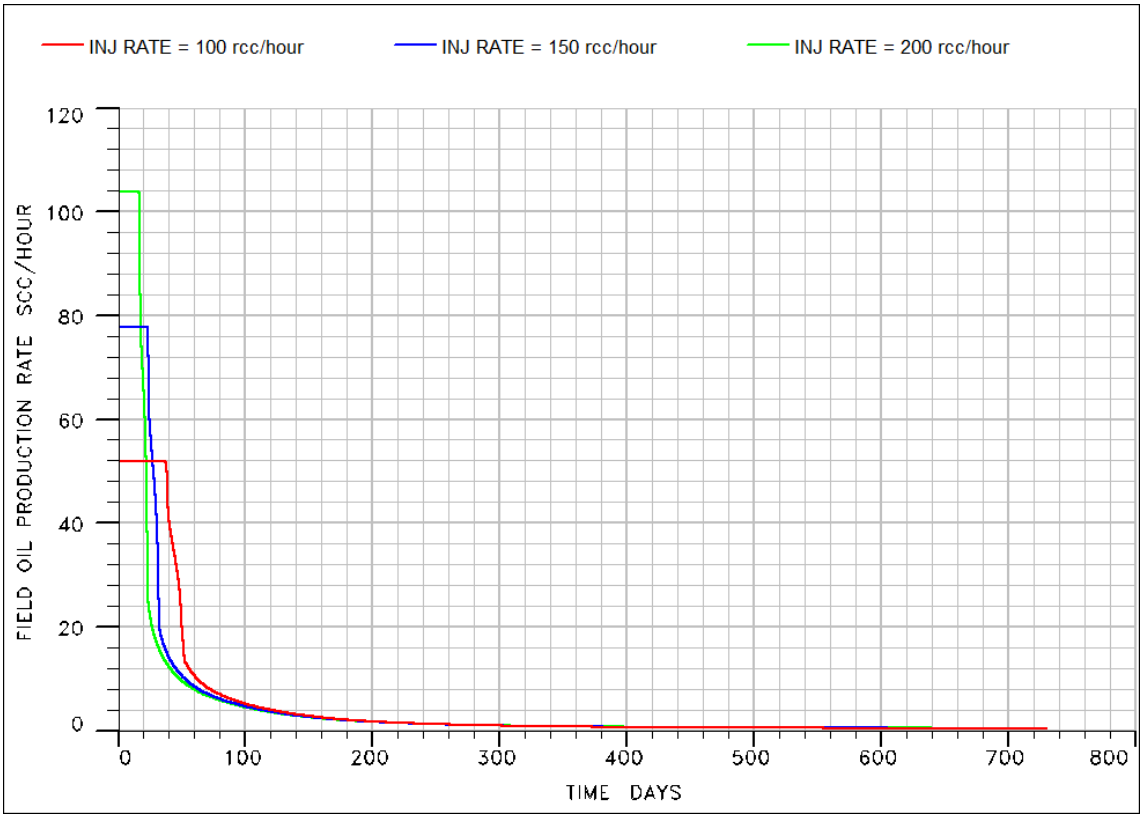

Figure 9.6 – Field oil production rate for three injection rate cases, 100 (red line), 150 (blue line) and 200 rcc/hour (green line)

The oil production rate for the three injection rate cases is plotted in Figure 9.6. It can be observed that the production rate at the surface corresponds to the injection rates into the reservoir.

A high injection rate yield a higher initial constant oil production for a shorter time, compared to the cases with lower injection rate. Green line represents an injection rate of 200 rcc/hr, and has an oil production rate of 104 scc/hr for 15 days before a sharp decline down to about 22.0 scc/hr after 23 days. The blue line represents an injection rate of 150 rcc/hr and has a constant oil production rate of 78.0 scc/hr for 37 days before declining. The case with low injection rate of 100 rcc/hr is represented by the red line. The production rate is constant at 52 scc/hr for 37 days before declining.

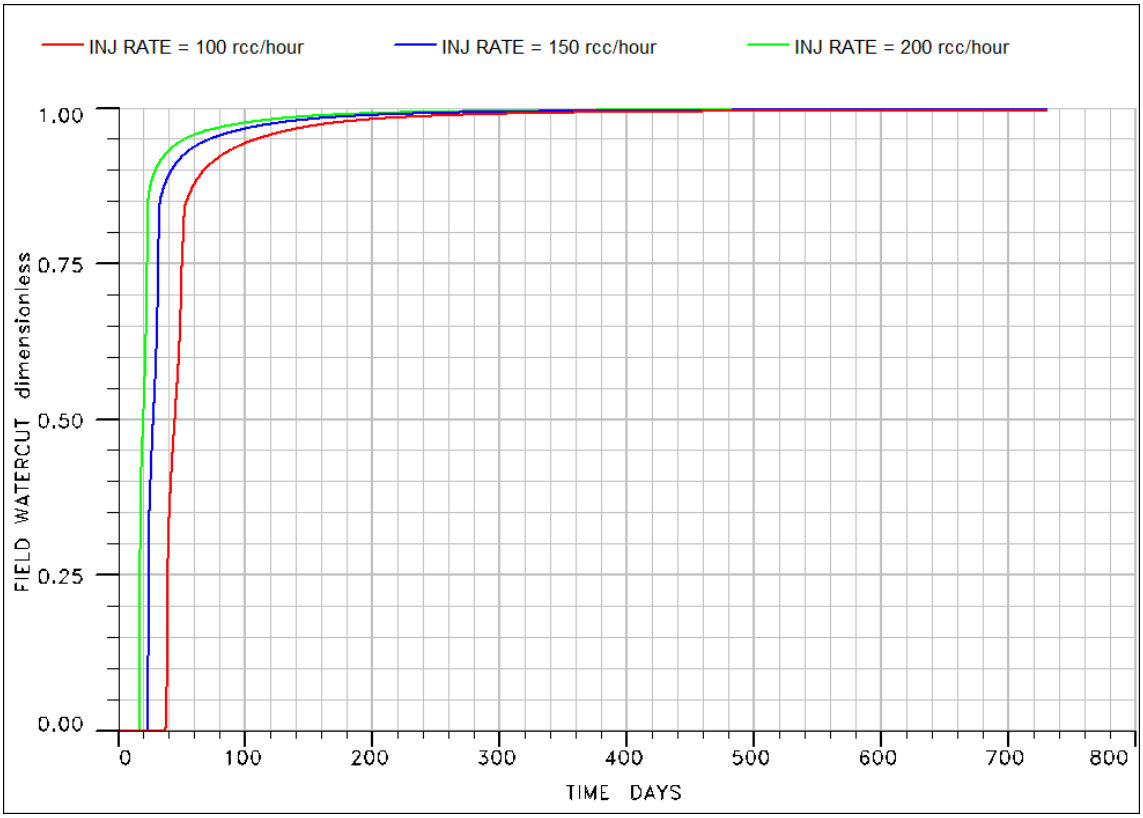

Figure 9.7 – Field watercut for three injection rate cases, 100 (red line), 150 (blue line) and 200 rcc/hour (green line)

In Figure 9.7, it can be observed that the three injection rate cases follow the same trend with water breakthrough at different times. The case with the highest injection rate starts producing water after 16 days, while the water breakthrough for injection rate of 150 and 100 rcc/hr occur after 23 and 37 days, respectively.

9.2 Waterflooding – Three Matrix Block (Basecase)

The waterflooding case presented in this section called basecase, is the same model that has been compared with the surfactant models introduced in Chapter 9.3.

The basecase parameters was introduced in Chapter 8.1.3, with injection and production rate of 200 rcc/hr.

9.2.1 Effect of Fracture Width

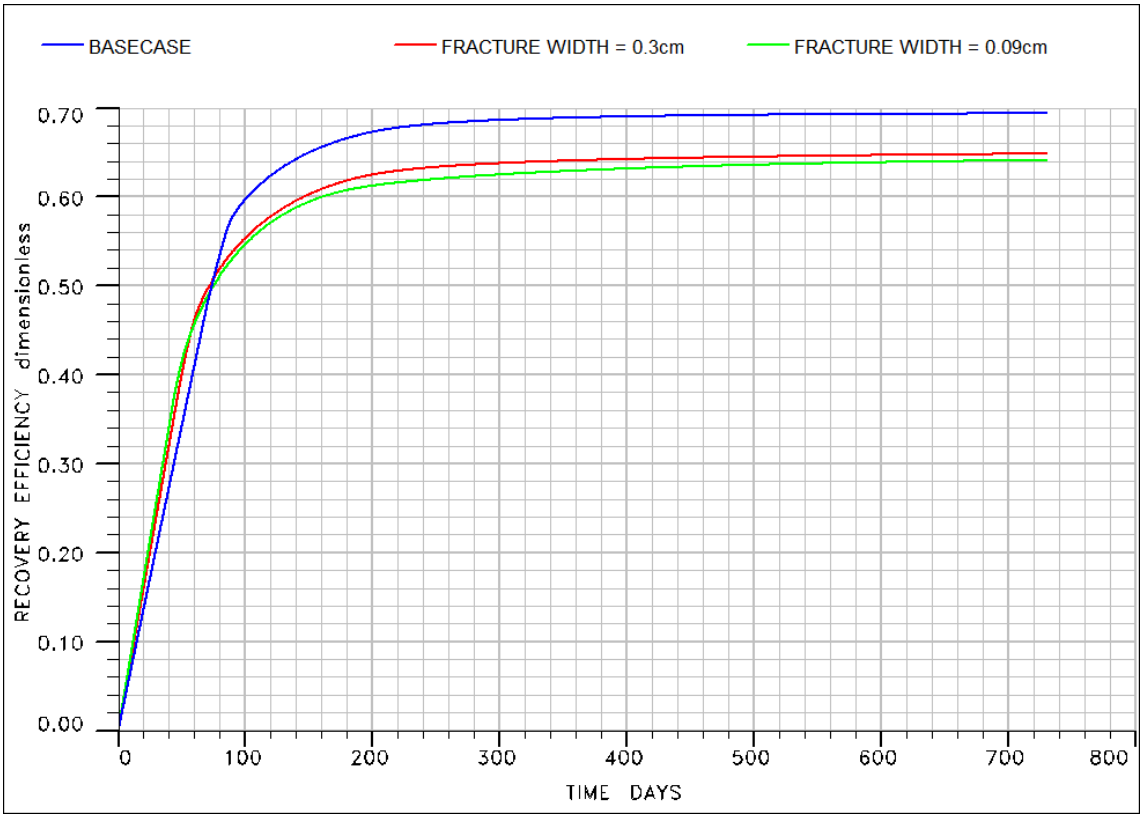

Figure 9.8 – Oil recovery efficiency for three different fracture widths. Basecase fracture width of 0.9cm (blue line) compared with 0.3cm (red line) and 0.09cm (green line).

Figure 9.8 shows the oil recovery efficiency for different fracture widths. It can be observed that the recovery curves with smaller fracture opening increases at a higher rate than the cases with bigger fracture opening. However, the final recovery is higher for the case with the biggest fracture opening. The case with fracture width of 0.09cm, increases at the highest rate until 45% recovery before intersecting with the two other cases. The case with fracture width of 0.3cm increases until 51% where it intersects with the basecase curve. The final recovery for fracture width 0.09cm, 0.3cm and basecase has a final recovery of 64%, 64.9% and 69.4%, respectively.

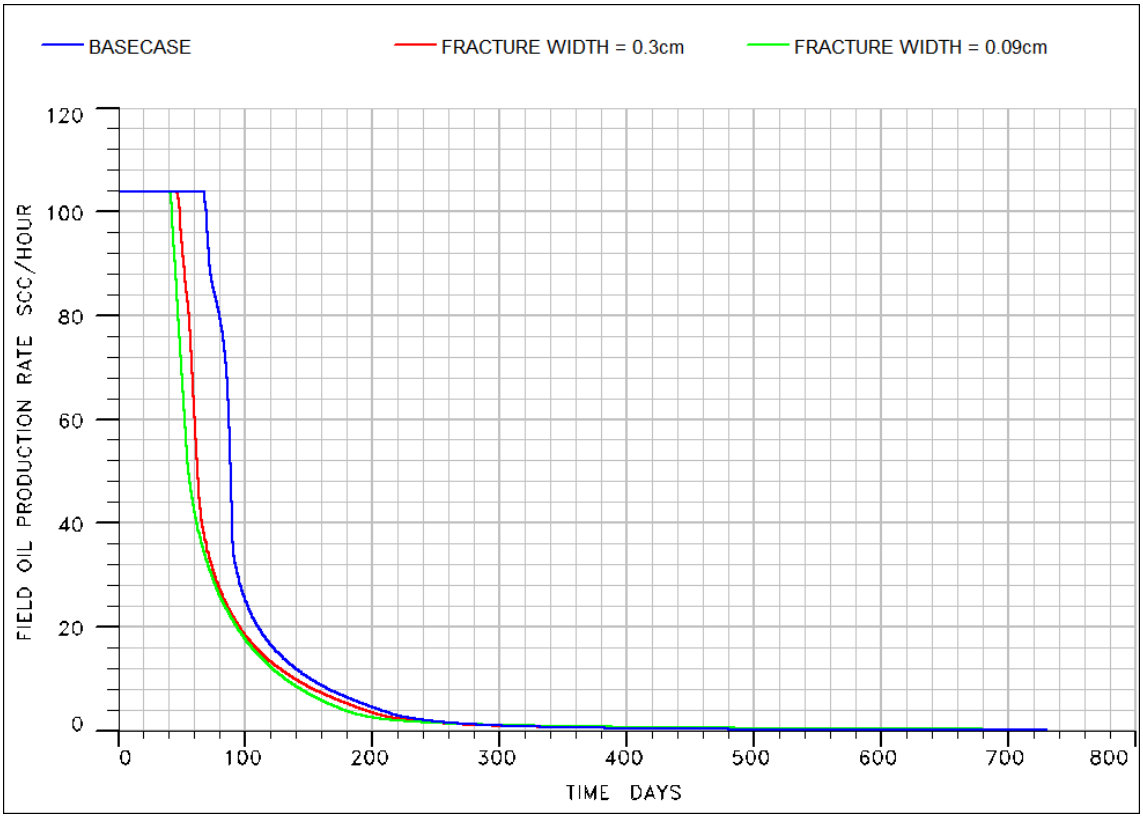

Figure 9.9 – Field oil production rate for three different fracture widths. Basecase fracture width of 0.9cm (blue line) compared with 0.3cm (red line) and 0.09cm (green line).

The oil production rate for the different fracture opening cases are plotted in Figure 9.9. All the cases has an initial production rate of about 104 scc/hr. The smallest fracture opening cases decrease in production rate first. The fracture width cases of 0.09cm, 0.3cm and Basecase start decreasing after 40, 46 and 67 days, respectively.

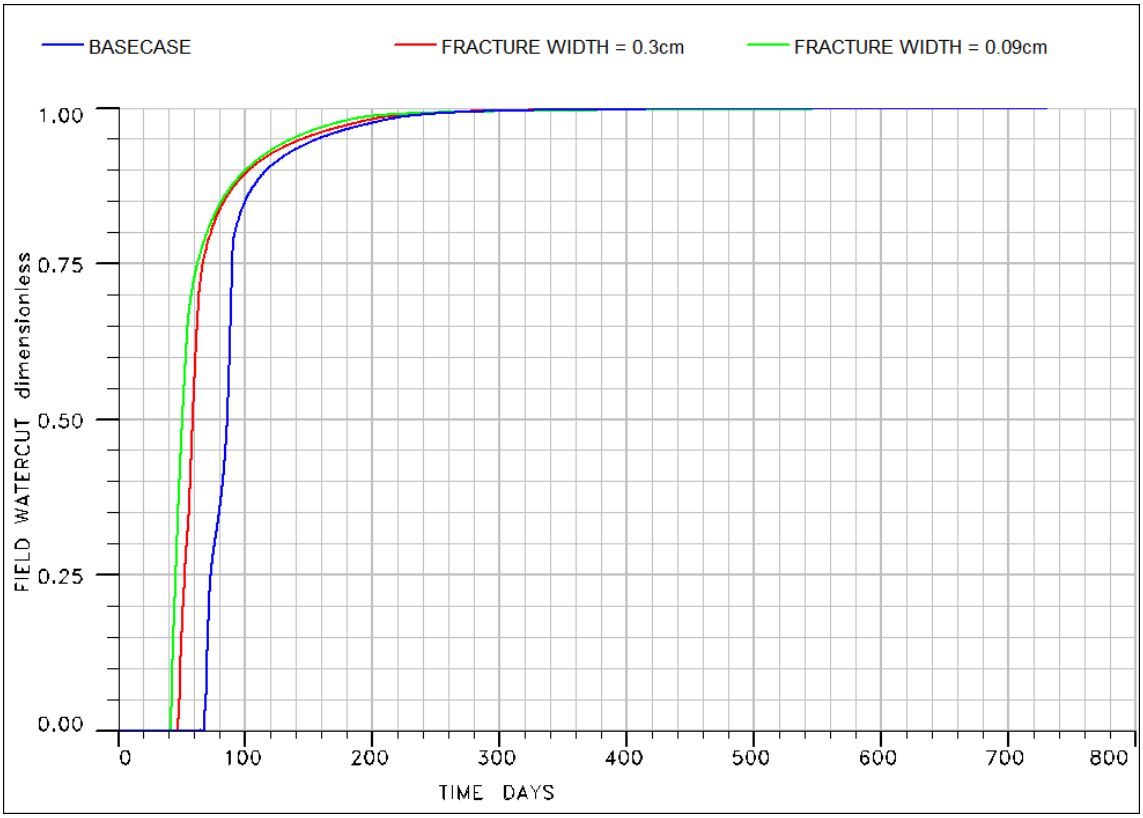

Figure 9.10 – Field watercut for three different fracture widths. Basecase fracture width of 0.9cm (blue line) compared with 0.3cm (red line) and 0.09cm (green line).

Figure 9.10 describes the watercut for all the three fracture opening cases. Water breakthrough for fracture opening 0.09cm, 0.3cm and basecase are 41, 46, 68 days, and follow the same trend.

9.2.2 Effect of Injection Rate

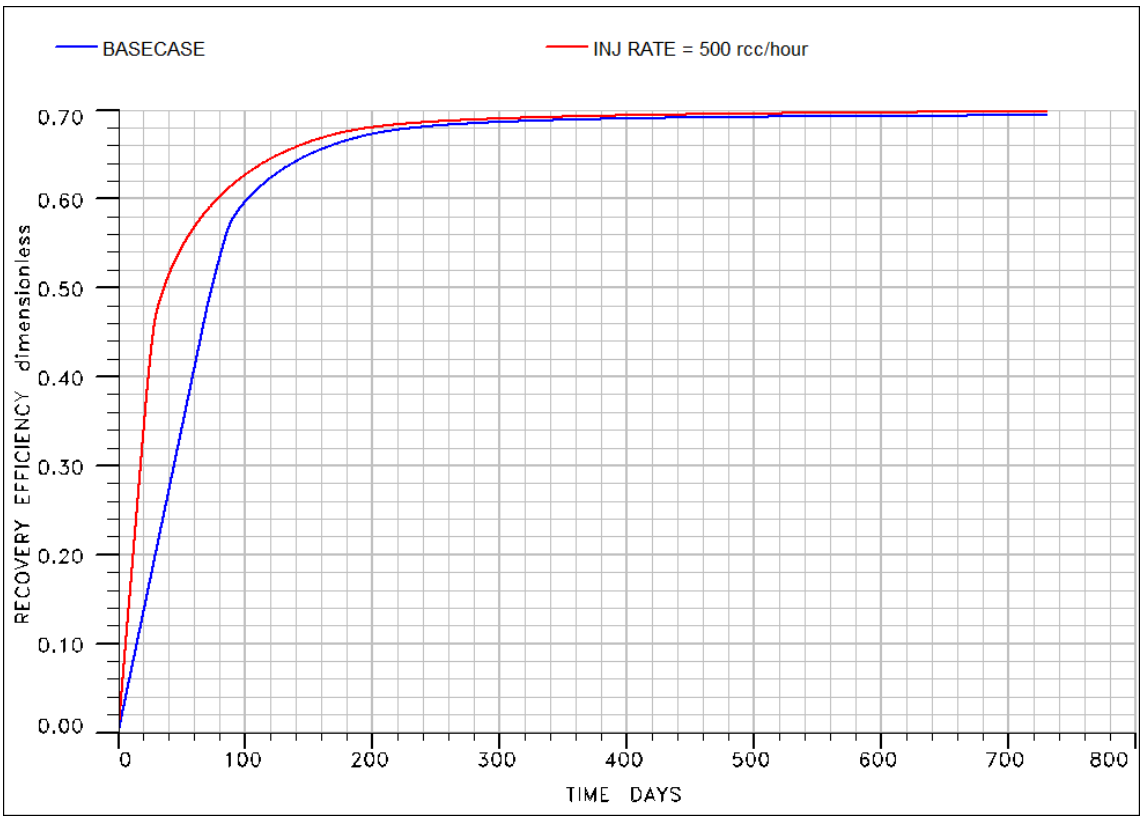

Figure 9.11 – Oil recovery efficiency for two injection rate cases. Basecase injection rate = 150rcc/hr and a case with injection rate = 500 rcc/hr.

Recovery efficiency for the two different injection rate cases has been plotted in Figure 9.11. It can be observed that a higher injection rate will yield a higher recovery rate at the beginning, before reaching a point close to residual oil saturation. Basecase increases with a lower rate, before the recovery curve flattens out and reaches a final recovery of 69.4%, which is 0.4% less than the final recovery of the high injection rate case.

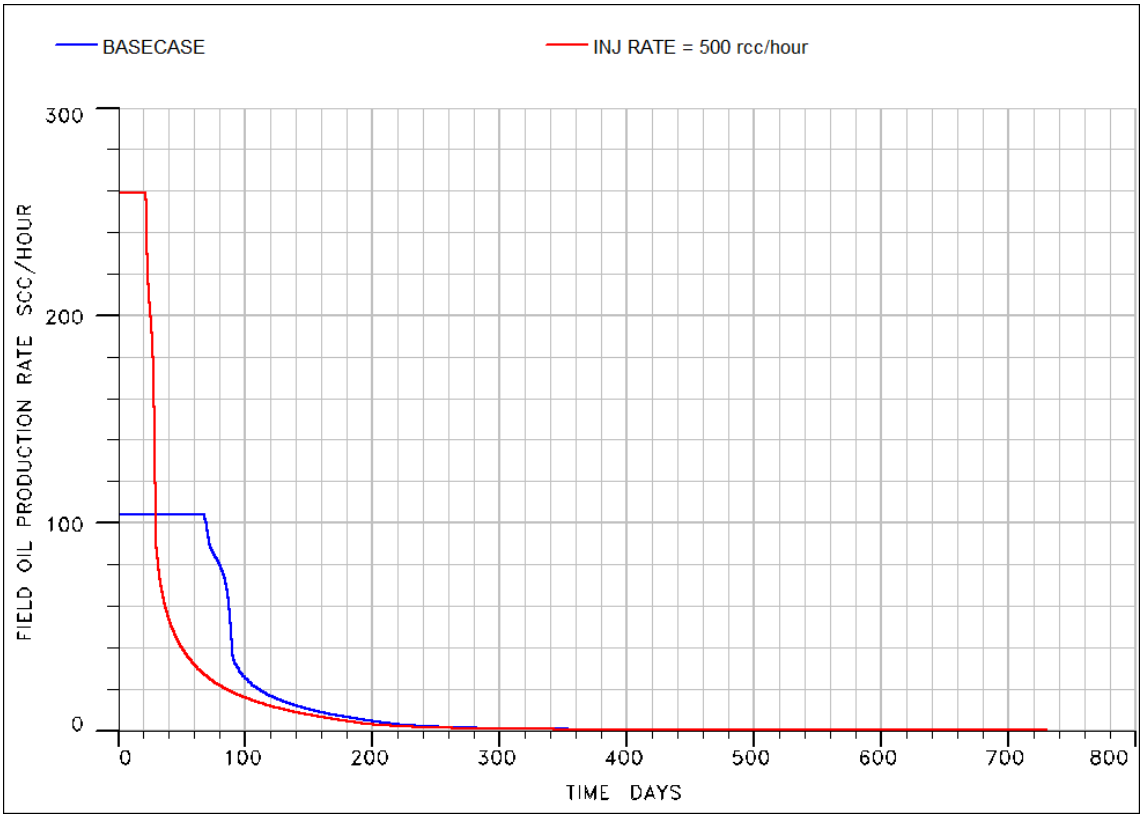

Figure 9.12 – Field oil production rate for two injection rate cases. Basecase injection rate = 150rcc/hr and a case with injection rate = 500 rcc/hr.

Figure 9.12 shows the field oil production rate for the two injection rate cases. It can be observed that the production rate is held constant at about 259 scc/hr in 21 days, before decreasing with an inversely proportional trend. The basecase production rate is constant at about 104 scc/hr in about 104 days before decreasing.

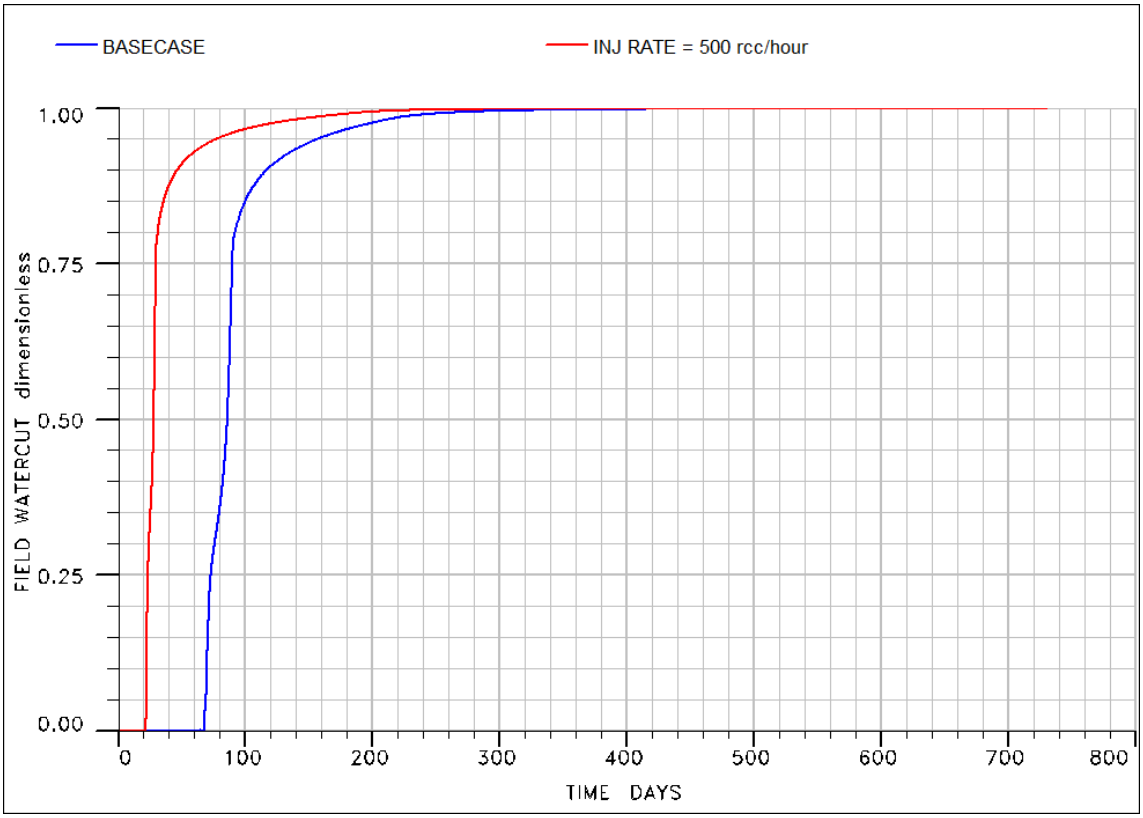

Figure 9.13 – Field watercut for two injection rate cases. Basecase injection rate = 150rcc/hr and a case with injection rate = 500 rcc/hr.

The watercut for the different injection rate cases can be observed in Figure 9.13.Water breakthrough for the high injection rate occurs after 21 days, while it is 67 days for basecase.

9.3 Surfactant flooding

Several sensitivity analyses on the surfactant flooding in both models was conducted.

9.3.1 Effect of Surfactant Concentration

Three different surfactant concentration has been simulated and compared with the basecase. Surfactant concentrations of 0.003 and 0.0003 g/cm^3 and an extreme case of 0.03 g/cm^3 with no adsorption was studied. Assuming continuous flooding of surfactants.

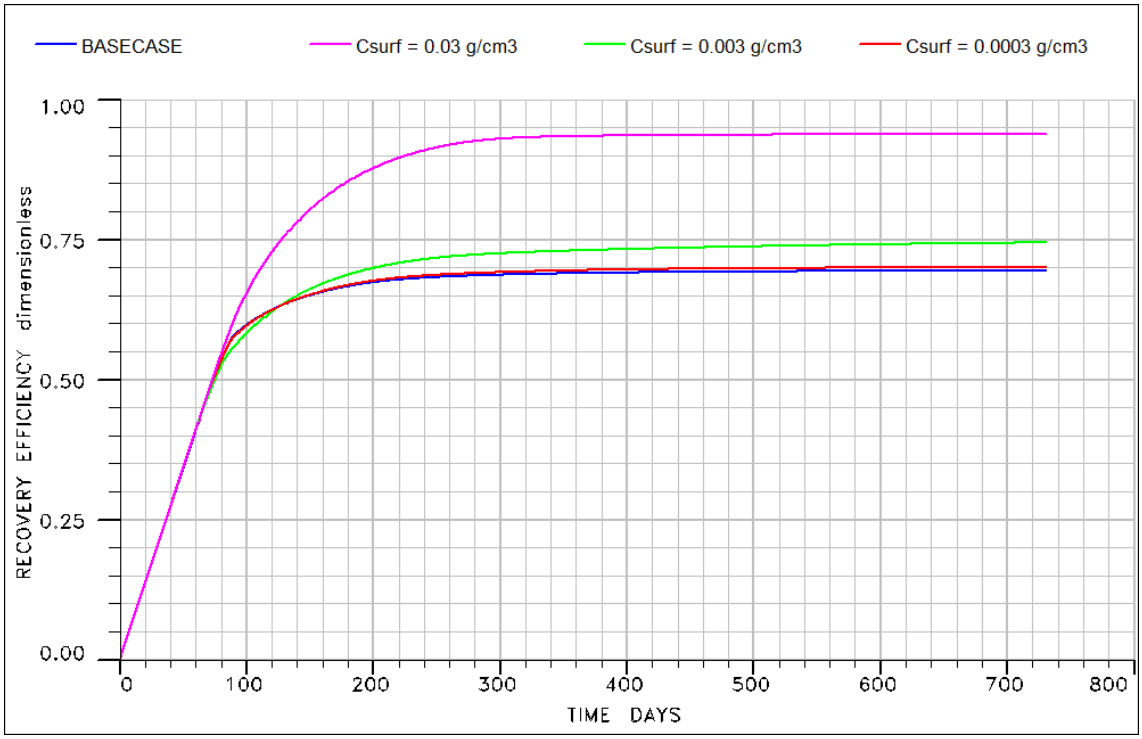

Figure 9.14 - Oil recovery efficiency for three different surfactant concentrations (0.03, 0.003 and 0.0003 g/cm^3) compared to basecase.

Figure 9.14 shows that the recovery efficiency increases with increased surfactant concentration. All cases follow the same trend until T = 80 Days, before splitting up with different final recoveries. It can also be observed that the green case declines in recovery rate after 90 days, but increases and intersect the low surfactant concentration case and basecase as their recovery rate reduces.

The basecase curve (blue line) with pure water has a final recovery of 69.5% while the final recovery of the surfactant concentration cases of 0.03g/cm3 (pink line), 0.003g/cm3 (green line) and 0.0003g/cm3 (red line) are 93.8%, 74.4% and 70.0%, respectively.

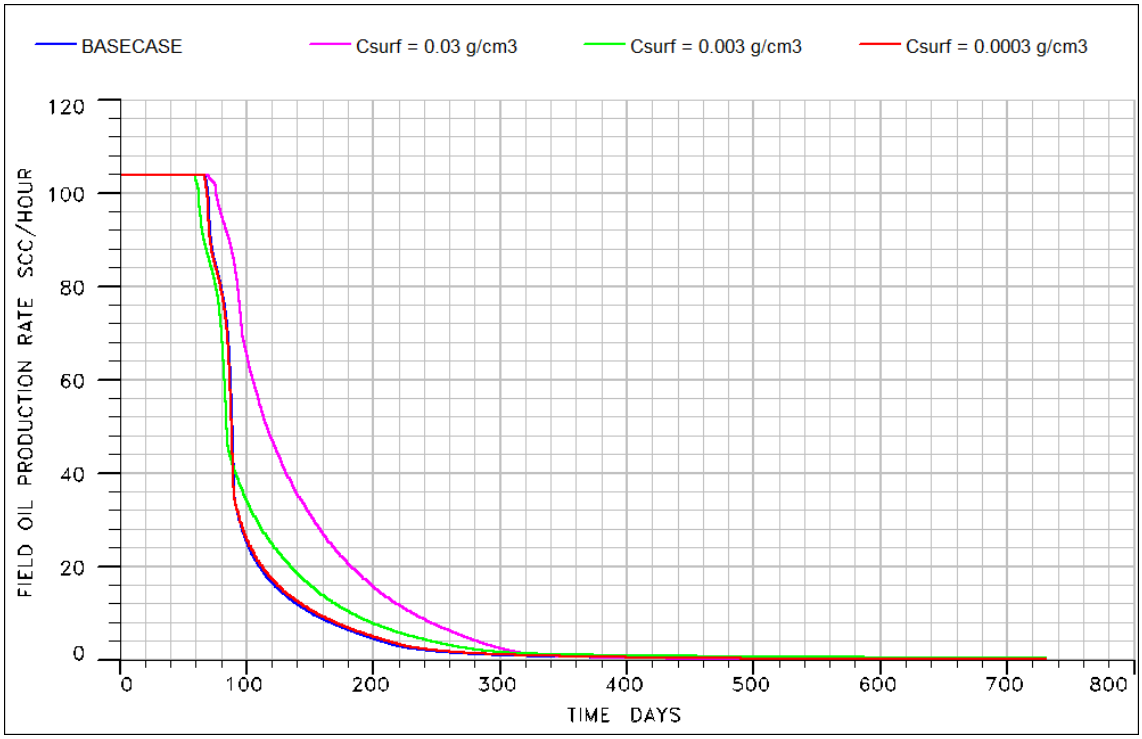

Figure 9.15 - Oil production rate in scm^3/hr for three different surfactant concentrations (0.03, 0.003 and 0.0003 g/cm^3) compared to basecase.

In Figure 9.15, it can be observed that the oil production rate will decrease much slower with higher surfactant concentration. All cases has the same initial production rate of 104 scc/hr.

The case with lowest surfactant concentration follow the exact same trend as the basecase, but with a slightly higher production rate. The case with 0.003g/cm^3 decrease faster and earlier than basecase, but intersects after 90 days of production with a higher oil production rate.

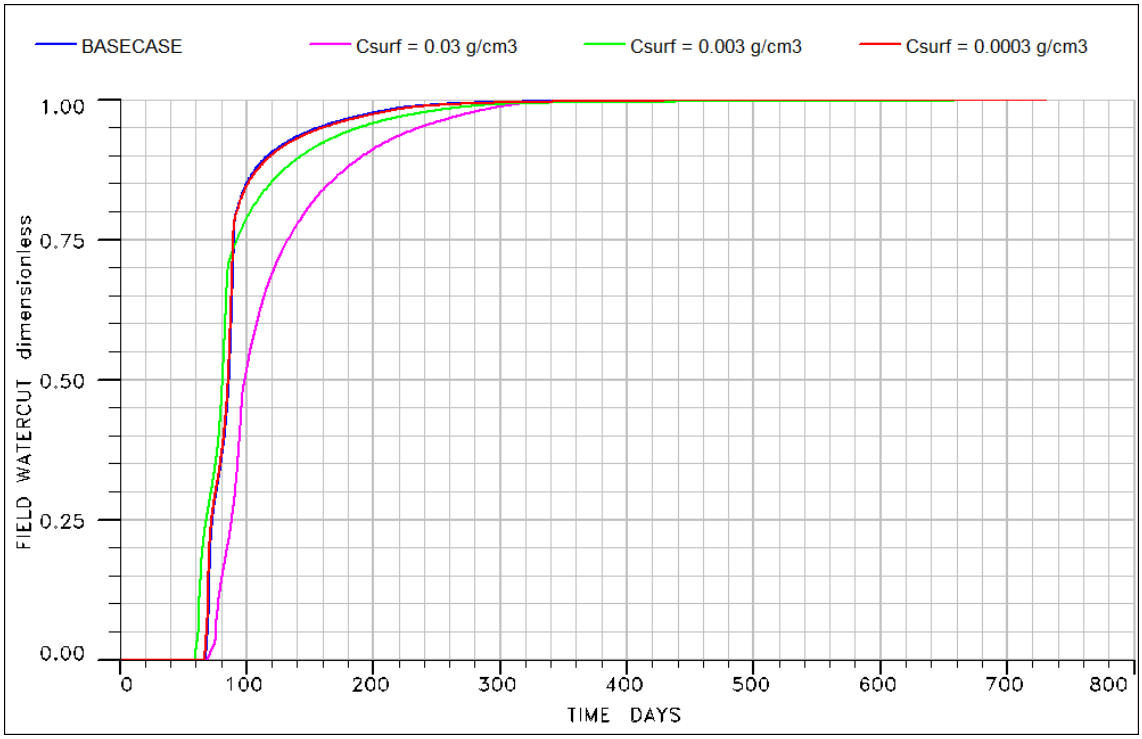

Figure 9.16 - Field watercut for three different surfactant concentrations (0.03, 0.003 and 0.0003 g/cm^3) compared to basecase.

Figure 9.16 shows that the rate of watercut decreases with increased surfactant concentration. The lowest surfactant concentration of 0.0003g/cm^3 follows the exact same line as basecase, similar to the oil production curve.

The surfactant concentration of 0.003g/cm^3 has an earlier watercut than basecase and the high surfactant concentration case.

9.3.2 Effect of Adsorption

The adsorption values show the amount of surfactant in the local solution surrounding the rock that is adsorbed onto the rock surface.

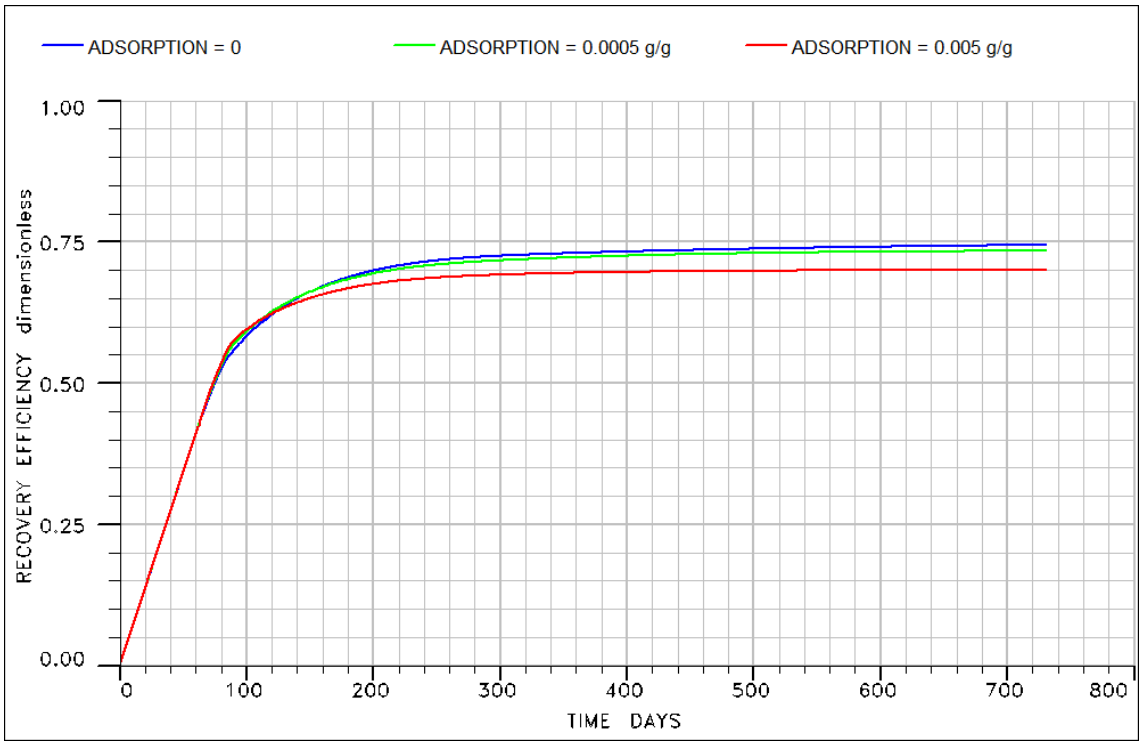

Figure 9.17 – Recovery efficiency for three cases of surfactant adsorption (0, 0.0005 and 0.005 g/g)

As more surfactants is adsorbed on the rock surface, see Figure 9.17, the final oil recovery efficiency decreases. The case with the highest recovery is the surfactant basecase with no adsorption at a final recovery of 74.4% after 2 years. With 0.0005 and 0.005 grams of surfactants adsorbed result in a lower recovery of 73.4% and 70.0%, respectively.

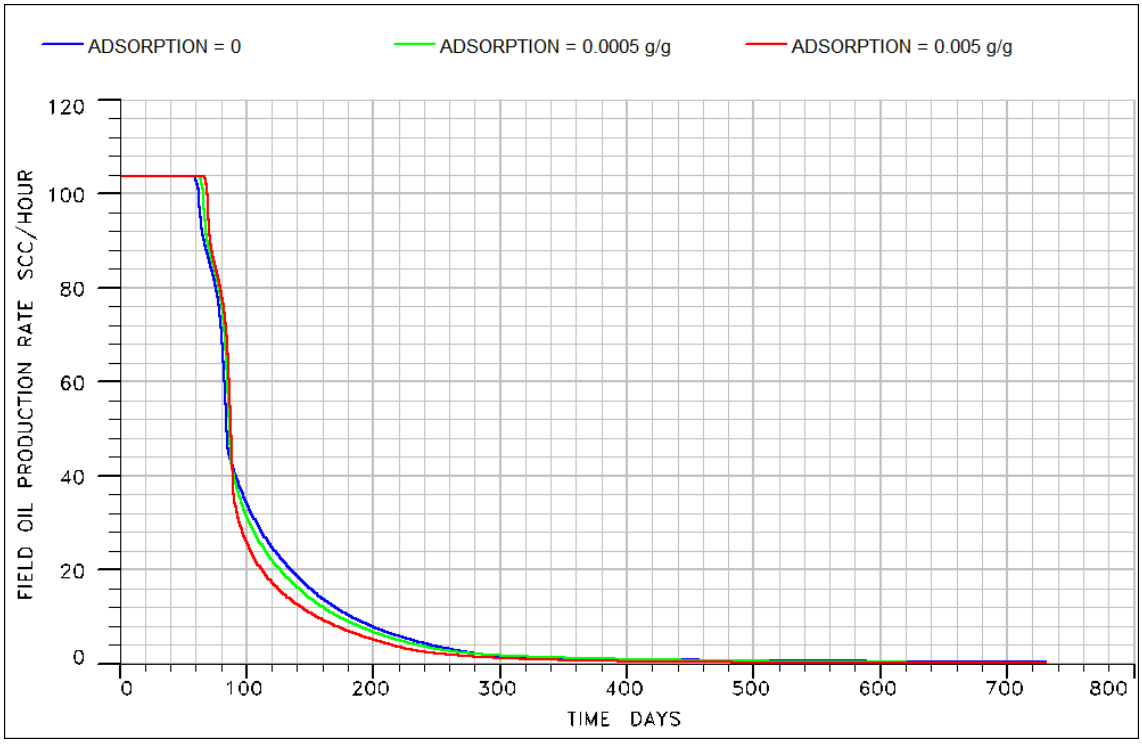

Figure 9.18 – Field oil production rate for three cases of surfactant adsorption (0, 0.0005 and 0.005 g/g)

Figure 9.18 indicate that the oil production rate is delayed a few days when adsorption takes place. The rate also decreases faster with higher adsorption. The initial oil production rate is the same for all cases at 104scc/hr.

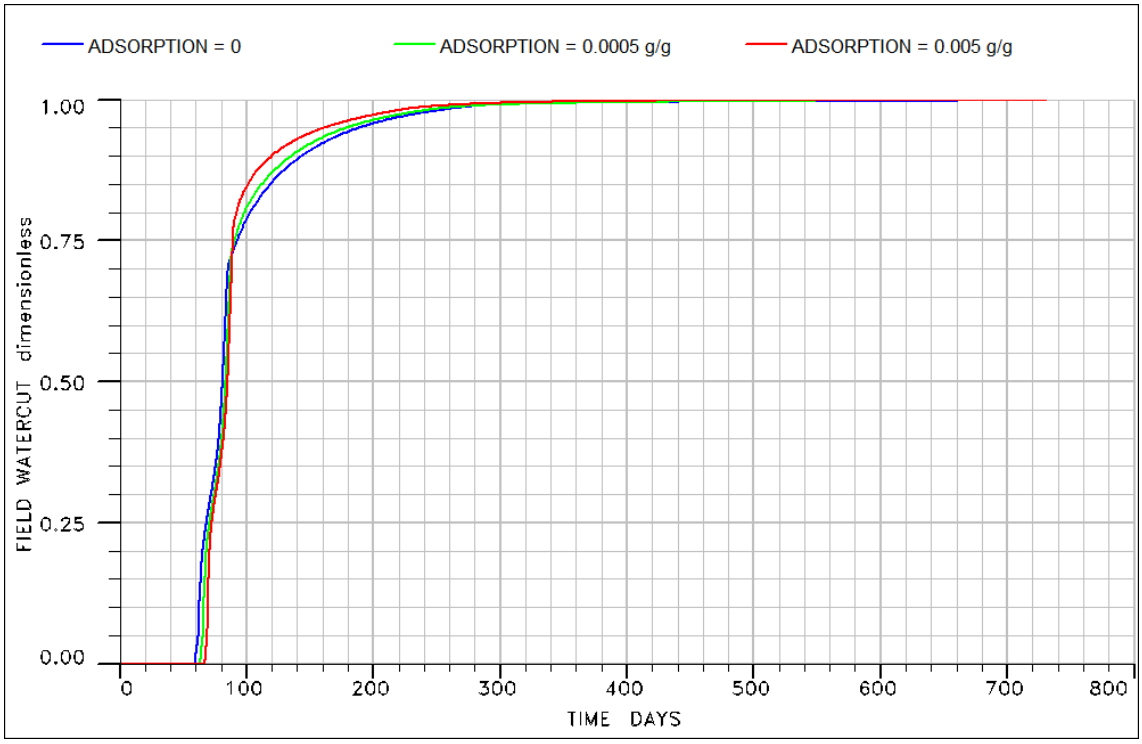

Figure 9.19 – Field watercut for three cases of surfactant adsorption (0, 0.0005 and 0.005 g/g)

Figure 9.19 shows the watercut of the field for different adsorption cases. The watercut increases at a slightly lower rate for the case with no adsorption and the case with 0.0005 g/g compared to the case with higher adsorption of 0.005g/g represented in the red line.

9.3.3 Effect of Surfactant Injection after Waterflooding

Sensitivity on when to start injecting surfactants has been done. The different cases that has been simulated are continuous surfactant flooding after 2 and 6 months of waterflooding with no adsorption and a surfactant concentration of 0.003 g/cm^3.

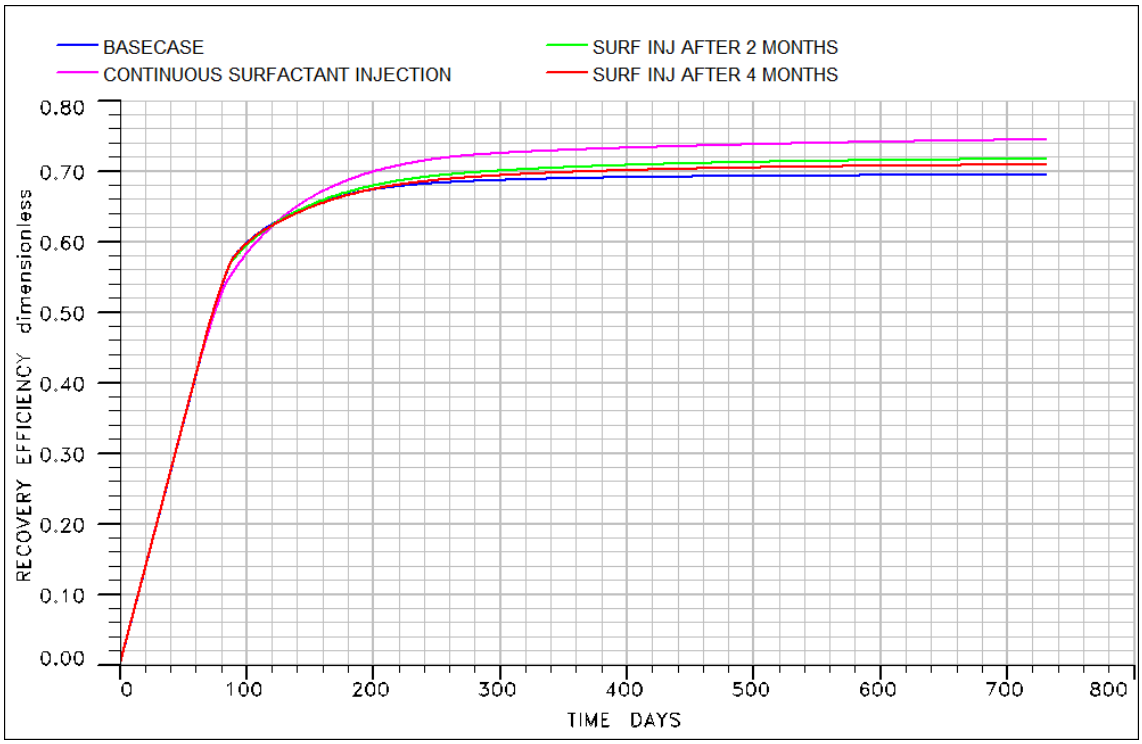

Figure 9.20 – Oil recovery efficiency for waterflooding, continuous surfactant injection and delayed surfactant injection.

With a delayed surfactant injection following the waterfront, it can be observed in Figure 9.20 that the oil recovery curves for the cases with surfactant follow the basecase at the beginning before continuing to increase at a slightly higher rate. This result in a final recovery factor of 71.7% and 70.9% for the 2 and 4 months surfactant injection delay cases, respectively. Compared to basecase at 69.5%. The continuous case has a final recovery of 74.4%.

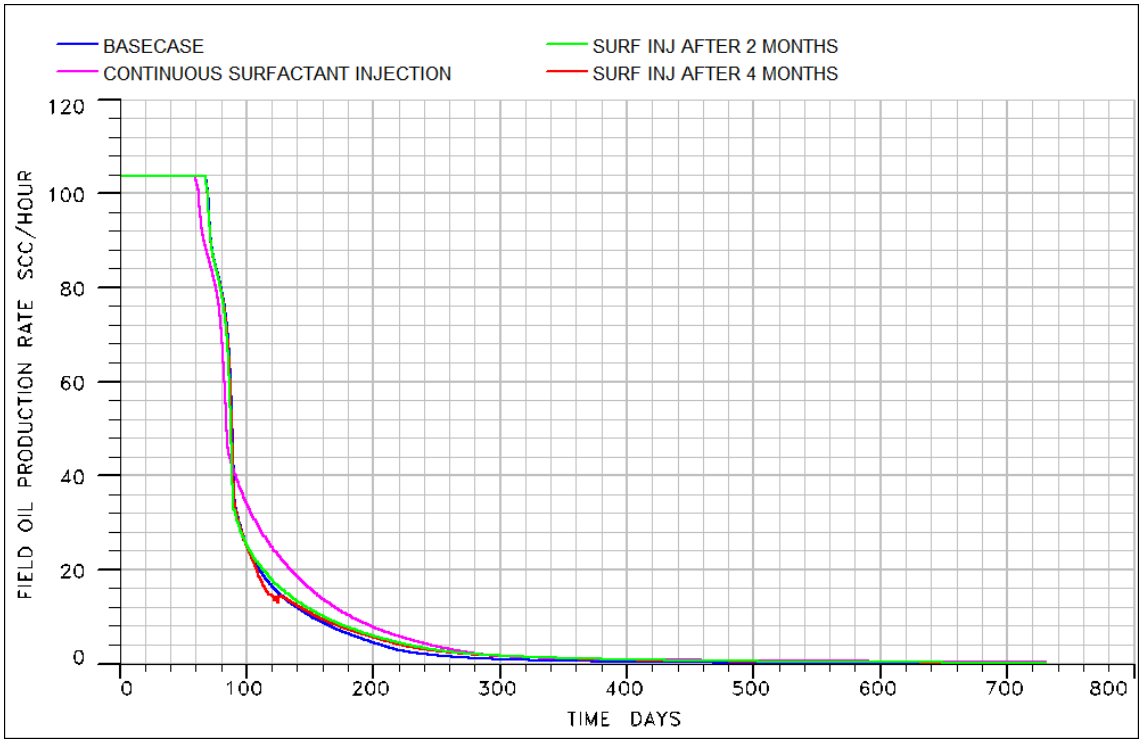

Figure 9.21 – Oil production rate for waterflooding, continuous surfactant injection and delayed surfactant injection.

Figure 9.21 describes the field oil production rate for basecase compared to different surfactant injection cases. It can be observed that the case with continuous surfactant injection drops in production first, but decreases in oil production rate slower than the other cases.

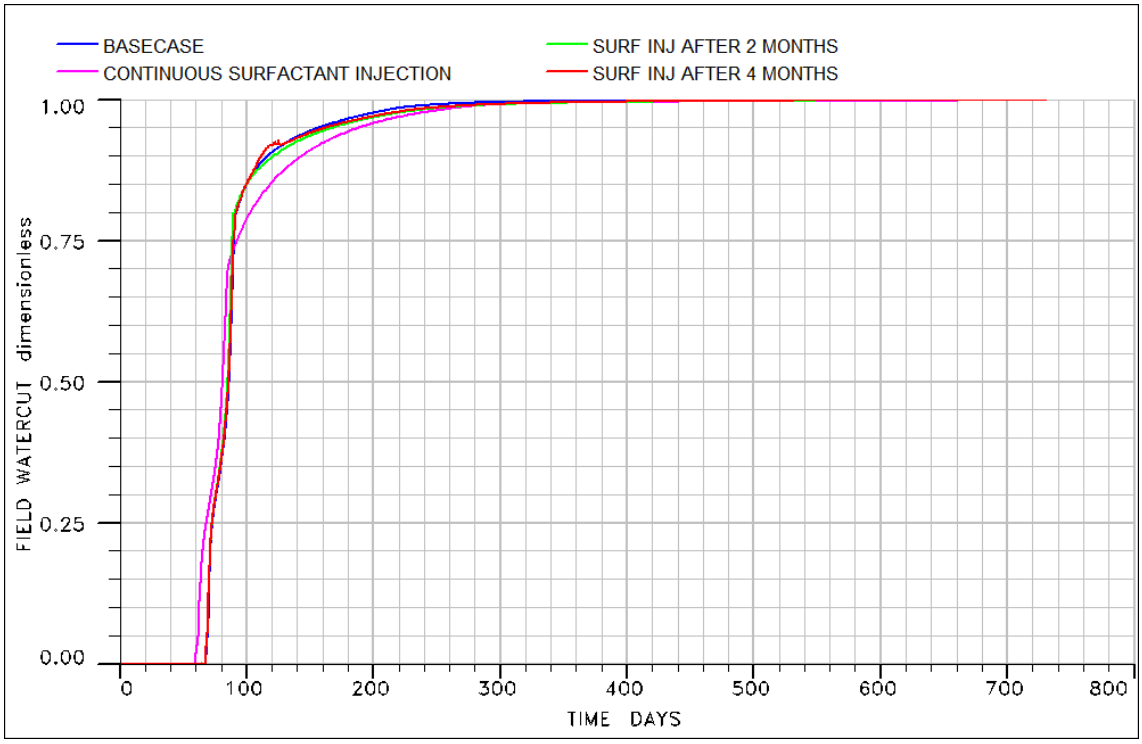

Figure 9.22 – Field watercut for waterflooding, continuous surfactant injection and delayed surfactant injection.

It can be observed in Figure 9.22, that the water breakthrough for the case with continuous surfactant flooding occurs at 60 days, 8 days before the water reaches the production well for basecase and the delayed surfactant injection case. The watercut for the continuous surfactant injection case intersects with the other cases after about 88 days, and flattens out at a lower watercut level compared to the other cases.

9.3.4 Effect of Surfactant Slug

The basecase with water injection and the case with continuous surfactant injection acts as a lower and upper limit. Different scenarios of slug size was simulated, assuming no adsorption onto the rock surface expect for one case. Surfactant concentration is kept constant for all the surfactant cases.

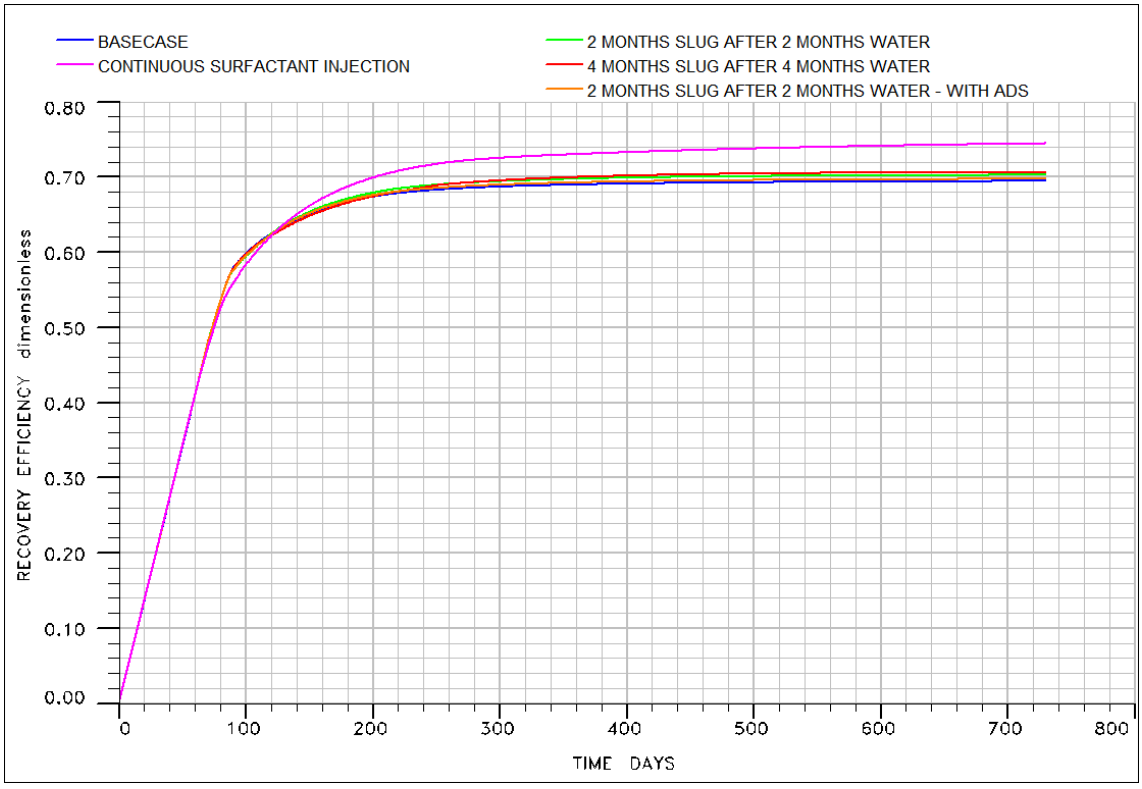

Figure 9.23 – Oil recovery efficiency for waterflooding, continuous surfactant injection and different slug sizes.

As seen in Figure 9.23, the recovery efficiency for the continuous surfactant injection case increases at the same rate as the other cases in 80 days. The surfactant slug cases and basecase increase in recovery at a higher rate than the continuous surfactant injection case after 80 days for 40 days before the continuous case intersects and result in a higher final recovery. The slug cases follow the basecase in 120 days, before the curves starts deviate from each other and result in different final recoveries that can be observed in Figure 9.24 and described in Table 9.1.

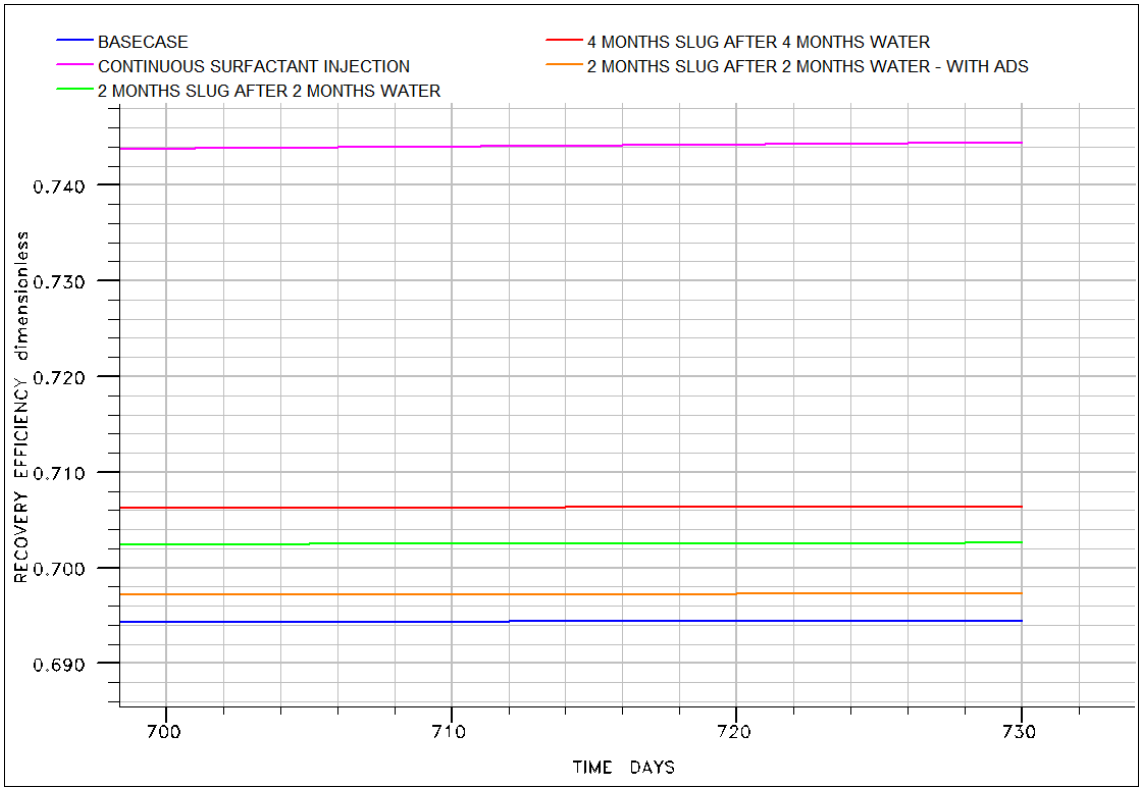

Figure 9.24 – A part of oil recovery efficiency for waterflooding, continuous surfactant injection and different slug sizes found in Figure 9.23.

Table 9.1 – Oil recovery efficiency for waterflooding, continuous surfactant injection and slug size cases.

Case	Recovery
Continuous surfactant injection	74.4%
2 month slug after 2 month water injection	70.3%
4 month slug after 4 month water injection	70.6%
2 month slug after 2 month water - adsorption	69.7%
Basecase	69.4%

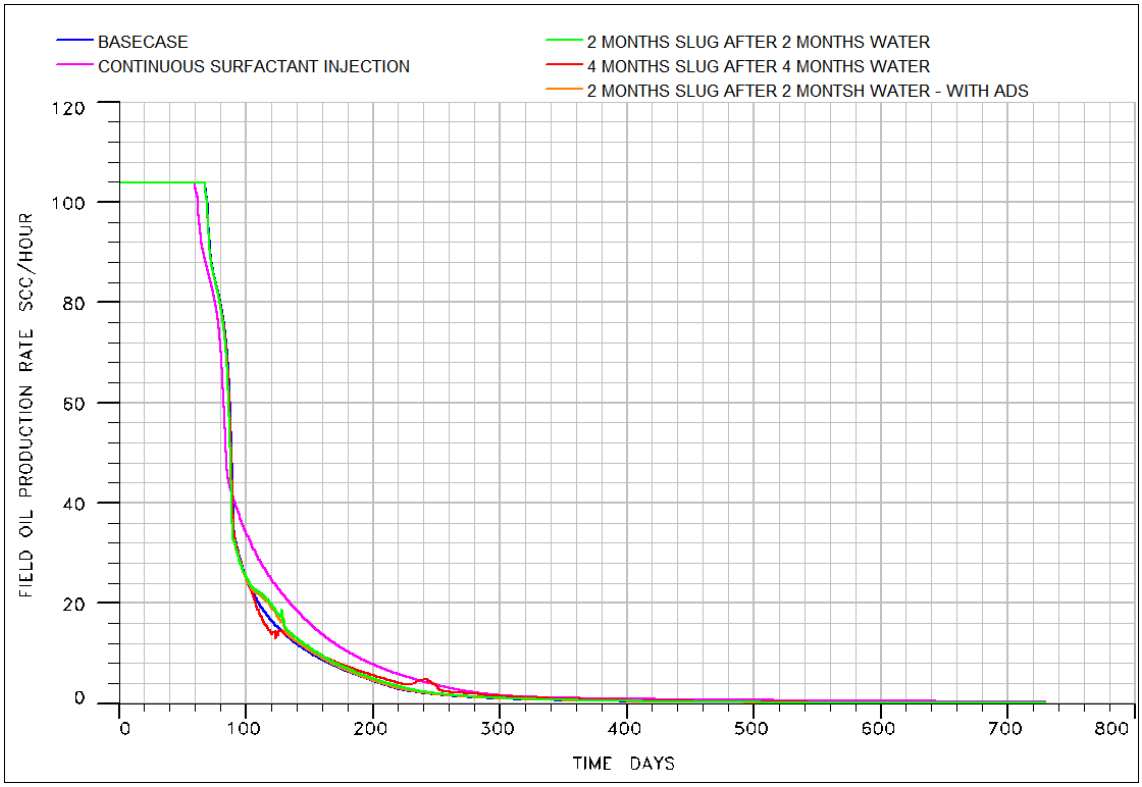

Figure 9.25 – Oil production rate for waterflooding, continuous surfactant injection and different slug sizes.

Figure 9.25 describes the field oil production trends of the different cases. The plot indicate that the continuous surfactant injection case starts decreasing in oil production after 60 days while the other cases starts decrease in oil production after 68 days.

The green case, gets a small bump in production rate right after 100 days, before declining at the same trend as basecase. The red case, which is a 4 month big slug, declines at higher rate than basecase before surfactants is introduced after 120 days. Another boost in oil production rate can be observed after 227 days.

The case with 2 months slug injection including adsorption tend to follow the same case without adsorption in parallel, but at a slightly lower rate.

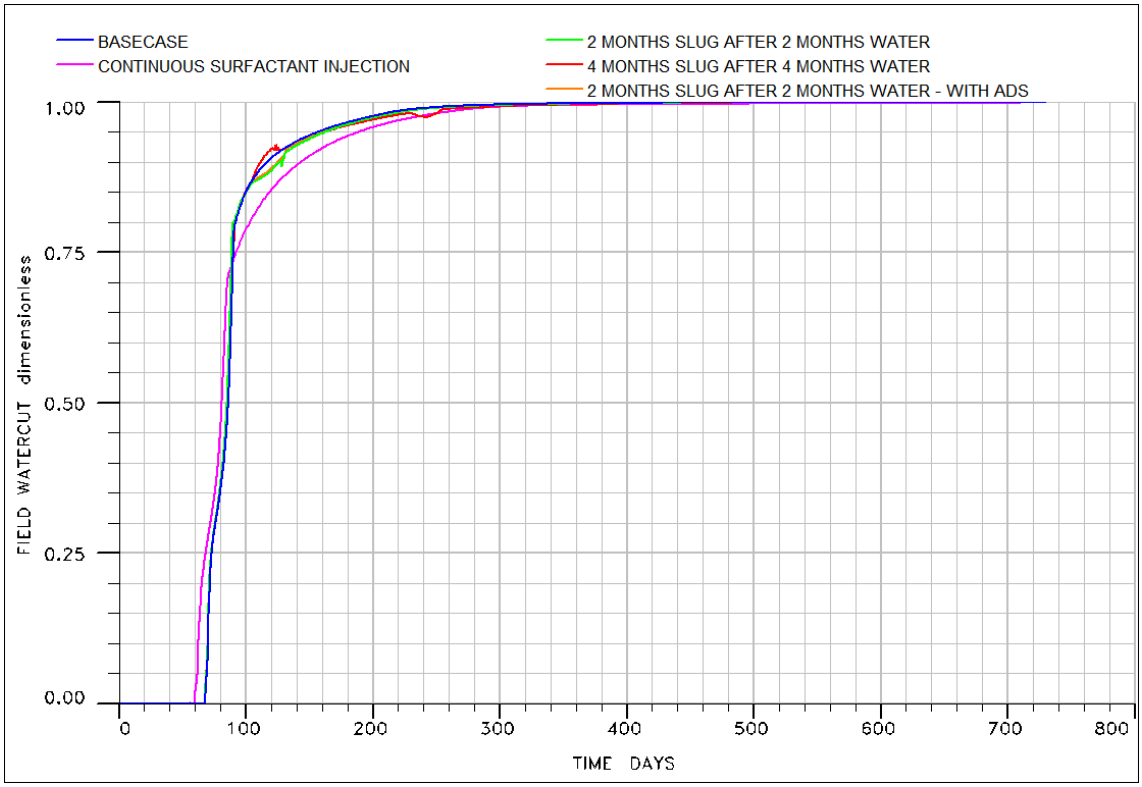

Figure 9.26 – Field watercut for waterflooding, continuous surfactant injection and different slug sizes.

The water breakthrough for waterflooding, continuous surfactant injection, and different slug sizes can be observed in Figure 9.26. Continuously injection surfactant result in an early water breakthrough than the other cases that starts with water injection. The case with continuous surfactant injection starts producing water after 60 days, while the water reaches the production well after 68 days for the other cases. The rate of watercut decreases for the continuous surfactant injection case and intersects with the other cases after 89 days of flooding.

The surfactant slug cases follow the basecase curve with a few bumps in watercut rate when surfactant is being injected and reaches the production well.

9.3.5 Comparison of Basecase, Slug and Continuous Surfactant Flooding

To study the actual effect of different surfactant injection cases on the matrix block, different surfactant cases has been compared with the basecase in terms of the amount of injected fluid that has been imbibed into the matrix blocks and the amount of oil that has been displaced and recovered from the matrix blocks.

The cases that has been compared is given in Table 9.2. The amount fluid outflow and inflow between matrix and fracture are reported in Table 9.3. Full report can be found in Appendix A.2 - Fluid in Place – Regions

Table 9.2 – Cases for comparison

A	Basecase
B	Continuous surfactant injection
C	Continuous surfactant injection after 2 months water
D	2 months slug after 2 months water
E	2 months slug after 2 months water with adsorption

Table 9.3 - Fluid in place report from Eclipse for matrix and fracture

	A	**B**	**C**	**D**	**E**
Outflow from matrix to fracture [cm^3]	173631	194194	182603	176819	174893
Inflow from fracture to matrix [cm^3]	173631	194194	182603	176819	174893
Ratio of displaced oil to initial OIP in matrix	0.61256	0.68510	0.64421	0.62381	0.61702
Ratio of displaced oil to initial OIP in fracture	0.98	0.9534	0.9736	0.98	0.98

Table 9.4 – Comparison of oil saturation in the three block model for five different cases.

	T = 60 days	T=90 days	T=730 days
A	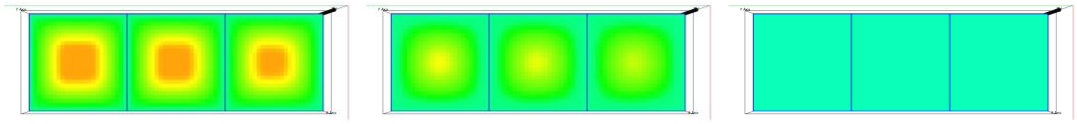		
B	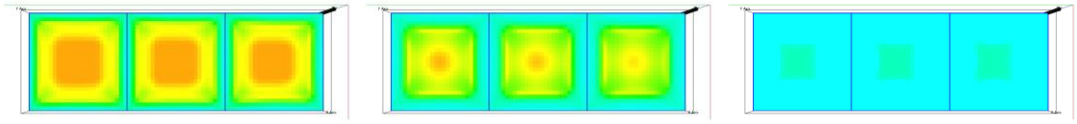		
C	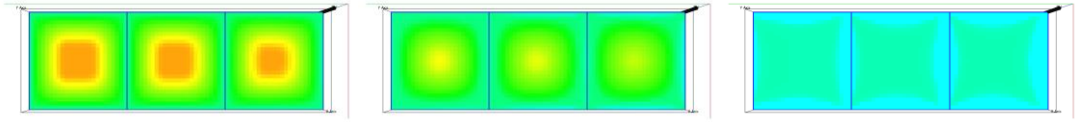		
D	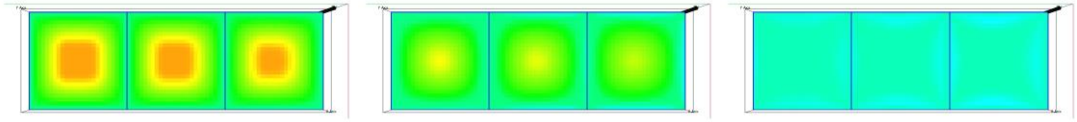		
E	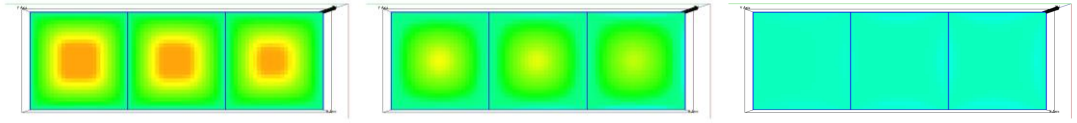		
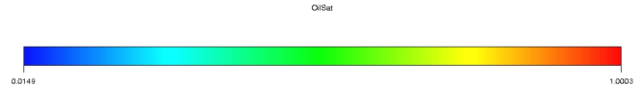			

Table 9.4 shows the a x, y slice of the model in the middle of the matrix block showing the effect of surfactant injection compared to water injection. The cross sections indicate that the most favorable situation is case B, which is continuously flooding with surfactants. The case which is most realistic in terms of profitability of injecting surfactants would be case E, where a surfactants is injected for two months after flooding the matrix with two months of water.

Table 9.3 represents the fluid in place at T=730 days in Table 9.4, and indicate that with more amount of surfactant in the system, a higher amount of oil will flow out from the matrix while the same amount of injected fluid will imbibe into the matrix.

10 Discussion

Sensitivity analysis on both models have been conducted with both water and surfactants. The properties that will be discussed are the effect on production by changing the capillary pressure, relative permeability and injection rate effect on production.

The main driving force is desired is imbibition and gravity force, but to be able to produce from the matrix with only water, viscous displacement forces could play an important role.

10.1 Reservoir Parameters

Choice of fracture porosity and permeability values are discussed in this section.

10.1.1 Fracture Permeability

In this simulation study, the fracture opening is 0.9 cm. The real fracture permeability can then be calculated using equation (2.7) given in Chapter 2.1.2:

$$k_f = \frac{e^2}{12} = \frac{0.0009^2}{12} = 6.75 \cdot 10^{-8}\ m^2$$

Converting to Darcy:

$$k_f = \frac{1\ D}{10^{-12}\ m^2} \cdot 6.75 \cdot 10^{-8}\ m^2 = 67500\ D$$

A fracture opening of 0.9 cm yields a permeability of 67500 D, which is much higher than the permeability used in the simulation of 5 D. The fracture opening assumes that there is an open channel of 0.9 cm, meaning that the fluid in the fracture flows freely, hence the high permeability.

In a real reservoir there exist capillary continuity between the matrix-blocks that is in touch with one another, with open channel in between. See Figure 10.1.

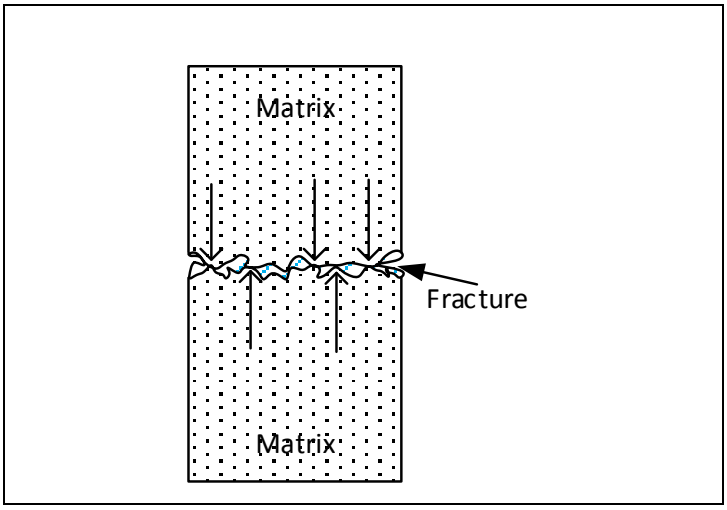

Figure 10.1 – Fracture between two matrix blocks. Arrows showing the capillary continuity between the matrix blocks, separated by high permeability zones in between.

Each gridblock in the simulator has an average fracture permeability of 5 D. Instead of assigning a certain amount of the fracture gridblocks with the same properties as the matrix to simulate the capillary continuity, the permeability is set to 5 D as an average permeability for simplicity reasons.

10.1.2 Fracture Porosity

The fracture porosity was initially set to 1.0, to simulate an open channel of fluid. In Eclipse E100, the porosity for any region must be less than 1.0 when the surfactant model is activated. The porosity in this study is therefore 0.99.

10.2 Simulation Model

The models that has been designed for this particular study is looking at the details of different displacement forces that acts on the matrix blocks in an actual reservoir, assuming that the matrix block is totally surrounded by fractures in all directions.

The model is built up by 31x31x31 = 29791 gridblock in the single matrix block and 31x87x31 = 83607 gridblocks in the three matrix block model. Both models is therefore very fine gridded to look at the imbibition process and the fluid exchange between matrix and fracture in more details.

The fracture in both models designed has been allocated three gridblock on each surface. Since the idea behind the fractures in this study was to have an open channel, decreasing the number of gridblocks allocated to the fractures could reduce the simulation time.

The idea behind the single matrix block model was to try to compare the simulation result with a similar case in the laboratory, but scaled down from $1m^3$ as matrix block to a more convenient core size. A core fully saturated with oil, placed in an Amott cell to study the displacement of oil by imbibition and gravity forces, would be of interest.

Expanding the model by two, makes it easier to study the nature of capillary continuity between the matrix blocks and its effect on production rate and recovery efficiency. The three matrix block model that was designed in this study, does not take capillary continuity into account. The fractures acts as an open flow channel primarily for the fluid to be transported in.

10.3 Waterflooding – Single Matrix Block Model

The single matrix block model was designed to find the most convenient and most representable well placement and geometry, as well as the choice of injection rate due to viscous displacement forces.

10.3.1 Effect of Well Geometry

Placing the wells vertically in the middle of the fracture surface as seen on the right side of Figure 9.1, result in a more radial flow pattern. The case with vertical wells perforates all layers from z=1 to z=31 for both injector and producer.

The case with horizontal wells only perforates at the horizontal plane. The producer of the horizontal well case is placed at z=1 parallel and diagonal to the injector at z =31.

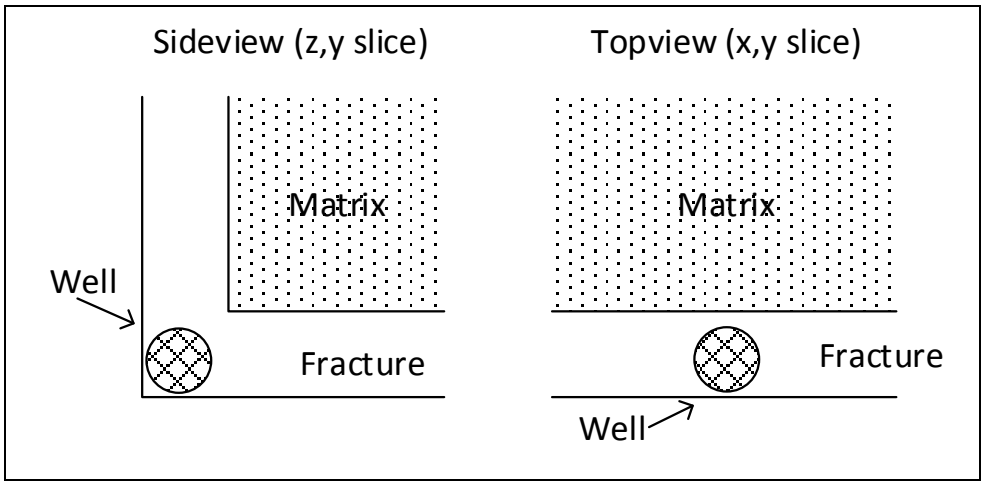

Figure 10.2 – Sideview of horizontal well and topview of vertical well.

Figure 10.2 shows that the injected water can displace the oil from two of the matrix surfaces with the horizontal well as well as the first three (y=1, 2, 3) and the last three gridblocks (y = 29, 30, 31) in y-direction. The vertical well only displaces oil from one of the matrix surfaces together with the first three (z=1, 2, 3) and the last three gridblocks (z=29, 30, 31) in z-direction.

The decision of well geometry is therefore important in term of recovery efficiency. The injected water is in contact with a bigger area of the matrix block, which result in a more effective recovery since it displaces the oil from the fracture more efficiently from primarily two surfaces and the water can then imbibe and displace the oil in the matrix from a bigger area compared to the vertical well case.

The vertical well has a shorter distance from injector to producer, compared to the horizontal well case where the distance is equal to the diagonal of the model. This result in an earlier watercut and earlier drop in oil production rate for the conventional case.

10.3.2 Effect of Injection Rate

A higher injection rate yields a higher recovery factor due to a larger amount of water will be in contact with the matrix surfaces per Δt. The result of the high injection rate is that the imbibition process will occur more uniform around the matrix block.

For lower injection rate the water will start the imbibition process more in the lower part of the model since it takes longer time to fill the fracture volume with water.

Figure 10.3 is a z-y slice of the model with two different injection rate cases. It can be observed that the water imbibes more in the lower part of the low injection rate case compared to a more uniform imbibition in the high injection rate case. The cases has been compared at a time where all parts of the fracture that surrounds the matrix has been filled with water.

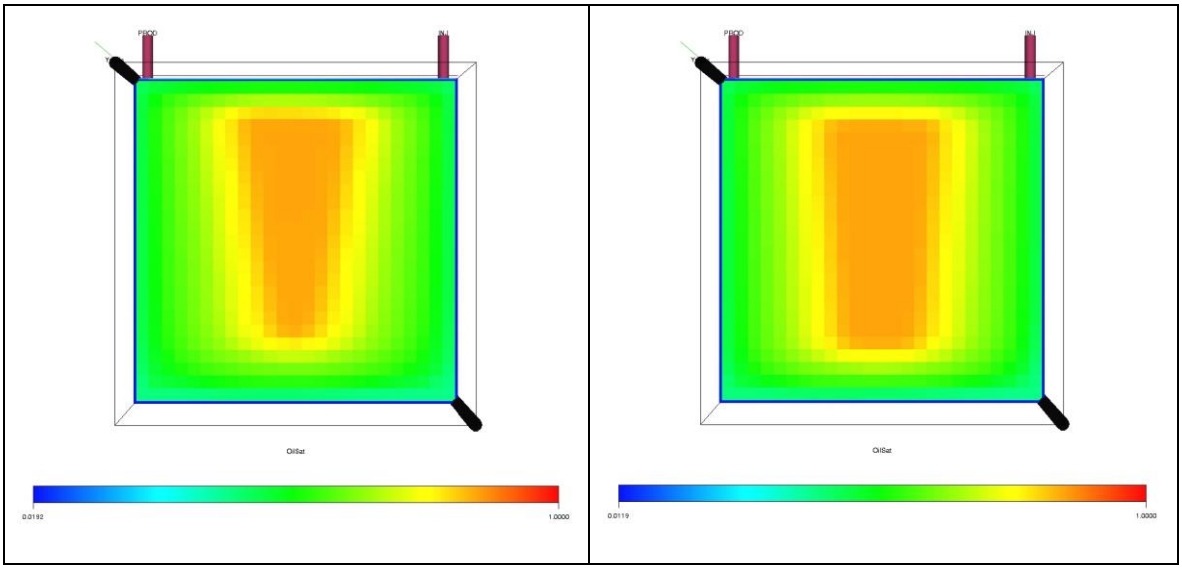

Figure 10.3 – Comparison of the effect of injection rate of 100 rcc/hr after 60 days of water injection (left) and 200 rcc/hr (right) after 44 days of water injection.

10.4 Waterflooding – Three Matrix Block Model

By expanding the model, it is possible to see the effect of matrix-fracture-matrix on displacement patterns. In this case the effect of different fracture openings has been studied and its effect on reservoir performance.

It is assumed discontinuity in capillary pressure between the matrix blocks, meaning that there are no connection in the fractures between the matrices.

10.4.1 Effect of Gravity

By studying the model visually it is possible to observe the gravitational contribution on the flow pattern.

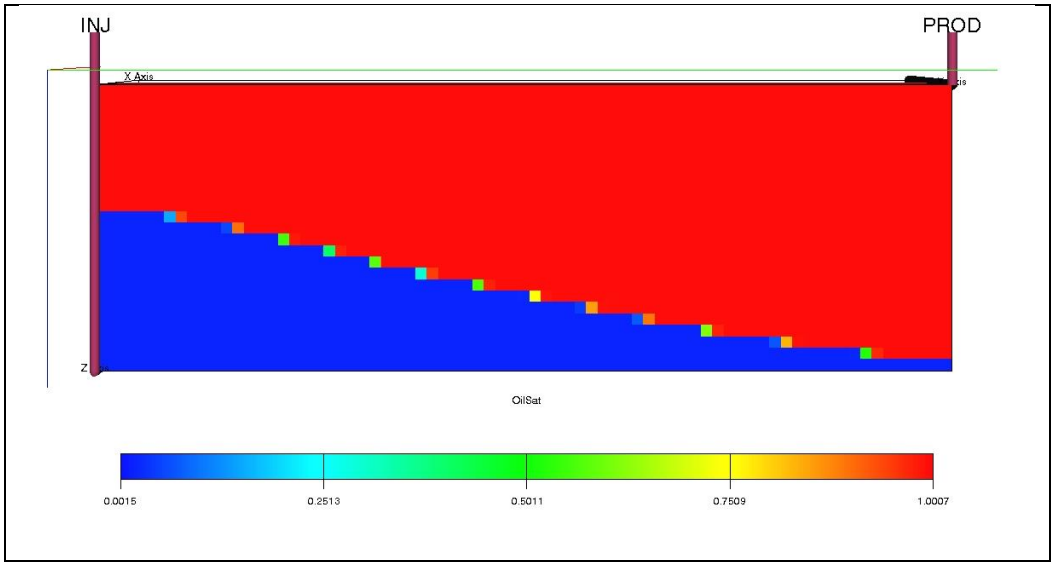

Figure 10.4 – Sideview (y, z) of fracture, showing the effect of gravity, after 14 days of waterflooding. Fracture width = 0.3cm

Figure 10.4 shows a clear trend in the contribution of gravity when injecting fluids. The injector perforates and injects at two surface areas which is why the water-level is higher close to the injector. The gravity contribution can have an impact on the imbibition process of the matrix blocks closest to the well.

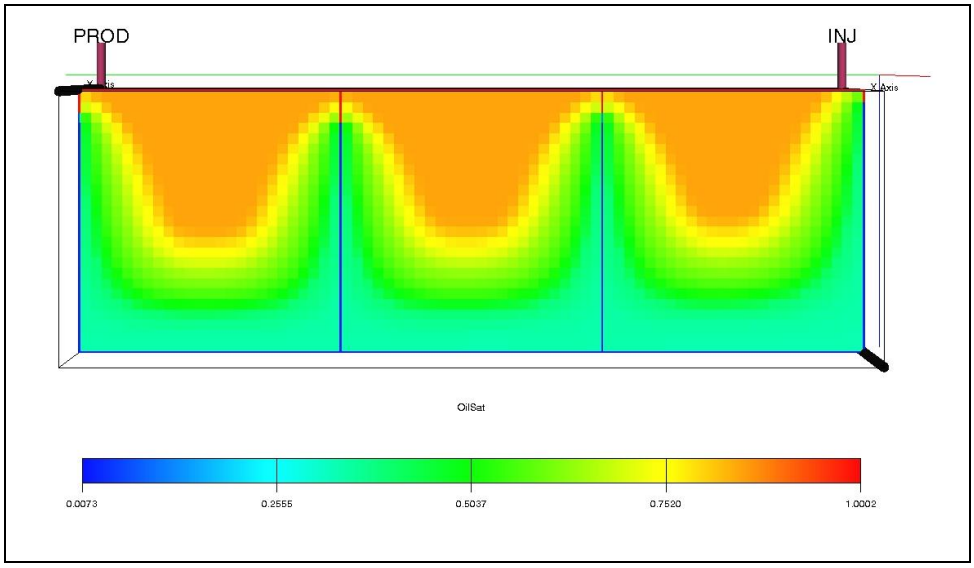

Figure 10.5 – Sideview (y, z) of fracture, showing the effect of gravity, after 60 days of waterflooding . Fracture width = 0.9cm

As seen in Figure 10.5, the matrix block closest to the well has displaced slightly more oil than the other two matrix blocks further away from the injector. It can also be observed that the water level in the fractures reaches approximately the same height, due to the nature of gravity and that the fractures act as an open flow channel.

The pattern of the oil displacement in the matrix indicate that the water imbibes more in the lowest part of all the matrix blocks and slowly also displacing the oil close to the x, z plane fractures.

Chilingarian et al. (1996) states that the capillary forces and gravity forces act in favor of an upward displacement of oil. This can be observed in the simulation model in Figure 10.5.

10.4.2 Effect of Fracture Opening

In an actual reservoir the fracture openings can vary between 10 and 200 microns, but the most frequent range is studied to be between 10-40 microns (Van Golf-Racht, 1982). In this study the fracture opening of the basecase is assumed to be 0.9 cm which is 9000 microns, for simulation conveniences.

Reducing the fracture width and keeping the production and injection rate constant gives the same effect as increasing the injection rate according to Darcy's law, described in Equation (4.5) in Chapter 4.2.

To study the effect of fracture opening, plots against pore volume should be made because of the change in bulk volume and fracture pore volume. The plots for the cases with modified fracture opening, is therefore misleading and not representable.

10.5 Surfactant flooding – Three Matrix Block Model

Using surfactants alters the interfacial tension between the oil and water phase. The fractures that surround the matrix blocks has an initial oil saturation that is produced first which is why the oil production curves are sharp in the beginning of all cases simulated.

Many factors with surfactant flooding was studied to see which parameter that affect the oil production the most.

10.5.1 Effect of Surfactant Concentration – Continuous Flooding

Continuous flooding with surfactants in an actual reservoir is not likely to happen due to high expenditures and result in a lower net profit.

Continuous flooding with surfactants is the case that result in the highest recovery factor. This is most likely because the surfactants are continuously being injected and are then able to reach out and affect a bigger area of the model. According to the relative permeability curves in Figure 8.9, the areas that has miscible fluid displacement are the areas where the surfactants has been introduced, resulting in a decrease in residual oil saturation.

Figure 9.14 indicate that as the surfactant concentration increases the oil production efficiency will increase. The simulated cases assume no adsorption in the rock surface, which means that even with higher local surfactant concentration in the solution, the surfactant will not attach to the rock surface and reach more of the capillary trapped oil.

However, one of the possible reasons why increased surfactant concentration affect the recovery, could be that the CMC is reached much faster and result in a more rapid decrease in interfacial tension and decrease in residual oil saturation in all areas of the model. The cases with lower surfactant concentration will tend to take longer time before reaching the point of CMC, and will take longer time for the effect of surfactants to take place.

It can be observed in Figure 9.14, that the extreme case with $0.03 g/cm^3$ in surfactant concentration continues to increase in recovery and reaches the residual oil saturation that has

been preset in the relative permeability curves much faster than the cases with lower concentration.

According to the SURFCAPD keyword in Eclipse, see Chapter 8.7.5, the miscible relative permeability curve will be applied to areas of the model where the capillary number is 10^{-4} or higher. By increasing the surfactant concentration to the point where the CMC is reached faster in all areas together with the reduction of interfacial tension that has affected the capillary number the most, the miscible relative permeability curve will be applied faster. This result in a lower residual oil saturation in the swept areas compared to the lower surfactant concentration cases.

In Figure 9.15, it can also be observed that at a point the case with surfactant concentration of $0.003 g/cm^3$ will drop in production rate faster than the waterflooding case, but has a higher oil production rate after 90 days of surfactant flooding and end up with a higher oil recovery. This can be explained by the reduction in IFT.

By slightly reducing the interfacial tension, the capillary pressure will be reduced and lead to less effective displacement efficiency at the matrix-fracture interface. When the injected fluid starts to imbibe, and the surfactant and water mix reaches the CMC. A capillary number of more than 10^{-4} is reached and result in the activation of miscible relative permeability and capillary pressure curve, leading to reduced residual oil saturation.

10.5.2 Effect of Adsorption – Continuous Flooding

Adsorption is one of the main challenges when it comes to injecting chemicals. With high adsorption, the net profit of a chemical injection project will decrease.

By continuously flooding with surfactants the final oil recovery efficiency can be observed as lower for the cases where the adsorption function is activated, see Figure 9.17. Since surfactant is continuously supplied, it will eventually sweep and reach the middle of the low permeable matrix blocks, and displace the capillary trapped oil until residual oil saturation in the miscible relative permeability table has been reached. When the adsorption function is activated but surfactants is continuously supplied, the final recovery for all the cases will eventually intersect with longer simulation time.

According to the SURFADS keyword in Chapter 8.7.5, which states the local surfactant concentration against adsorption, the adsorption is restricted to a maximum local surfactant concentration of 1.0 g/cm^3. When the local surfactant concentration has reached this level for one gridblock, no more adsorption can takes place in that particular gridblock. This leads to a delay in the time it takes before the surfactant reaches the middle of the matrix. In other words, it takes longer time for the surfactant to reach the areas of the model that is furthest away from the injector.

Figure 10.6 shows the topview of an adsorption case and a case with no adsorption. The color coding indicate the oil saturation, where it increases from blue to red. It can be observed that the matrix areas that is closest to the fracture has displaced more oil in the no adsorption, but as the surfactant concentration is lower due to adsorption, the tension between oil and water is reduced. This means that the water-surfactant mixture are able to reach more of the oil in the middle of the matrix earlier than the case with no adsorption and result in a slightly higher recovery at the beginning, see Figure 9.17.

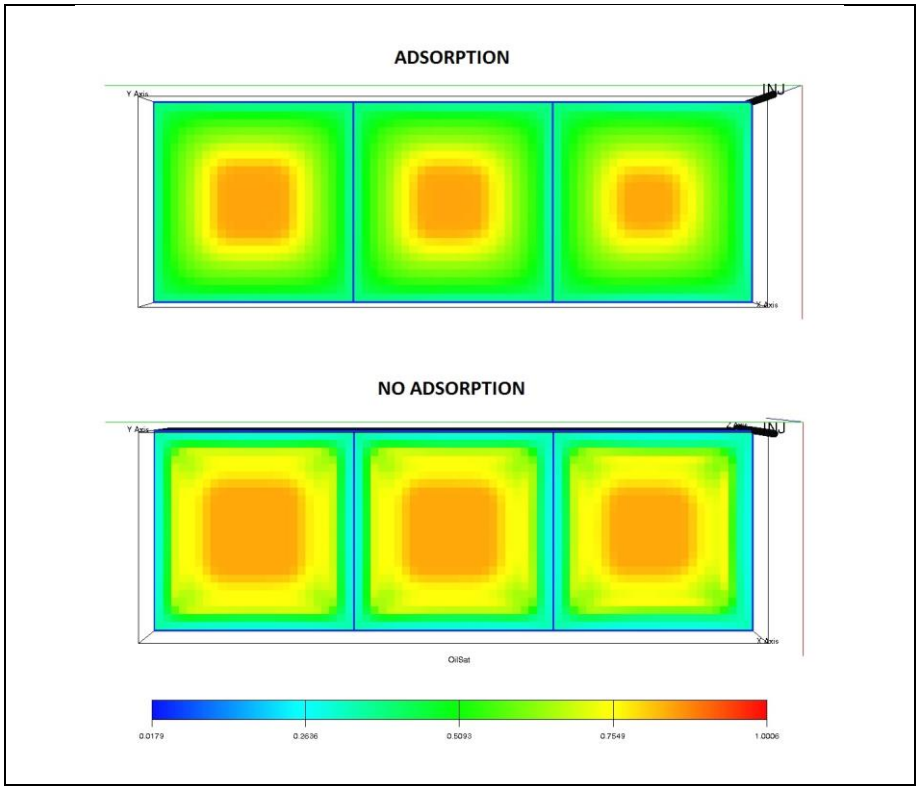

Figure 10.6 – Topview comparing adsorption and no adsorption case with same surfactant concentration. Model sliced in the middle of the matrix at T=60days. Adsorption of 0.005g/g, surfactant concentration of 0.003g/cm^3.

10.5.3 Effect of Surfactant Slug Size

The continuous surfactant injection cases that has been studied is only conceptual. In a real reservoir case, the surfactants is usually injected as slugs, see Figure 10.7.

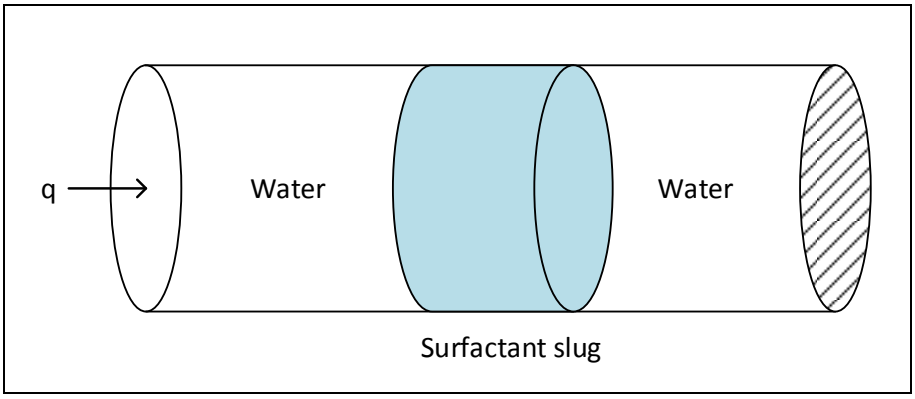

Figure 10.7 – Water injection followed by a surfactant slug and then water injection.

In Figure 9.23, it can be observed that the recovery is dependent on surfactant slugs. A larger surfactant slug for this study indicate that the surfactant is in contact with the swept areas for a longer time before pure water is injected and pushes the slug out of the model, assuming that no adsorption takes place.

With more surfactants in the system, the formation of micelles can occur at a higher pace and eventually reach CMC if enough surfactants is supplied. The oil production case with two months of slug injection after two months of water injection can be observed in Figure 9.25. It indicates that the production is following the exact trend as basecase until the point where the surfactant has been injected and contributed to the decrease in interfacial tension and reduced residual oil saturation at the areas that has been swept by surfactant mixture. The bump in oil production after 100 days of production is the result of this. The same trend can be observed for the 4 months big slug after 210 days of production.

10.6 Simulation Uncertainties

There are many uncertainties related to reservoir simulation, due to several reservoir assumptions and simplifications. The result for this study is less plausible due to no production history to match the model with.

Other uncertainties is related to how representable the models in this study is in an actual reservoir case, in terms of reservoir pressure, bottom hole pressure in production and injection well, capillary and relative permeability curves; which all can impact the model's production performance.

The surfactant model in Eclipse does not take the surfactant composition into account, by which different surfactant types can have an impact on production and recovery efficiency according to laboratory experiments.

10.7 Complete Evaluation

This study has shown the importance of well placement and geometry to recovery efficiency. To take advantage of the fractures to transport fluids it is important to localize and map the fractures to place the well where it can perforate several fractures, and with higher injection rate more amount of injected fluid is in contact with the matrix surface per Δt and imbibe into the matrix more uniformly.

The fracture width between the matrix blocks can impact the reservoir performance in terms of higher injection rate and change in flow condition. Natural fracture widths in real reservoirs are not uniformly distributed which can have an impact on flow and the dominating displacement force.

Continuously injecting surfactants will yield the highest recovery due to a higher amount of surfactants in the system that lead to a more rapid formation of micelles, similar to increasing the surfactant concentration.

Adsorption is one of the greatest challenges when injecting chemicals to alter interfacial tension, relative permeability and capillary forces, due to the loss of chemicals. Adsorption constrains the surfactant to reach to the areas furthest away from the well, but can also alter the wettability to a more water-wet state and reduce the residual oil saturation.

According to Shen et al. (2010), the IFT has a significant effect on the empirical exponents n_o and n_w that is used in the Corey correlation. When designing the miscible relative permeability curve, the empirical exponent for both water and oil was reduced from 2.0 to 1.5 that resulted in more straight relative permeability that could represent the effect of surfactants in the model.

11 Conclusion

- Injection of surfactants into a fractured network that surrounds a matrix block will lead to increased recovery.
- Surfactants alters the relative permeability curves due to reduced interfacial tension, which result in improved reservoir performance.
- High adsorption will reduce the effect of surfactant, but can alter the wettability to a more preferred state under right conditions.
- Well location have an impact on the reservoir performance when injecting in a fractured network.
- Higher amount of surfactant in the system yields the best surfactant effect due to CMC being reached faster.
- High surfactant concentration is more effective than low surfactant concentration.
- Large surfactant slugs are more effective than small surfactant slugs.

12 Recommendation

- In this simulation study, it is assumed that the fracture act as an open gap between the matrix blocks. In an actual reservoir, there is capillary continuity between the matrix blocks that can change the imbibition and fluid flow patterns in the reservoir. To get a better understanding of this, it is recommended to study the act of capillary continuity between the matrix blocks by defining a certain amount of the gridcells that lies in the fracture with the same properties as the actual matrix block.

- When taking use of an enhanced oil recovery mechanism by using chemicals, the economic feasibility is of great importance and should be thoroughly investigated.

- The surfactant model in Eclipse E100 does not take the chemical composition of the surfactant into account. This means that effect of different types of surfactants such as anionic and cationic surfactants is being neglected. Other simulation tools are therefore recommended to use in order to check the accuracy of the simulation.

- Laboratory measurements including relative permeability and capillary pressure should be conducted and set as input data in the simulation model. Result from flooding and imbibition experiments with both water and surfactants can be correlated with a numerical model to check if the result is the same.

Nomenclature

Γ	Transferability of fluid between the fracture and the matrix
δ	Azimuth
θ	Contact angle
λ_1	Mobility of displacing fluid
λ_2	Mobility of displaced fluid
λ_w	Pore size distribution constant for water relative permeability
λ_o	Pore size distribution constant for oil relative permeability
μ	Viscosity of the flowing fluid (cP)
μ_1	Viscosity of displacing fluid
μ_2	Viscosity of displaced fluid
μ_w	Viscosity of water
μ_{ws}	Viscosity of the water-surfactant mixture
ρ_o	Oil density
ρ_w	Water density
σ	Block shape factor
σ	Interfacial tension between displaced and displacing fluid
σ_{os}	Tension between oil droplet and surface
σ_{wo}	Tension between water and oil droplet
σ_{ws}	Tension between water and surface
φ	Porosity
φ_f	Fracture porosity (secondary)
φ_m	Matrix porosity (primary)
φ_{tot}	Total porosity
ω	Dip angle

∇P_P	Phase potential
A	Cross-sectional area across which flow occurs (cm^2)
b	Fracture width
$CA(C_{surf})$	Adsorption isotherm as a function of local surfactant concentration in solution
CMC	Critical Micelle Concentration
C_N	Unit conversion constant, ≈1 for SI-units
C_{surf}	Surfactant concentration
D	Average fracture width and where the fracture plane is parallel to the fluid pressure gradient
dP/dL	Pressure drop per unit length (atm/cm)
dP/dx	Pressure gradient
e	Fracture width, m
f(t)	Function of time
F_c	Capillary force
FINT	Fracture intensity
F_v	Viscous force
g	Gravity constant
g_c	Conversion factor
H	Capillary rise
IFT	Interfacial Tension
k	Permeability
k_1	Permeability in the displacing fluid medium
k_2	Permeability in the displaced fluid medium
k_f	Fracture permeability, mD
k_m	Matrix permeability, mD
k_t	System permeability, mD
L	Fracture length
L	Length of capillary tube
LFDH	Linear fracture density (horizontal)
LFDV	Linear fracture density (vertical)

L_x	Length
M	Mobility ratio
MD	Mass density of rock
N_c	Capillary number
n_f	Number of fractures
n_o	Empirical exponent for oil phase
n_w	Empirical exponent for water phase
P	Fluid pressure at a location (x, y) in a 2D flow geometry
P_c	Capillary pressure
p_f	Fracture pressure
P_g	Gravity force
p_m	Matrix pressure
$P_{non\text{-}wetting}$	Pressure in the non-wetting phase
P_{ref}	Reference pressure in the PVTW keywords
PV	Pore volume
$P_{wetting}$	Pressure in the wetting phase
q	Volumetric flow rate
q	Flow rate through the porous medium (cm/s)
r	Capillary radius
r_1	Radius of curvature
r_2	Radius of curvature
S_g	Gas saturation
S_i	Saturation of fluid i
S_o	Oil saturation
S_{or}	Residual oil saturation
S_w	Water saturation
S_w^*	Normalized water saturation
S_{wr}	Residual water saturation
$\bar{v}$	Average velocity in the capillary tube
v	Darcy velocity of the displacing fluid

V	Volume of the matrix block
v	Apparent velocity
V_b	Bulk volume
V_f	Fracture volume
V_i	Total volume of fluid i
V_m	Matrix volume
V_p	Pore volume
$V_{p,\,f}$	Pore volume of fracture
$V_{p,\,m}$	Pore volume of matrix
$V_{p,\,tot}$	Total pore volume
x	Characteristic length of the matrix block

Bibliography

Abdallah, W., Buckley, J. S., Carnegie, A., Edwards, J., Herold, B., Fordham, E., . . . Signer, C. (2007). Fundamentals of wettability. *Schlumberger Oilfield Review, 19*(2).

Ahmed, T. (2010a). Chapter 4 - Fundamentals of Rock Properties. In T. Ahmed (Ed.), *Reservoir Engineering Handbook (Fourth Edition)* (pp. 189-287). Boston: Gulf Professional Publishing.

Ahmed, T. (2010b). Chapter 5 - Relative Permeability Concepts. In T. Ahmed (Ed.), *Reservoir Engineering Handbook (Fourth Edition)* (pp. 288-330). Boston: Gulf Professional Publishing.

Ahmed, T. (2010c). Chapter 17 - Fractured Reservoirs. In T. Ahmed (Ed.), *Reservoir Engineering Handbook (Fourth Edition)* (pp. 1338-1432). Boston: Gulf Professional Publishing.

Chilingarian, G. V., Mazzullo, S. J., & Rieke, H. H. (1996). Carbonate Reservoir Characterization - A Geologic-Engineering Analysis, Part II: Elsevier.

Dake, L. P. (1983). *Fundamentals of reservoir engineering*: Elsevier.

Dandekar, A. Y. (2013). *Petroleum reservoir rock and fluid properties*: CRC press.

Donaldson, E. C., & Alam, W. (2008). *Wettability*. Houston, Tex.: Gulf Pub. Co.

Donaldson, E. C., Chilingarian, G. V., & Yen, T. F. (1989). *Enhanced Oil Recovery, II: Processes and Operations*: Elsevier Science.

Fanchi, J. R. (2006a). Chapter 3 - Multiphase Flow Concepts. In J. R. Fanchi (Ed.), *Principles of Applied Reservoir Simulation (Third Edition)* (pp. 27-50). Burlington: Gulf Professional Publishing.

Fanchi, J. R. (2006b). Chapter 4 - Fluid Displacement. In J. R. Fanchi (Ed.), *Principles of Applied Reservoir Simulation (Third Edition)* (pp. 51-64). Burlington: Gulf Professional Publishing.

GeoQuest, S. (2013). ECLIPSE Technical Description Manual (2013.2 ed.): 2003A.

Green, D. W., & Willhite, G. P. (1998). *Enhanced oil recovery*. Richardson, TX: Henry L. Doherty Memorial Fund of AIME, Society of Petroleum Engineers.

Kalnæs, P. E. (2009). *An introduction to applying surfactant simulation on the Norne field.* (Master Project), Norwegian University of Science and Technology.

Kjosavik, A., Ringen, J., & Skjaeveland, S. (2002). Relative permeability correlation for mixed-wet reservoirs. *SPE JOURNAL-RICHARDSON-, 7*(1), 49-58.

Kleppe, J. (2014). Handout note 3: Review of relative permeabilities and capillary pressures. *TPG4150 Reservoir Recovery Techniques 2014*.

Lowe, D. F., Oubre, C. L., & Ward, C. H. (1999). *Surfactants and Cosolvents for NAPL Remediation A Technology Practices Manual*: Taylor & Francis.

Nelson, R. A. (2001). 1 - Evaluating Fractured Reservoirs: Introduction. In R. A. Nelson (Ed.), *Geologic Analysis of Naturally Fractured Reservoirs (Second edition)* (pp. 1-100). Woburn: Gulf Professional Publishing.

Nind, T. E. W. (1989). *Hydrocarbon Reservoir and Well Performance*: Springer.

Salehi, M., Johnson, S. J., & Liang, J.-T. (2008). Mechanistic study of wettability alteration using surfactants with applications in naturally fractured reservoirs. *Langmuir, 24*(24), 14099-14107.

Satter, A., Iqbal, G. M., & Buchwalter, J. L. (2008). *Practical enhanced reservoir engineering: assisted with simulation software*. Tulsa, Okla.: PennWell Corp.

Shen, P., Zhu, B., Li, X.-B., & Wu, Y.-S. (2010). An Experimental Study of the Influence of Interfacial Tension on Water–Oil Two-Phase Relative Permeability. *Transport in Porous Media, 85*(2), 505-520. doi: 10.1007/s11242-010-9575-y

Sheng, J. J. (2011). Chapter 7 - Surfactant Flooding. In J. J. Sheng (Ed.), *Modern Chemical Enhanced Oil Recovery* (pp. 239-335). Boston: Gulf Professional Publishing.

Skår, H. (2014). *Simulation of Surfactant EOR in a Mechanistic Model with Fracture and Ekofisk Properties.* (Master), Norwegian University of Science and Technology.

Slider, H. C. (1983). *Worldwide Practical Petroleum Reservoir Engineering Methods*: PennWell Books.

Standnes, D. C., & Austad, T. (2000). Wettability alteration in chalk: 2. Mechanism for wettability alteration from oil-wet to water-wet using surfactants. *Journal of Petroleum Science and Engineering, 28*(3), 123-143. doi: http://dx.doi.org/10.1016/S0920-4105(00)00084-X

Tadros, T. F. (2006). *Applied Surfactants: Principles and Applications*: Wiley.

Torsæter, O. (2014). *Naturally Fractured Reservoir, Course Compendium*. Trondheim: Norwegian University of Science and Technology.

Torsæter, O., & Abtahi, M. (2003). Experimental reservoir engineering laboratory workbook. *Department of Petroleum Engineering and Applied Geophysics, Norwegian University of Science and Technology (NTNU), Trondheim*.

Van Golf-Racht, T. D. (1982). Fundamentals of Fractured Reservoir Engineering: Elsevier.

Warren, J., & Root, P. J. (1963). *The behavior of naturally fractured reservoirs*: SPE Journal.

Zolotukhin, A. B., & Ursin, J. R. (2000). *Introduction to Petroleum Reservoir Engineering*: Høyskoleforlaget, Norwegian Academic Press.

APPENDIX A

All parameters in this section is given in lab units.

A.1 – Table of Input Parameters

Relative permeability and capillary pressure table given in SWOF.inc input file:
Calculated matrix ($N_o = N_w = 2.0$) and miscible condition ($N_o = N_w = 1.5$) relative permeability by using equation (8.3), (8.4) and (8.5).

Table of relative permeability and Capillary pressure

SW	KRW	KROW	PCOW [atm]
0.00	0.00	1.00	0.00
0.10	0.10	0.90	0.00
0.20	0.20	0.80	0.00
0.25	0.25	0.75	0.00
0.30	0.30	0.70	0.00
0.35	0.35	0.65	0.00
0.40	0.40	0.60	0.00
0.45	0.45	0.55	0.00
0.50	0.50	0.50	0.00
0.55	0.55	0.46	0.00
0.60	0.60	0.40	0.00
0.70	0.70	0.30	0.00
0.80	0.80	0.20	0.00
0.90	0.90	0.10	0.00
0.98	0.98	0.00	0.00/Fracture
0.15	0.000	0.800	0.148
0.20	0.003	0.672	0.099
0.25	0.013	0.556	0.069
0.30	0.028	0.450	0.049
0.35	0.050	0.356	0.035
0.40	0.078	0.272	0.020
0.45	0.113	0.200	0.010
0.50	0.153	0.139	0.005
0.55	0.200	0.089	0.001
0.60	0.253	0.050	0.000
0.65	0.313	0.022	-0.010
0.70	0.378	0.006	-0.049
0.75	0.450	0.000	-0.197/Matrix
0.05	0.000	1.000	0.296
0.10	0.013	0.918	0.148
0.20	0.068	0.761	0.049
0.30	0.146	0.614	0.017
0.40	0.243	0.478	0.002
0.50	0.354	0.354	0.000
0.60	0.478	0.243	-0.015
0.70	0.614	0.146	-0.049
0.80	0.761	0.068	-0.089
0.90	0.918	0.013	-0.158
0.95	1.000	0.000	-0.345/Miscible

Ekofisk PVT data from Skår (2014).

P [atm]	Bo	Viscosity [cP]
394.3	1.9927	0.18
418.9	1.9727	0.19
443.6	1.9543	0.2
468.3	1.9373	0.21
473.5	1.9338	0.21
483.4	1.9275	0.22
492.9	1.9215	0.22
503.1	1.9153	0.23
522.8	1.9038	0.24
572.3	1.8776	0.26
574.2	1.8766	0.26
584.1	1.8718	0.27
603.8	1.8625	0.28
623.6	1.8536	0.29
672.9	1.833	0.31

A.2 - Fluid in Place – Regions

Basecase

FIPNUM REPORT REGION 1
PAV = 483.22 ATMOSA
PORV= 600000. RCC

	OIL LIQUID	OIL SCC VAPOUR	OIL SCC TOTAL	WAT SCC TOTAL	GAS SCC FREE	GAS SCC DISSOLVED	GAS SCC TOTAL
CURRENTLY IN PLACE	109819.		109819.	412601.		36026286.	36026286.
OUTFLOW TO OTHER REGIONS	173631.		173631.	-320321.		56959628.	56959628.
OUTFLOW THROUGH WELLS			0.	0.			0.
MATERIAL BALANCE ERROR.			-0.	-0.			-5.
ORIGINALLY IN PLACE	283450.		283450.	92280.		92985909.	92985909.
OUTFLOW TO REGION 2	173631.		173631.	-320321.		56959628.	56959628.

FIPNUM REPORT REGION 2
PAV = 483.25 ATMOSA
PORV= 144817. RCC

	OIL LIQUID	OIL SCC VAPOUR	OIL SCC TOTAL	WAT SCC TOTAL	GAS SCC FREE	GAS SCC DISSOLVED	GAS SCC TOTAL
CURRENTLY IN PLACE	1610.		1610.	145516.		528152.	528152.
OUTFLOW TO OTHER REGIONS	-173631.		-173631.	320321.		-56959628.	-56959628.
OUTFLOW THROUGH WELLS			252507.	-465836.			82834902.
MATERIAL BALANCE ERROR.			1.	-2.			355.
ORIGINALLY IN PLACE	80487.		80487.	0.		26403781.	26403781.
OUTFLOW TO REGION 1	-173631.		-173631.	320321.		-56959628.	-56959628.

FIPNUM OIL RECOVERY FACTORS

REGION	MOBILE OIIP (W.R.T WATER)	MOBILE OIIP (W.R.T GAS)	RATIO OF DISPLACED OIL TO INITIAL OIP	RATIO OF DISPLACED OIL TO INITIAL MOBILE OIL (WATER)	RATIO OF DISPLACED OIL TO INITIAL MOBILE OIL (GAS)	RATIO OF WELL FLOW TO INITIAL OIP	RATIO OF WELL FLOW TO INITIAL MOBILE OIL (WATER)	RATIO OF WELL FLOW TO INITIAL MOBILE OIL (GAS)
FIELD	2.604E+05		0.69382	0.96975		0.69382	0.96974	
1	1.868E+05		0.61256	0.92970		0	0	
2	7.363E+04		0.98000	1.07133		3.13724	3.42963	

Continuous Surfactant Flooding

FIPNUM REPORT REGION 1
PAV = 483.22 ATMOSA
PORV= 600000. RCC

	OIL LIQUID	OIL SCC VAPOUR	OIL SCC TOTAL	WAT SCC TOTAL	GAS SCC FREE	GAS SCC DISSOLVED	GAS SCC TOTAL
CURRENTLY IN PLACE	89258.		89258.	450535.		29280934.	29280934.
OUTFLOW TO OTHER REGIONS	194194.		194194.	-358252.		63705197.	63705197.
OUTFLOW THROUGH WELLS			0.	0.			0.
MATERIAL BALANCE ERROR.			-1.	-4.			-222.
ORIGINALLY IN PLACE	283450.		283450.	92280.		92985909.	92985909.
OUTFLOW TO REGION 2	194194.		194194.	-358252.		63705197.	63705197.

FIPNUM REPORT REGION 2
PAV = 483.23 ATMOSA
PORV= 144817. RCC

	OIL LIQUID	OIL SCC VAPOUR	OIL SCC TOTAL	WAT SCC TOTAL	GAS SCC FREE	GAS SCC DISSOLVED	GAS SCC TOTAL
CURRENTLY IN PLACE	3751.		3751.	141567.		1230421.	1230421.
OUTFLOW TO OTHER REGIONS	-194194.		-194194.	358252.		-63705197.	-63705197.
OUTFLOW THROUGH WELLS			270930.	-499823.			88878476.
MATERIAL BALANCE ERROR.			0.	4.			80.
ORIGINALLY IN PLACE	80487.		80487.	0.		26403781.	26403781.
OUTFLOW TO REGION 1	-194194.		-194194.	358252.		-63705197.	-63705197.

FIPNUM OIL RECOVERY FACTORS

REGION	MOBILE OIIP (W.R.T WATER)	MOBILE OIIP (W.R.T GAS)	RATIO OF DISPLACED OIL TO INITIAL OIP	RATIO OF DISPLACED OIL TO INITIAL MOBILE OIL (WATER)	RATIO OF DISPLACED OIL TO INITIAL MOBILE OIL (GAS)	RATIO OF WELL FLOW TO INITIAL OIP	RATIO OF WELL FLOW TO INITIAL MOBILE OIL (WATER)	RATIO OF WELL FLOW TO INITIAL MOBILE OIL (GAS)
FIELD	2.604E+05		0.74444	1.04049		0.74444	1.04050	
1	1.868E+05		0.68510	1.03980		0	0	
2	7.363E+04		0.95340	1.04226		3.36613	3.67985	

Continuous Surfactant Flooding after 2 months of Water

FIPNUM REPORT REGION 1
PAV = 483.22 ATMOSA
PORV= 600000. RCC

	OIL SCC LIQUID	OIL SCC VAPOUR	OIL SCC TOTAL	WAT SCC TOTAL	GAS SCC FREE	GAS SCC DISSOLVED	GAS SCC TOTAL
CURRENTLY IN PLACE	100848.		100848.	429153.		33083028.	33083028.
OUTFLOW TO OTHER REGIONS	182603.		182603.	-336867.		59902924.	59902924.
OUTFLOW THROUGH WELLS			0.	0.			0.
MATERIAL BALANCE ERROR.			-0.	-6.			-42.
ORIGINALLY IN PLACE	283450.		283450.	92280.		92985909.	92985909.
OUTFLOW TO REGION 2	182603.		182603.	-336867.		59902924.	59902924.

FIPNUM REPORT REGION 2
PAV = 483.23 ATMOSA
PORV= 144817. RCC

	OIL SCC LIQUID	OIL SCC VAPOUR	OIL SCC TOTAL	WAT SCC TOTAL	GAS SCC FREE	GAS SCC DISSOLVED	GAS SCC TOTAL
CURRENTLY IN PLACE	2129.		2129.	144559.		698397.	698397.
OUTFLOW TO OTHER REGIONS	-182603.		-182603.	336867.		-59902924.	-59902924.
OUTFLOW THROUGH WELLS			260960.	-481430.			85607871.
MATERIAL BALANCE ERROR.			1.	4.			436.
ORIGINALLY IN PLACE	80487.		80487.	0.		26403781.	26403781.
OUTFLOW TO REGION 1	-182603.		-182603.	336867.		-59902924.	-59902924.

FIPNUM OIL RECOVERY FACTORS

REGION	MOBILE OIIP (W.R.T WATER)	MOBILE OIIP (W.R.T GAS)	RATIO OF DISPLACED OIL TO INITIAL OIP	RATIO OF DISPLACED OIL TO INITIAL MOBILE OIL (WATER)	RATIO OF DISPLACED OIL TO INITIAL MOBILE OIL (GAS)	RATIO OF WELL FLOW TO INITIAL OIP	RATIO OF WELL FLOW TO INITIAL MOBILE OIL (WATER)	RATIO OF WELL FLOW TO INITIAL MOBILE OIL (GAS)
FIELD	2.604E+05		0.71705	1.00221		0.71705	1.00221	
1	1.868E+05		0.64421	0.97774		0	0	
2	7.363E+04		0.97355	1.06428		3.24226	3.54444	

2 months Surfactant Slug after 2 months of Water

FIPNUM REPORT REGION 1
PAV = 483.22 ATMOSA
PORV= 600000. RCC

	OIL SCC LIQUID	OIL SCC VAPOUR	OIL SCC TOTAL	WAT SCC TOTAL	GAS SCC FREE	GAS SCC DISSOLVED	GAS SCC TOTAL
CURRENTLY IN PLACE	106631.		106631.	418483.		34980283.	34980283.
OUTFLOW TO OTHER REGIONS	176819.		176819.	-326203.		58005633.	58005633.
OUTFLOW THROUGH WELLS			0.	0.			0.
MATERIAL BALANCE ERROR.			-0.	-0.			-7.
ORIGINALLY IN PLACE	283450.		283450.	92280.		92985909.	92985909.
OUTFLOW TO REGION 2	176819.		176819.	-326203.		58005633.	58005633.

FIPNUM REPORT REGION 2
PAV = 483.25 ATMOSA
PORV= 144817. RCC

	OIL SCC LIQUID	OIL SCC VAPOUR	OIL SCC TOTAL	WAT SCC TOTAL	GAS SCC FREE	GAS SCC DISSOLVED	GAS SCC TOTAL
CURRENTLY IN PLACE	1610.		1610.	145517.		528062.	528062.
OUTFLOW TO OTHER REGIONS	-176819.		-176819.	326203.		-58005633.	-58005633.
OUTFLOW THROUGH WELLS			255695.	-471718.			83880867.
MATERIAL BALANCE ERROR.			1.	-2.			486.
ORIGINALLY IN PLACE	80487.		80487.	0.		26403781.	26403781.
OUTFLOW TO REGION 1	-176819.		-176819.	326203.		-58005633.	-58005633.

FIPNUM OIL RECOVERY FACTORS

REGION	MOBILE OIIP (W.R.T WATER)	MOBILE OIIP (W.R.T GAS)	RATIO OF DISPLACED OIL TO INITIAL OIP	RATIO OF DISPLACED OIL TO INITIAL MOBILE OIL (WATER)	RATIO OF DISPLACED OIL TO INITIAL MOBILE OIL (GAS)	RATIO OF WELL FLOW TO INITIAL OIP	RATIO OF WELL FLOW TO INITIAL MOBILE OIL (WATER)	RATIO OF WELL FLOW TO INITIAL MOBILE OIL (GAS)
FIELD	2.604E+05		0.70258	0.98200		0.70258	0.98199	
1	1.868E+05		0.62381	0.94677		0	0	
2	7.363E+04		0.98000	1.07134		3.17685	3.47293	

2 months Surfactant Slug after 2 months of Water with 0.0005g/g Adsorption

FIPNUM REPORT REGION 1
PAV = 483.22 ATMOSA
PORV= 600000. RCC

	OIL SCC			WAT SCC	GAS SCC		
	LIQUID	VAPOUR	TOTAL	TOTAL	FREE	DISSOLVED	TOTAL
CURRENTLY IN PLACE	108557.		108557.	414930.		35612141.	35612141.
OUTFLOW TO OTHER REGIONS	174893.		174893.	-322649.		57373767.	57373767.
OUTFLOW THROUGH WELLS			0.	0.			0.
MATERIAL BALANCE ERROR.			0.	-1.			2.
ORIGINALLY IN PLACE	283450.		283450.	92280.		92985909.	92985909.
OUTFLOW TO REGION 2	174893.		174893.	-322649.		57373767.	57373767.

FIPNUM REPORT REGION 2
PAV = 483.25 ATMOSA
PORV= 144817. RCC

	OIL SCC			WAT SCC	GAS SCC		
	LIQUID	VAPOUR	TOTAL	TOTAL	FREE	DISSOLVED	TOTAL
CURRENTLY IN PLACE	1610.		1610.	145517.		528080.	528080.
OUTFLOW TO OTHER REGIONS	-174893.		-174893.	322649.		-57373767.	-57373767.
OUTFLOW THROUGH WELLS			253769.	-468165.			83249062.
MATERIAL BALANCE ERROR.			1.	-1.			406.
ORIGINALLY IN PLACE	80487.		80487.	0.		26403781.	26403781.
OUTFLOW TO REGION 1	-174893.		-174893.	322649.		-57373767.	-57373767.

FIPNUM OIL RECOVERY FACTORS

REGION	MOBILE OIIP (W.R.T WATER)	MOBILE OIIP (W.R.T GAS)	RATIO OF DISPLACED OIL TO INITIAL OIP	RATIO OF DISPLACED OIL TO INITIAL MOBILE OIL (WATER)	RATIO OF DISPLACED OIL TO INITIAL MOBILE OIL (GAS)	RATIO OF WELL FLOW TO INITIAL OIP	RATIO OF WELL FLOW TO INITIAL MOBILE OIL (WATER)	RATIO OF WELL FLOW TO INITIAL MOBILE OIL (GAS)
FIELD	2.604E+05		0.69729	0.97460		0.69729	0.97459	
1	1.868E+05		0.61702	0.93646		0	0	
2	7.363E+04		0.98000	1.07134		3.15292	3.44678	

APPENDIX B

```
--VINH VUONG TRAN
--MSC THESIS - NTNU 2015
--IMBIBITION PROCESS
--BASECASE FOR THREE MATRIX BLOCKS SURROUNDED BY FRACTURES


--
RUNSPEC
--

TITLE
SIMULATION OF THREE MATRIX BLOCKS SURROUNDED BY FRACTURES IN 3D

DIMENS
31        87        31/

OIL
WATER
SURFACT

--METRIC
LAB

TABDIMS
3         1         40        40        2         20/

WELLDIMS
2         90        1         2/

NUPCOL
150/

NSTACK
100/

START
1 'DEC'  2005/

UNIFOUT
UNIFIN

MESSAGES
3*        1000      5*        1000      2*/

--NOSIM

--
GRID
--
```

```
INIT
OLDTRAN

EQUALS
--VALUE          I1    I2    J1    J2    K1    K2
'TOPS'  3e5      1     31    1     87    1     1     / TOTAL MODEL
'DX'    4        1     31    1     87    1     31    /
'DY'    4        1     31    1     87    1     31    /
'DZ'    4        1     31    1     87    1     31    /
'PERMX'          1     1     31    1     87    1     31    /
'PERMY'          1     1     31    1     87    1     31    /
'PERMZ'          1     1     31    1     87    1     31    /
'PORO'  0.2      1     31    1     87    1     31    /
/

EQUALS
'DX'    0.3      1     3     1     87    1     31     / X FRACTURE
'PERMX'          5000  1     3     1     87    1     31    /
'PERMY'          5000  1     3     1     87    1     31    /
'PERMZ'          5000  1     3     1     87    1     31    /
'PORO'  0.99     1     3     1     87    1     31    /
/

EQUALS
'DX'    0.3      29    31    1     87    1     31     / X FRACTURE
'PERMX'          5000  29    31    1     87    1     31    /
'PERMY'          5000  29    31    1     87    1     31    /
'PERMZ'          5000  29    31    1     87    1     31    /
'PORO'  0.99     29    31    1     87    1     31    /
/

EQUALS
'DY'    0.3      1     31    1     3     1     31     / Y FRACTURE
'PERMX'          5000  1     31    1     3     1     31    /
'PERMY'          5000  1     31    1     3     1     31    /
'PERMZ'          5000  1     31    1     3     1     31    /
'PORO'  0.99     1     31    1     3     1     31    /
/

EQUALS
'DY'    0.3      1     31    29    31    1     31     / Y FRACTURE
'PERMX'          5000  1     31    29    31    1     31    /
'PERMY'          5000  1     31    29    31    1     31    /
'PERMZ'          5000  1     31    29    31    1     31    /
'PORO'  0.99     1     31    29    31    1     31    /
/

EQUALS
'DY'    0.3      1     31    57    59    1     31     / Y FRACTURE
'PERMX'          5000  1     31    57    59    1     31    /
'PERMY'          5000  1     31    57    59    1     31    /
'PERMZ'          5000  1     31    57    59    1     31    /
'PORO'  0.99     1     31    57    59    1     31    /
/

EQUALS
'DY'    0.3      1     31    85    87    1     31    / Y FRACTURE
'PERMX'          5000  1     31    85    87    1     31    /
'PERMY'          5000  1     31    85    87    1     31    /
'PERMZ'          5000  1     31    85    87    1     31    /
```

```
'PORO'  0.99    1       31      85      87      1       31      /
/

EQUALS
'DZ'    0.3     1       31      1       87      1       3       / Z FRACTURE
'PERMX'         5000    1       31      1       87      1       3       /
'PERMY'         5000    1       31      1       87      1       3       /
'PERMZ'         5000    1       31      1       87      1       3       /
'PORO'  0.99    1       31      1       87      1       3       /
/

EQUALS
'DZ'    0.3     1       31      1       87      29      31      / Z FRACTURE
'PERMX'         5000    1       31      1       87      29      31      /
'PERMY'         5000    1       31      1       87      29      31      /
'PERMZ'         5000    1       31      1       87      29      31      /
'PORO'  0.99    1       31      1       87      29      31      /
/

--MULTZ
--83607*0.1/

RPTGRID
/


--
PROPS
--

--INCLUDE WATER-OIL RELPERM
INCLUDE
'SWOFX2Z.INC'/

ROCK
1.00    1.43e-4/

PVTW
--      PREF    BW              CW                      VW              VISCOSIBILITY
1.00    1.07    4.93E-05        0.61    1.10e-3/

DENSITY
--      OIL     WATER
        0.7222  0.99735/

RSCONST
328.05  394.277/

PVDO
--Po     Bo              Viscosity
394.3   1.9927          0.18
418.9   1.9727          0.19
443.6   1.9543          0.2
468.3   1.9373          0.21
473.5   1.9338          0.21
483.4   1.9275          0.22
492.9   1.9215          0.22
503.1   1.9153  0.23
522.8   1.9038  0.24
572.3   1.8776  0.26
```

```
574.2    1.8766   0.26
584.1    1.8718   0.27
603.8    1.8625   0.28
623.6    1.8536   0.29
672.9    1.833    0.31
/

SURFVISC
0        0.61
0.03     0.8
1.00     1.0/
/

SURFADS
0.0      0
0.001    0.000
0.03     0.000
1.00     0.000/
/
/

SURFST
0                5
0.001    0.5
0.005    1.0E-8
0.01     1.0E-9
0.3      1.0E-9
1                1.0E-9/

SURFCAPD
-10      0.0
-5               0.0
-4               1.0
-3               1.0
10               1.0/
/
/

SURFROCK
2        0.253/
2        0.253/
2        0.253/


RPTPROPS
/

--
REGIONS
--
EQUALS
SATNUM      2    1    31    1    87    1    31    /TOTAL MODEL
SATNUM      1    1    3     1    87    1    31    /X FRACTURE
SATNUM      1    29   31    1    87    1    31    /X FRACTURE
SATNUM      1    1    31    1    3     1    31    /Y FRACTURE
SATNUM      1    1    31    29   31    1    31    /Y FRACTURE
SATNUM      1    1    31    57   59    1    31    /Y FRACTURE
SATNUM      1    1    31    85   87    1    31    /Y FRACTURE
SATNUM      1    1    31    1    87    1    3     /Z FRACTURE
SATNUM      1    1    31    1    87    29   31    /Z FRACTURE
```

```
/

SURFNUM
83607*3/
/

INCLUDE
FIPNUMX3.FIPNUM /

--
SOLUTION
--
EQUIL
--Datum Datum   OWC          OWC          GOC          GOC          RSVD  RVVD  SOLN
--Depth Press   Depth  PCOW  Depth  PCOG  Tab   Tab    Meth
3E5    483.21  3.05E5 0     0            0             0            1             0
               0/

--RSVD


RPTSOL
--'PRES''SOIL'  'SWAT' 'RS'  'PWAT' /
'FIP' /

--
SUMMARY
--
ALL
FPR
FRPV
FOPV
FOE
FOPR
FOPT
FGOR
FGPR
FWPR
FWPT
FWIR
FWIT
WBHP
/

FTPRSUR
FTPTSUR
FTIRSUR
FTITSUR
FTADSUR

WTPRSUR
'PROD'/

RUNSUM
EXCEL
SEPARATE

--
SCHEDULE
--
```

```
RPTSCHED
--'PRES''SOIL'   'SWAT' 'RS'      'RESTART=2'    'SUMMARY=1'  'CPU=1' 'PWAT'
RESTART=2 CPU=1 FIP=2 WELLS=1 /

RPTRST
BASIC=2 /

DRSDT
0 /

WELSPECS
--Name  Group   i       j       Dbh     Phase
PROD    G1      1       87      1*      OIL/
INJ     G1      1       1       1*      WAT/
/

COMPDAT
--      i       j       k1      k2      OP/SH
PROD    1       87      1       1       'OPEN'  1*      1       /
PROD    2       87      1       1       'OPEN'  1*      1       /
PROD    3       87      1       1       'OPEN'  1*      1       /
PROD    4       87      1       1       'OPEN'  1*      1       /
PROD    5       87      1       1       'OPEN'  1*      1       /
PROD    6       87      1       1       'OPEN'  1*      1       /
PROD    7       87      1       1       'OPEN'  1*      1       /
PROD    8       87      1       1       'OPEN'  1*      1       /
PROD    9       87      1       1       'OPEN'  1*      1       /
PROD    10      87      1       1       'OPEN'  1*      1       /
PROD    11      87      1       1       'OPEN'  1*      1       /
PROD    12      87      1       1       'OPEN'  1*      1       /
PROD    13      87      1       1       'OPEN'  1*      1       /
PROD    14      87      1       1       'OPEN'  1*      1       /
PROD    15      87      1       1       'OPEN'  1*      1       /
PROD    16      87      1       1       'OPEN'  1*      1       /
PROD    17      87      1       1       'OPEN'  1*      1       /
PROD    18      87      1       1       'OPEN'  1*      1       /
PROD    19      87      1       1       'OPEN'  1*      1       /
PROD    20      87      1       1       'OPEN'  1*      1       /
PROD    21      87      1       1       'OPEN'  1*      1       /
PROD    22      87      1       1       'OPEN'  1*      1       /
PROD    23      87      1       1       'OPEN'  1*      1       /
PROD    24      87      1       1       'OPEN'  1*      1       /
PROD    25      87      1       1       'OPEN'  1*      1       /
PROD    26      87      1       1       'OPEN'  1*      1       /
PROD    27      87      1       1       'OPEN'  1*      1       /
PROD    28      87      1       1       'OPEN'  1*      1       /
PROD    29      87      1       1       'OPEN'  1*      1       /
PROD    30      87      1       1       'OPEN'  1*      1       /
PROD    31      87      1       1       'OPEN'  1*      1       /
INJ     1       1       1       31      'SHUT'  1*      1       /
INJ     2       1       31      31      'OPEN'  1*      1       /
INJ     3       1       31      31      'OPEN'  1*      1       /
INJ     4       1       31      31      'OPEN'  1*      1       /
INJ     5       1       31      31      'OPEN'  1*      1       /
INJ     6       1       31      31      'OPEN'  1*      1       /
INJ     7       1       31      31      'OPEN'  1*      1       /
INJ     8       1       31      31      'OPEN'  1*      1       /
INJ     9       1       31      31      'OPEN'  1*      1       /
INJ     10      1       31      31      'OPEN'  1*      1       /
```

```
INJ     11      1       31      31      'OPEN'  1*      1       /
INJ     12      1       31      31      'OPEN'  1*      1       /
INJ     13      1       31      31      'OPEN'  1*      1       /
INJ     14      1       31      31      'OPEN'  1*      1       /
INJ     15      1       31      31      'OPEN'  1*      1       /
INJ     16      1       31      31      'OPEN'  1*      1       /
INJ     17      1       31      31      'OPEN'  1*      1       /
INJ     18      1       31      31      'OPEN'  1*      1       /
INJ     19      1       31      31      'OPEN'  1*      1       /
INJ     20      1       31      31      'OPEN'  1*      1       /
INJ     21      1       31      31      'OPEN'  1*      1       /
INJ     22      1       31      31      'OPEN'  1*      1       /
INJ     23      1       31      31      'OPEN'  1*      1       /
INJ     24      1       31      31      'OPEN'  1*      1       /
INJ     25      1       31      31      'OPEN'  1*      1       /
INJ     26      1       31      31      'OPEN'  1*      1       /
INJ     27      1       31      31      'OPEN'  1*      1       /
INJ     28      1       31      31      'OPEN'  1*      1       /
INJ     29      1       31      31      'OPEN'  1*      1       /
INJ     30      1       31      31      'OPEN'  1*      1       /
INJ     31      1       31      31      'OPEN'  1*      1       /
/

WCONPROD
PROD    OPEN    RESV    4* 200  444.01/
/

WECON
PROD    0       1*      98      2*      CON             YES/
/

WCONINJE
INJ     WATER           OPEN    RESV    1* 200  493.34/
/

WSURFACT
'INJ'   0.003/
/

TUNING
0.24    1.2     0.24    0.72    2/
/
20      1*      100/

DATES
1 DEC 2005 00:00:10/
1 DEC 2005 12:00:00/
2 DEC 2005/
3 DEC 2005/
4 DEC 2005/
5 DEC 2005/
6 DEC 2005/
7 DEC 2005/
14 DEC 2005/
21 DEC 2005/
1 JAN 2006 /
7 JAN 2006/
14 JAN 2006/
21 JAN 2006/
1 FEB 2006 /
```

```
/

TUNING
24      24      1.2     0.24    2/
/
20      1*      100/

DATES
1 MAR 2006 /
1 APR 2006 /
1 MAY 2006 /
1 JUN 2006 /
1 JUL 2006 /
1 AUG 2006 /
1 SEP 2006 /
1 OCT 2006 /
1 NOV 2006 /
1 DEC 2006 /
1 JAN 2007 /
1 FEB 2007 /
1 MAR 2007 /
1 APR 2007 /
1 MAY 2007 /
1 JUN 2007 /
1 JUL 2007 /
1 AUG 2007 /
1 SEP 2007 /
1 OCT 2007 /
1 NOV 2007 /
1 DEC 2007 /
/

END
```